BENDING FATIGUE AND CREEP

OF TOUGH MATRIX LAMINATES

by

RIZWAN MAHMOOD GUL
B.Sc (Mechanical Engineering); Peshawar, Pakistan
(1990)

submitted to
The Department of Materials Science and Engineering
in partial fulfillment of the requirement for the degree of

MASTER OF SCIENCE
IN MATERIALS SCIENCE AND ENGINEERING

at the
Massachusetts Institute of Technology
May, 1994

Signature of Author _____
Department of Materials Science and Engineering
May 6, 1994

Certified by _____
Frederick J. McGarry
Professor of Polymer Engineering
Thesis Supervisor

Accepted by _____
Carl V. Thompson III
Professor of Electronic Materials
Chair, Departmental Committee on Graduate Students

BENDING FATIGUE AND CREEP OF TOUGH MATRIX LAMINATES

by

RIZWAN MAHMOOD GUL

Submitted to the Department of Materials Science and Engineering on May 6, 1993 in partial fulfillment of the requirement for the degree of Master of Science in Materials Science and Engineering

ABSTRACT

A toughened polyester epoxy network (MNS) with a 10 fold increase in fracture energy (G_{Ic}) by the addition of reactive rubber has been developed in a previous study. The purpose of this study is to characterize the fatigue and creep behavior of this polymer as a matrix, and to study the general effect of toughening on these properties. Flexural fatigue (R=-1) is used for the tests. The reinforcements used are chopped strand mat, glass fabric and carbon fabric, while MNS is used as the matrix with different rubber contents (0%, 7.5%, 12.5% and 17.5%) and unmodified polyester for comparison. There is much controversy about the effect of toughening of the matrix on the fatigue behavior of composites. In this study it has been observed that the fatigue behavior improves with increasing flexibility provided that the modulus does not drop too much. The S-N curves are linear on a Log-Log plot and can be characterized by the value of m ($S/S_o = N^{-1/m}$). The comparison of the value of m for different rubber contents with a particular reinforcement shows that the fatigue performance generally improves with increasing rubber content; the increase is most obvious in the case of carbon composites. Damage mechanisms also are discussed.

Creep tests have been performed in flexure, with chopped strand mat and glass fabric, and MNS as the matrix with different rubber contents (0%, 7.5%, 12.5% and 17.5%). The tests shows that the creep does not increase to a large extent with increasing rubber content. The performance has been characterized by Schapery's non-linear constitutive equation. The difference between the predicted and experimental values at 2188 hrs. ranges from 0.5%-8.57% for glass fabric composites and ranges from 1.31-8.76% for chopped strand mat composites.

Thesis Supervisor: Professor Frederick J. McGarry

Title: Professor of Polymer Engineering

Table of Contents

List of Tables

List of Figures

Figure

Acknowledgements

I acknowledge Prof. F. J. McGarry for his guidance and support during my stay here. His comments gave me inspiration and encouragement, leading me to work with the best of my abilities.

I acknowledge my parents for their patience, because I should be serving them instead of giving them the agony of staying away.

I acknowledge Dr. Mary Chan, Dr. Ramnath Subramaniam, Dr. Peter Flueler, Maria Raposo, Stephen and Arthur Rudolph for their help and valuable suggestions. Specially Mary whom I should always be grateful for teaching me many things and for being a friend in need.

Chapter 1

Introduction

Polymer composites are widely used because of their high strength and stiffness to weight ratios, ease of manufacture and corrosion resistance. Among the different matrices, epoxy and polyester are the most common. Usually glass composites are made with polyesters because of their low cost, but the drawbacks are that they are brittle and have very low fracture toughness compared to epoxies. Many attempts have been made to increase the toughness of polyester, but usually they result in a significant loss of stiffness, strength and chemical resistance [1]. The search to make a tougher polyester with a modest loss in other properties has led to the development of an interpenetrating polymer network (I.P.N): a styrene cross linked polyester, intimately combined on a molecular scale with a rubber toughened epoxy, which has been named a Molecular Network System (MNS) [2]. The purpose of this study is to characterize the fatigue and creep behavior of reinforced MNS composites and to study the effect of toughening the matrix resin on these properties.

1.1 Fatigue :-

Fatigue is defined as the loss in strength of a material due to repeated cycles of loading and unloading. This study examines the fatigue behavior under fully reversed flexure with the ratio of minimum to maximum stress (R) equal to -1; this is also called bending fatigue or full flexural fatigue. The reasons for choosing bending fatigue are as follows:

(1) Components and structures made of composites are commonly subjected to flexural fatigue. For example in the case of boats, the surfaces in contact with water are subjected to repeated pounding of waves, producing flexural fatigue. In aircraft the wings and control surfaces are subjected to wind induced flutter and engine noise producing flexural fatigue [3]. In wind turbine blades the rotation and changing wind direction produce flexural fatigue.

(2) In flexural fatigue the behavior of a composite is matrix dependent. This is because in flexural fatigue a compression component is involved which leads to matrix dependent properties. Since the purpose of this work is to study the effect of toughening of the matrix on the fatigue behavior, it was logical to use flexural fatigue.

The fatigue of composites is different from that of metals. In metals a single crack is formed near the end of the sample life and that crack propagates across the entire cross section causing failure of the specimen. In composites, fatigue loading causes multiple damage sites and the damage usually begins to appear at the start of sample life, even on the first loading cycle [4]. The damage is in the form of matrix cracking, delamination, fiber breakage and interfacial debonding. Normally, fibers lying transversely with respect to the stress axis serve as sites for the initiation of debonding followed by matrix cracking and fiber breakage or delamination [5]. This sequence is not universal and it may vary widely depending on many factors. In fact, the fatigue behavior depends on the type of matrix, the fibers, stacking sequence, the length of fibers, fiber content, void content, the method of processing, the R value and on other factors. Adding to the complexity is the fact that it may be difficult even to define the fracture criteria. Fracture in composites does

not always mean complete separation of the specimen and in some cases physical integrity is maintained long after the load carrying capacity of a specimen has been exhausted. Usually failure is defined either when a surface crack penetrates across the whole width or when the initial stiffness is reduced by 20-40% [6].

There is controversy about the effect of rubber toughening of the matrix on the fatigue behavior of composites, but usually the fatigue behavior degrades with flexibilizing the matrix. Although it may be expected that an increase in fracture toughness from the use of rubber particles leads to a decrease in fatigue degradation rate, this is not what is always observed. Murakami *et al* [7] studied the tensile fatigue behavior of neat resins blended with NBR. He found the fatigue life as measured in the S-N curve decreased with a increase in rubber content, the slope of S-N curve improved somewhat. Konur *et al* [11] reported improved fatigue life in unidirectional composites when rubber was used to toughen the epoxy matrix. Curtis [10] observed that in unidirectional composites, toughened epoxies improved the static strength but the fatigue behavior was degraded, with steeper Strain-N curves. Mandell *et al* [12] studied the tensile fatigue behavior of unimpregnated glass strands and of their composites with polyester, epoxy and rubber modified epoxy, and found that the S-N slope for all of the composites and for the unimpregnated strands were about the same: approximately equal to 10. He also plotted the S-N curve slopes for a variety of materials and showed they were approximately equal to 10. In relation to increasing the flexibility of the matrix, Hertzberg [8] cited two references for glass-fabric-reinforced laminates; in one, toughening the epoxy led to better fatigue life, while in the other, flexibilizing a polyester resin neither

improved the fatigue life nor the fracture toughness. Joneja [9] studied the effect of adding flexible polyester to standard polyester resin on the fatigue behavior of unidirectional composites. He found the fatigue life and the slope of the S-N curve decreased with a high quantity of flexible polyester present.

With unidirectional composites loaded parallel to the fibers in tensile fatigue, high modulus fiber composites are much more fatigue resistant than low modulus ones: in the S-N curves, the slope of glass fiber composites (low modulus) is much steeper than that for carbon fiber composites (high modulus). However when a composite made of off-axis plies is subjected to tensile fatigue or when a composite with any stacking sequence is subjected to flexural fatigue (R=-1), all the composites behave in approximately the same way: the glass composites have the same slope as carbon composites. Studying the environmental fatigue behavior, Jones *et al* [13] pointed out that in tensile fatigue of unidirectional composites the behavior improved with increasing modulus of the composite [Fig. 1], but he also observed that for $\pm 45^0$ laminates, both glass fiber and carbon fiber composites had exactly the same fatigue life and slope. According to Mandell [14], with unidirectional composites loaded along the fiber direction, high modulus materials are more fatigue resistant than low modulus ones, but with off-axis plies or when loading in compression, the modulus does not affect the fatigue behavior, which approximately follows the glass composite trend line. Rotem [14] studied the fatigue behavior of graphite/epoxy laminate for different R values (R=0.1, 10 and -1) and for two lay-ups ($0^0/90^0$ and $\pm 45^0$). He found that for R=0.1 the S-N slopes for $\pm 45^0$ and $0^0/90^0$ laminates are 9.45% and 1.11% respectively. For R=10 the slopes for $\pm 45^0$ and $0^0/90^0$ laminates are 5.5% and 7.11% respectively. Interestingly however, for R=-1, the slope for $\pm 45^0$ and

$0^0/90^0$ laminates are 11.22% and 10.02% respectively, which are similar. Finally, Osborn [3] tested a variety of specimens with stacking sequences of $\pm 25^0$, $\pm 20^0$, $\pm 10^0$ and woven cloth, for a variety of fiber types including S glass, E glass and Graphite, under exactly our testing conditions. He found all these various specimens followed approximately the same S-N slope [Fig. 2]; since the only common factor was the matrix, he concluded that the fatigue behavior was matrix dependent.

To represent the complex nature of the fatigue of composites, Talrega [5] developed a critical strain model based on Strain-N curves. It characterizes fatigue strain ranges according to different damage mechanisms. He contrasts the high strain range in which fiber breakage and interfacial debonding are predominant, to the low strain range where matrix cracking and interfacial shear failures control [Fig 3]. His model is a conceptual framework for comparing fatigue behavior of composites with different constituents and for characterizing the damage mechanisms [11]. In our study the tests emphasize Stress-N curves instead of Strain-N curves, but the Stress-N curves can be transformed by using the initial modulus of the samples.

We tested chopped strand glass mat , glass fabric and carbon fabric composites, all made with MNS (rubber modified polyester). Glass and carbon fabric composites made with unmodified polyester also were tested for comparison. Different fatigue curves are characterized and compared by the value of b, where b is the slope of S-Log N curve normalized by the single cycle strength of the composite:

$$b = \frac{S/S_o - 1}{\log N}$$

Here N is the number of cycles required to break the specimen at stress S, and S_0 is the one cycle strength of the material. The higher the value of b, the more rapid is the fatigue degradation. Since the S-N curves are not linear (indicating a change in failure mechanism), they were also characterized and compared by the value of m, where 1/m represents the slope of the linear Log-Log plot and is defined by the following equation :

$$\frac{S}{S_0} = N^{-1/m}$$

The smaller the value of m, the more rapid is the fatigue degradation.

1.2 Creep :-

Increasingly, composite materials are used in applications, where creep is important: the increase of deformation with time under constant load. The magnitude of creep deformation depends on laminate lay-up, stress level, humidity, temperature and the previous thermal history [27]. Most creep studies are performed in tension or shear, while the flexural mode, which is important in many cases, has received little attention. In this study the creep tests were performed in bending.

Unidirectional composites tested axially in tensile creep show less time dependent response, because the properties are fiber dominated. When the matrix properties control, as in a crossply composite in tension or any composite in compression, significant viscoelasticity becomes evident [16]. Composites both with short and long fibers exhibit non-linear visco-elasticity [17]. The common ways to describe this non-linear creep are (i) the modified Boltzmann superposition principle, (ii) the multiple integral representation

(iii) the Findlay procedure and (iv) Schapery's constitutive equation [18]. Of these, the Schapery constitutive equation is most used for composites, and it is the one used in our study.

Chapter : 2

Materials

Three different reinforcements, chopped strand mat, glass fabric and carbon fabric were used with unmodified polyester and with MNS of varying rubber contents to form the composites. The rubber contents used were 0%, 7.5%, 12.5% and 17.5% of the total resin weight.

Chopped strand mat has randomly oriented two inch long glass fibers, of 15 micron diameter. The glass fabric was 181 style with a satin weave [Boatex], while the carbon fabric was G117 style with a satin weave [Textile Technologies]. The carbon fiber is a Hercules AS4G6K with a epoxy compatible sizing, while the glass fiber has a Volan coating. The reasons for using the woven fabric were easier handling and the more isotropic in plane properties, compared to uni-directional reinforcement. The MNS resin was composed of unsaturated polyester (MR13006 from Aristech Corporation), liquid epoxy (Epon 828 from Shell Chemical), styrene monomer (Aldrich Chemical) and an amine terminated butadiene acrylonitrile rubber (ATBN 1300x16 from B. F. Goodrich Co.). Catalysts were Ancamine, a tertiary amine salt and t-butyl peroxybenzoate. A description of the composites is given in Table. 1.

All the composites are made by the wet, hand lay-up technique. In the case of glass composites the stacking sequence was the aluminum mold plate covered with non-porous Teflon sheet, the laminate, a peel ply, a aluminum press plate, a breather fabric and the Mylar vacuum bag. Alternate layers of glass mat or glass fabric and resin were applied, and the resin was worked into

the fibers with a corrugated roller. The roller reduces voids between the laminae. Eight layers of glass mat and thirteen layers of glass fabric were used. When all the layers had been applied, the lay-up was sealed in the vacuum bag by tape and degassed under a vacuum of 17-18 inches of Hg for about five minutes. The vacuum removed the entrapped air and voids; the lay-up was then cured at 100 ^{o}C for 10 hrs. under atmospheric pressure. The fabrication of the carbon composites was the same with a few exceptions. With only one vacuum bag the laminate was full of voids, so two bags were used to simulate the autoclave process. To the inner bag a vacuum of 18 inches of Hg was applied for five minutes to remove the entrapped air and then to the outer bag a vacuum of 20-25 in of Hg was applied for 10 minutes. This reduced the void content. Another problem with the carbon composite was poor surface finish, so a new stacking sequence was used. This was mold plate, non-porous Teflon sheet, laminate, porous Teflon sheet, bleeder ply, non-porous Teflon sheet, press plate, breather ply, first vacuum bag, breather ply and the second vacuum bag. Since all the composites were cured at atmospheric pressure the void content was expected to be higher than for autoclave or press cures.

Chapter : 3

Specimens

The specimen were 5.5 in long by 1 in wide and the support span was 4 in. The thickness ranged from 0.11 to 0.18 in. The size of the specimen was chosen according to ASTM standard D790 [19], so that it can be considered as a beam. According to the standard the span should be at least 16 times the thickness of the specimen; a higher ratio reduces the shear stress in the center plane of the beam. The ratio in our specimens varied from 22 to 32. According to the standard, the width should not exceed 1/4 of the span and in our case it was is exactly 1/4 of the span. Overhang should be sufficient to prevent the specimen from slipping through the supports, at least 10% of the support span. In our case the overhang was around 19%. Other considerations in choosing the specimen size involved effective handling in the testing fixture and convenience of machining.

The specimens were cut from the plate with a diamond saw, which was water cooled. The machined surfaces of the cut specimens were then wet sanded, ground and dried in an oven. The specimens were stored in a desiccator until testing to reduce moisture absorption effects. In the fabric composites, we tried to keep a proper alignment of the weave along the specimen length, but some distortion occurred in fabrication and some misalignment took place in the cutting process.

The surface of the glass composites was very rough so they were wet ground and then a thin layer of resin was applied to cover the fibers so

exposed, and then cured. This surface finishing did not appear to affect the fatigue behavior but it was not necessary with the carbon composites.

Chapter : 4

Stress Analysis

4.1 Stresses in the specimen

The specimen is considered to be a homogeneous, elastic beam loaded in three point bending [Fig. 4]. The shear stresses in the center of the specimen are neglected. The maximum stress in the outer fibers, as defined by ASTM D 790 is given by:

$$\sigma = \frac{3PL}{2bd^2}$$

Where :

σ = Stress in the outer fibers at mid span, (Pa)

P = Load at a given point on the load-deflection curve,

L = Support span, (m)

b = Width of beam tested, (m)

d = depth of beam tested, (m)

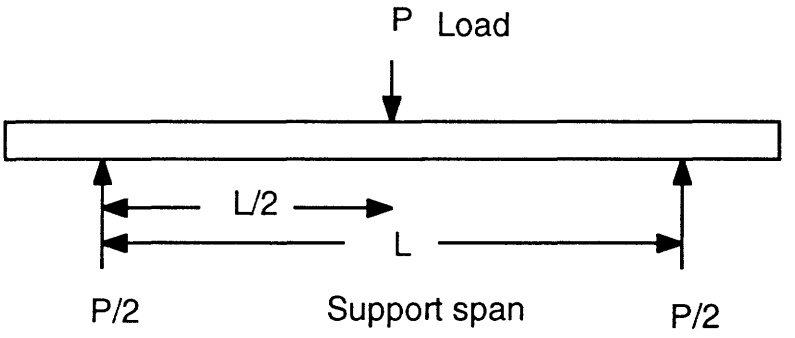

Fig : 4 : Loading diagram

The bending modulus of the specimen is calculated as :

$$E = \frac{PL^3}{4\delta d^3 b}$$

Where δ is the deflection in the center of the specimen. The maximum strain in the outer fibers also occurs at mid span, and is :

$$\varepsilon = \frac{\sigma}{E}$$

4.2 Loading rate

Force control, constant amplitude, sine wave loading was used in testing the specimens. A constant stress was applied to the specimen and the stiffness degraded due to fatigue. Most polymer composites behave in a visco-elastic manner: their response to a given deformation depends on the loading rate. Thus if all the specimen are tested at the same frequency the specimens tested at high stress will experience a higher loading rate than the specimen loaded to lower stress. This will cause scatter in the results so to reduce this, all the specimens were tested at the same loading rate but somewhat different frequencies. The frequency for a particular stress level can be calculated from the expression for simple harmonic motion. The displacement, S, of a particle rotating at angular speed ω with amplitude A is given as :

$$S = A \text{ Sin } \omega t$$

The velocity V can be calculated as :

$$V = A\omega \text{ Cos } \omega t$$

Velocity will be maximum at t=0 and since $\omega = 2\pi f$:

$$V = 2\pi f A$$

The amplitude A of the sinusoidal loading wave represents stress level, f is the frequency and V the loading rate. So the frequency can be expressed as :

$$f = \frac{V}{2\pi\sigma}$$

A constant loading rate is also advantageous because at low stress levels the test frequency is higher so the time duration of the test is reduced. The loading rate was chosen as 3378 MPa/sec so our results could be compared to those of Osborn [3] who used the same rate.

4.3 Failure Definition

As mentioned earlier it can be difficult to locate the failure point in composites since the material fails progressively as it softens under fatigue. According to ASTM D 671 [20] fatigue failure is said to occur when the modulus decreases to 70% of its original value. In the case of the chopped strand mat composites we observed that cracks on the surface appeared to penetrate through the entire thickness when the modulus dropped to 60% of its original value, so we took this condition to define failure: a 40% decrease in the modulus of the sample.

Chapter : 5

Fatigue Tests

5.1 Test Equipment

The fatigue tests were performed on a servo-controlled Instron 8500 machine using a special fixture. The machine has automatic load control to cope with substantial changes in the specimen stiffness. The deflection is obtained directly from the machine, to calculate modulus and strain. All the tests are performed in a uncontrolled laboratory atmosphere, at approximately 20 ^{o}C. A fan was used to avoid any heating of the specimen from hysterises.

The fixture was specially designed and fabricated for use in reversed flexural fatigue [Fig. 5]. The frame is made of aluminum but the specimen support rollers are hardened steel, in bearings. Each support point has a pair of rollers, one of which can move to accommodate specimens of different thickness. Nylon bushings on the rollers prevent any sideways drift of the specimen, while nylon bumper plates keep it from displacing along its length. The rollers are 17.46 mm in diameter.

5.2 Static Tests

Static three point bend tests were performed at two different loading rates on Instron 4505 and Instron 8500 machines. First they were done at a cross-head rate of 5.08 mm/min, to determine the yield strength, yield strain, and modulus of all the composites, as presented in Table 2 (a typical stress-

strain curve is shown in Fig. 6). Three specimens were tested for each material and fracture was due to fiber breakage. The results show that modulus and strength decrease with increasing rubber content, except for the carbon composites where the absence of this trend may be due to varying quality and fiber content of the different laminates [Fig. 7]. In general the yield strains and stresses of the MNS composites are greater than with the unmodified polyester, but the yield strain does not vary much with increasing rubber content [Fig. 8 & 9].

Because the fatigue tests were done at a rate of 3378 MPa/sec, the static strength parameters measured at the same rate are shown in Table 3. A typical load-stroke curve is shown in Fig. 10. Comparing Table 2 and Table 3 it is clear that both modulus and strength increase appreciably with rate. With chopped strand mat the average increase in strength is around 110%, with the glass fabric it is 80% and with the carbon fabric it is 50%. Comparing Fig. 6 and Fig. 10 it can be observed that with the higher loading rate the load-deflection curve is straight and there are no knees, as observed at the low rate because of ply breakage.

5.3 Fatigue Tests

5.3.1 Chopped Strand Mat Composites

Fatigue tests were done with unmodified polyester and four different rubber contents: 0%, 7.5%, 12.5% and 17.5%. At each stress level three specimens of the 7.5% rubber content were tested to observe the scatter. As seen in Figure13, the scatter was modest, suggesting that both the procedure and the specimens were consistent. The S-N curves are presented in Figures 11-15 and the ε-N curves, based on the initial modulus, are shown in Figures 16-20. As shown in Table 4 the loss of strength per decade of cycles (parameter b) on a linear scale, for the laminates with unmodified polyester, 0%, 7.5%, 12.5% and 17.5% rubber is 14.74, 15.36, 13.27%, 13.58% and 13.67% respectively. There is a change in slope at 10^4 cycles. Table 3 show the b value before and after 10^4 cycles. The value of m (the inverse of the drop in strength per decade of cycles on a Log-Log plot) for the laminates with unmodified polyester, 0%, 7.5%, 12.5% and 17.5% rubber is 7.86, 7.44, 6.96, 7.43 and 7.59 respectively. The comparison of the value of m for laminate with 7.5% rubber, with the laminates with unmodified polyester and 0% rubber show that the degradation rate increases with the addition of rubber (the smaller the value of m the more rapid is the degradation). But as we further increase the rubber content the degradation rate decreases. The overall decrease and increase in degradation rate is small. From the values of b it is clear that before 10^4 cycles, the degradation rate increases with increasing rubber content (the larger the value of b the more rapid is the degradation), which may reflect the lower static strength trend with increasing rubber content. The decrease in slope after 10^4 cycles is large and this may signal the approaching endurance limit.

In Fig. 21 the S-N curves with different rubber contents are compared and in Fig. 22 the normalized curves are presented. The ε-N curves are shown in Fig. 23. It can be seen that the rubber level has little effect on the fatigue strength behavior but the strain-number of cycles performance is improved by the rubber.

Specimen	$b = \frac{S/S_o - 1}{\log N}$			$m = -\frac{Log(N)}{Log(S/S_0)}$
	for whole life, %	upto 10^4 cycles, %	after 10^4 cycles, %	for whole life
Chopped Strand mat				
Unmodified polyester	14.74	17.22	6.25	7.86
MNS 0% Rubber	15.36	18.83	5.93	7.44
MNS 7.5% Rubber	13.27	19.46	4.97	6.96
MNS 12.5% Rubber	13.58	18.89	5.14	7.43
MNS 17.5% Rubber	13.67	21.39	4.31	7.59

Table : 4 :- Value of fatigue characterizing parameters, b and m for chopped strand mat composites.

As seen in Figures 60-62 the damage zone can be observed by whitening of the specimens and this increases, reaches a maximum, and then decreases as the cycles increase. The maximum occurs at around 10^4 cycles and this suggests that the change in slope there is due to a change in damage mechanism. Microgrpahs taken of the side (free edge) of the fracture surfaces are shown in Fig. 66, Fig. 67 and Fig. 68 for laminates made of chopped strand mat with 7.5% ,12.5% and 17.5% rubber. The fracture surface was polished in the longitudinal direction, then coated with a thin layer of gold and examined in the S.E.M. (Cambridge Instruments) using back scattered electrons. The two

micrograph for each laminate show the top and bottom edges. The primary mode of failure is similar in all three cases: the crack starts at the surface due to interfacial debonding or matrix cracking in the resin rich area, then propagates inward by matrix cracking and some fiber breakage. Sometimes the crack moves longitudinally, because of the toughness of the matrix, until it finds a weaker location or until it reaches the end of the strand.

Since interfacial debonding is the dominant mode of failure, we have modified the Talrega diagram [Fig. 3] as shown in Figures 31-35. The top horizontal band determined from the static strain to failure represents fiber breakage, and the sloped data refers to transverse fiber debonding and matrix damage. The lower horizontal band is the limiting strain for the onset of transverse fiber debonding, $\varepsilon_{d.b.}$. This was taken to be 0.12%, as obtained by plotting the numbers of cycles for the onset of debonding against the maximum cyclic strain and recommended by Talrega for short fiber and cross laminate composites. According to this interpretation, the ε-N curves for all the laminates tested show that failures are based on matrix cracking and transverse fiber debonding; this is consistent with the fracture mechanisms evident in the micrographs.

The increase in deflection with cycles was observed for a few specimens as shown in Fig. 24 (In all of these cases the failure was defined as a 40% decrease in modulus). The curves can be divided into three stages. In the first (I) the modulus drops rapidly, then reaches a steady state (II). In the final stage, (III), near the end of fatigue life, again the modulus decreases rapidly.

In a few specimens, the temperature increase was monitored [Fig. 25]; increases of only a few degrees centigrades were found and these were judged to be inconsequential.

5.3.2 Glass Fabric Composites

Fatigue tests were performed on laminates with unmodified polyester, and with 0%, 7.5%, 12.5% and 17.5% rubber contents. Two specimen of the 7.5% rubber laminate were tested on each stress level to confirm that the scatter was not large. The S-N curves are shown in Figures 26-30 and ε-N curves, based on the initial modulus, are shown in Figures 31-35. The value of b [Table 5] for laminates with unmodified polyester, 0%, 7.5%, 12.5% and 17.5% rubber is 13.49%, 13.21%, 13.94%, 12.99% and 13.59% respectively. Here the change in slope occurs around 10^5 cycles instead at 10^4 cycles as was the case with the chopped strand mat. Table 5 show the b value before and after 10^5 cycles. The b values for the different composites are nearly the same; adding 7.5% rubber increased it somewhat, but with 12.5% rubber it decreased. One interesting point to note is that the unmodified polyester composite, after 10^5 cycles, degrades at a faster rate. than the MNS composites. This means that the latter have better long term behavior. The decrease in slope for the glass cloth composites after 10^5 cycles is not as large as for the chopped strand composites which means that the endurance limit is farther away.

The value of m for laminates made with unmodified polyester, with 0%, 7.5%, 12.5% and 17.5% rubber is 9.03, 8.77, 8.09, 9.14 and 9.55 respectively, which shows the same trends as the value of b. The S-N curves based on

stress are compared in Fig. 36 and the normalized curves are shown in Fig. 37. The MNS composites perform better at low cycles but the curves converge at high cycles. The difference was much less in the normalized curves. The ε-N curves for the different composites are compared in Fig. 38 where the advantage of the MNS system is clear. This correlates with the yield strains of these laminates [Table. 2].

Specimen	$b = \frac{S/S_o - 1}{\log N}$			$m = -\frac{Log(N)}{Log(S/S_0)}$
	for whole life, %	upto 10^5 cycles, %	after 10^5 cycles, %	for whole life
Glass Fabric				
Unmodified Polyester	13.49	15.67	7.61	9.03
MNS 0% Rubber	13.21	15.23	6.29	8.77
MNS 7.5% Rubber	13.94	15.01	7.13	8.09
MNS 12.5% Rubber	12.99	14.65	6.69	9.14
MNS 17.5% Rubber	13.59	14.93	3.20	9.55

Table : 5 :- Value of fatigue characterizing parameters, b and m for glass fabric composites.

All of the glass composites are compared in Fig. 39 and the normalized S-N curves are shown in Fig. 40. The fabric performs better than the chopped mat, but the differences become smaller in the normalized data. In the latter, at low cycles the fabric is superior, but the two types converge at high cycles. Since we did not test glass fabric/epoxy composites in our study, data from the literature were used for comparison. Osborn [3] performed such tests under exactly the same condition and Fig. 41 shows that the MNS curves are above

the epoxy and the unmodified polyester curves. On a normalized basis [Fig. 42], all the composites show similar behavior.

The size of the damage zones, revealed by whitening of the specimens [Fig. 63-65] varies with the number of cycles: at first it increases, reaches a maximum and then decreases as the cycles increase. This is most obvious in the 7.5% rubber composites. The maximum zone occurs around 10^5 cycles, where the change in slope of the S-N curve is seen. Micrographs taken of the sides of the fracture surfaces are shown in Fig. 69, Fig. 70 and Fig. 71 (The two micrographs for each specimen show the top and bottom surface of the edge). They show the primary mode of failure in the MNS composites is different from the unmodified polyester ones: interfacial debonding and matrix cracking, while in the case of unmodified polyester the fracture is delamination in the center caused by the interlaminar shear stress. In the MNS composites, the crack appears to start at the surface by interfacial debonding of transversely oriented fibers or by breakage of cross ply strands. It then extends inward due to matrix cracking, breaking cross ply strands in the process. When the crack encounters longitudinal ply strands, either it breaks them or passes around them. In the unmodified polyester laminate while there is some damage on both the surfaces the primary cause of failure is the delamination in the center.

The Talrega concept has been applied to the glass fabric results, as shown in Figures 31-35. The data suggest that the failures are due to transverse fiber debonding and matrix cracking (with delamination in case of the pure polyester): this is consistent with the fracture mechanisms evident in the micrographs.

5.3.3 Carbon Fabric Composites

Fatigue tests were performed on laminates based on unmodified polyester and 0%, 7.5%, 12.5% and 17.5% rubber. The S-N curves for each are shown in Fig. 43-47 and ε-N curves are shown in Fig. 48-52. The value of b [Table 6] for laminates made of unmodified polyester and with 0%, 7.5%, 12.5% and 17.5% rubber is 12.23%, 12.22%, 11.35%, 12.38% and 9.18% respectively. At 10^5 cycles there is change in slope, but with very few points beyond 10^5, only the b up to 10^5 cycles can be reported accurately, as shown in Table 6. The values of b show that rubber modified composites degrade at a slower rate as compared to unmodified polyester and 0% rubber composites. Generally the performance improves with increasing rubber content, except in the case of the 12.5% material which has a lower yield strain [Table 3]. The values of m for unmodified polyester, and with 0%, 7.5%, 12.5% and 17.5% rubber are 11.37, 11.07, 12.69, 11.66 and 17.79, respectively, which shows explicitly that the fatigue performance improves with increasing rubber content. The S-N curves for different composites are presented in Fig. 53 and normalized in Fig. 54 (The low strength of the 17.5% rubber laminate may be due to a higher matrix content or poor quality of manufacture). These normalized curves for the carbon composites show a behavior different from glass composites; in the latter, all the curves were nearly the same (see Fig. 37). The ε-N curves are presented in Fig. 55. The curve for the 7.5% rubber material is best and if the yield strains are considered (Table 2), it is seen the performance increases directly with increasing yield strain.

Specimen	$b = \frac{S/S_o - 1}{\log N}$			$m = -\frac{Log(N)}{Log(S/S_0)}$
	for whole life, %	upto 10^5 cycles, %	after 10^5 cycles, %	for whole life
Carbon Fabric				
Unmodified Polyester	12.23	15.00		11.37
MNS 0% Rubber	12.22	12.908		11.07
MNS 7.5% Rubber	11.35	12.24		12.69
MNS 12.5% Rubber	12.38	13.45		11.66
MNS 17.5% Rubber	9.18	9.97		17.79

Table : 6 :- Value of fatigue characterizing parameters, b and m for carbon fabric composites.

The carbon and glass fabric composites are compared in Fig. 56 and Fig. 57. With respect to stress, the trend is as follows: carbon with 7.5% rubber is the top, followed by carbon with 12.5% rubber, carbon with 0% rubber, carbon with 17.5% rubber, carbon with unmodified polyester, glass with 7.5% rubber, glass with 12.5% rubber, glass with 0% rubber, glass with unmodified polyester and glass with 17.5% rubber. For the normalized data the following trend is observed: carbon with 17.5% rubber, carbon with 7.5% rubber, carbon with 12.5% rubber, carbon with 0% rubber, carbon with unmodified polyester and then all the rest. In Fig. 58, a plain weave carbon with epoxy composite (reported by Chou *et al* [21]) tested in cantilever fashion performs better than the other composites, but it appears to degrade at a much higher rate: its slope is steeper.

Micrographs of the side of the fracture surface are shown for laminates of carbon cloth and unmodified polyester [Fig. 72], with 7.5% rubber [Fig. 73],

12.5% rubber [Fig. 74] and 17.5% rubber [Fig. 75]. The two micrographs for each material show the top and bottom surfaces at the edge. The primary mode of failure combines interfacial debonding and matrix cracking and there is much more debonding in the carbon composites than in the glass ones. The carbon fibers have an epoxy compatible sizing so the fiber may not adhere well due to the large amount of polyester present in the MNS. Apparently the damage starts at the surface due to interfacial debonding, then propagates inward by matrix cracking, interfacial debonding and infrequent fiber breakage.

Talrega diagrams are presented in Figures 48-52, and the curves show that failure is due to interfacial debonding and matrix cracking, which is consistent with the micrograph study.

The decrease in modulus as represented by an increase in deflection was observed for a few specimens, as shown in Fig. 59. One sample was tested until it reached the maximum deflection the test fixture could handle, while the other two were taken to a 40% decrease in modulus. All the curves are similar to those observed for chopped strand mat: they can be divided in three main stages. In the first (I) the modulus drops rapidly and reaches a steady state second stage (II). Finally, near the end of the fatigue life the modulus deteriorates rapidly (III).

5.4 Discussion of results

5.4.1 S-N behavior

Improved fatigue performance in composites with higher modulus fibers has been widely observed [11,14]. Since the modulus of the MNS composites decrease with increasing rubber content [Table 2], it could be expected that the fatigue performance might degrade. This was not observed. According to Mandell [14], in short fiber glass composites, if the matrix is fatigue resistant, it is possible that the behavior may be fiber dominated. This was observed both for the chopped strand mat and the glass fabric/MNS composites. When the normalized curves for different glass mat composites are compared [Fig. 15], all superpose. Similarly when the normalized curves for the glass fabric composites are compared [Fig. 26], all of them tend to follow the same line. Since the only common factor in these cases is the glass fibers, it can be concluded that the fatigue behavior was fiber dominated and was limited by the performance of the fibers. Matrix variations did not change this.

Carbon fibers have excellent fatigue properties, in contrast to glass [11]. Because of this, the fatigue behavior of carbon composites will be matrix dominated. Figure 41 illustrates this: the tougher the matrix the better the fatigue resistance . As the strain to failure in a static test increases, the fatigue resistance improves.

Fig. 57 presents the normalized data for all the fabric based composites tested. The carbon fabric composites have improved fatigue behavior

compared to glass fabric composites. This is a marked difference from the observation made by Osborn [Fig. 3], in which all the composites had the same normalized S-N curve. Similarly according to Mandell [14], with off axis plies or in compression loading the high modulus carbon composites tended to follow the glass trend line. In our study, because of yarn crossovers, weave distortions and the presence of the compression component, the behavior was expected to be similar to Osborn's: i.e. carbon composites performing the same way as glass. The observation that the carbon composites performed better than glass, however, is significant. In unidirectional composites, carbon performs better than glass, but both perform similarly in off-axis laminates and in compression loading. The off-axis plies fail at low strains and develop cracks before the plies in the dominant stress direction fail. With the MNS the strain to failure increases, so the fatigue resistance of the carbon fibers operates and gives a different slope from the glass composites. The fact that an increasing strain to failure improves the fatigue behavior has been observed previously. Hayashi *et al* [22] found with aramid fiber/epoxy composites (ε_f=1.5%) the rate of decrease of the maximum bending moment was slower than that for carbon fiber/epoxy composites (ε_f=0.8%). Similarly Newaz [23] found that a glass/epoxy composite had better fatigue performance compared to a glass/vinyl ester one, especially at high cycles because of the higher strain to failure of the glass/epoxy.

Because of the change in slope of the S-N curves it was difficult to fit a straight line ($S/S_0 = 1 - b \log N$), but when the data were plotted on a Log S-Log N basis a linear relationship is obtained: ($S/S_0 = N^{-1/m}$). Hence m is a fatigue parameter and as its value increases it denotes improved fatigue performance. For both chopped strand mat and glass fabric composites the

fatigue improvement required 12.5% rubber, and the 7.5% rubber did not show it, when we compare the performance with unmodified polyester. Since the glass fibers are Volan coated, this effect may be present because of better adhesion of glass fibers with polyester, as compared to the adhesion with MNS. With further increase in rubber content (17.5%) the fatgiue performance improves in both types of glass composites. With the carbon fabric, the m value showed the fatigue improvement with increasing rubber content. If Strain-N curves are examined (Figs. 23, 38 and 55) are examined, it will be seen that a consistent behavior prevails: the higher the strain to failure in the static test at 3378 MPa/sec, the better is the fatigue resistance. Thus the use of the rubber modification to toughen the matrix and to increase its ability to plastically deform, also provides better fatigue resistance in the fiber reinforced composites.

5.4.2 Damage development

Reversed flexural fatigue represents the most severe loading condition, because of the compression component involved. In compression, local resin and interfacial damage lead to fiber instability which is more severe than the fiber isolation mode which occurs in tensile loading [11]. The damage development as observed from the micrographs for chopped glass mat [Fig. 66-68], glass fabric [Fig. 69-71] and carbon fabric [Fig. 72-75] is similar, except for the glass fabric/unmodified polyester composite. Usually the damage starts on the surface with fiber/resin debonding of the transverse fibers. With increasing number of cycles, matrix cracking develops and some fiber breakage occurs. As the cycling continues, interfacial debonding and matrix cracking develop in strands oriented in the stress direction and the damage

moves toward the center of the thickness. Crack propagation through a fiber causing its breakage seems to follow the explanation presented by Joneja [9]: as interfacial debonding propagates along the fiber in the matrix which has low strength and modulus but high ductility, a high stress gradient develops at the microcrack tip and this searches out a weak segment of the fiber. Such explains the poor fatigue performance of some of the flexible matrix composites previously cited in section 1.1. This poor performance may be due to the large modulus drop which accompanies the increased flexibility for these polymers; in the MNS resins the modulus does not decrease so much and it causes the fatigue performance to improve instead of degrading.

The improvement in fatigue performance of the MNS composites is due to the delay of interfacial debonding and matrix cracking in high cycle fatigue. As observed by Newaz [23] in low cycle fatigue, damage is in the form of matrix cracking, interfacial debonding and fiber breakage, while in high cycle fatigue the damage is predominately matrix cracking and interfacial debonding. Since fiber breakage dominates low cycle fatigue, the normalized S-N curves overlap in the low cycle regime, but the difference in performance become more apparent at high cycles. This is most apparent in the case of carbon composites [Fig. 54]. The change of damage mechanism with increasing number of cycles explains the change in the slope of the S-N curve and the maxima of the damage zone as observed by whitening of the glass composites [Fig. 60-65]. Since the whitening is due to matrix cracking, the maximum in the damage zone can be explained as follows: at high stresses and in static tests the damage is mainly in the form of fiber breakage so the damage zone is small. As the stress reduces, matrix cracking increases causing the damage zone to reach its maximum value. With a further reduction in

stress, interfacial debonding becomes more pronounced and the damage zone decreases.

With carbon fiber composites, as observed by SEM micrographs Fig. 72-75, the interfacial debonding is much more pronounced, because the carbon fibers have an epoxy compatible sizing, and therefore do not adhere as well to the MNS because of the large amount of polyester present. Since the fatigue performance improves with adhesion [24], the fact that the carbon composites perform much better than glass composites with a less steep slope [Fig. 57] is quite remarkable.

5.4.3 Loss of Stiffness

In fiber reinforced composites the failure is progressive, resulting from a gradual accumulation of various types of damage. The damage growth is accompanied by a loss in stiffness: deflection increases when tested at a constant stress level. These effects are shown in Fig 24 and Fig 59, (which also note the percent of the ultimate tensile strength at which the tests were performed). The stiffness loss is divided into three stages. In the first there is a rapid decrease caused by matrix and interface damage, which reaches a saturation level at the end of the stage. In the second, the modulus remains nearly unchanged but the hysterises loss rapidly increases [8]. In this stage, cracks interact and start to spread to transverse plies. In the final stage the damage in the longitudinal and transverse directions coalesce and there is some fiber breakage. This final stage is characterized by a very high damage growth rate, such that a 40% loss in stiffness and complete fracture occurs at approximately the same number of cycles [Fig. 59].

Chapter : 6

Creep Tests

6.1 Test Results

When a continuous fiber reinforced composite is loaded along the fiber direction the properties are nearly time independent, but when the same composite is loaded in compression or in flexure, and in the case of off-axis laminates or discontinuous fiber composites, the properties usually are time dependent. Since our composites have time dependent or visco-elastic properties it is important to characterize their long term performance, so that structural components could be designed with confidence. Therefore flexural creep tests are performed on chopped strand mat with 7.5%, 12.5% & 17.5% rubber and on glass fabric with 7.5% & 12.5% rubber composites. The tests are performed at EMPA (Swiss Federal Laboratories for Materials Testing and Research), in Zurich, Switzerland [26], using ASTM 2990-90 standard [25] with three point flexural loading. Three specimens were tested at a constant stress level of 16.7% of the ultimate flexural strength (UFS) and one sample each was tested at 30%, 45% and 60% of the flexural strength. The total time for which the specimens were tested was 120 days (2188 hrs). All the tests were carried out in a laboratory atmosphere at 23 ^{o}C and 50% relative humidity (The effect of physical aging has not been investigated in this study). Only two failures were observed, one in chopped strand mat with 7.5% rubber (1200 hours) and the other in chopped strand mat with 17.5% rubber (400 hours), both at a stress level of 60% of ultimate.

The mid span deflection was measured as a function of time. The deflection-time curves for the chopped strand mat are shown in Fig. 76-78 and for the glass fabric are shown in Fig. 79-80. The creep modulus as a function of time is shown in Fig. 81-85.

The creep behavior of the composites at different stress levels is compared on the basis of their RCD (relative creep deflection) value, where RCD is defined as:

$$RCD\% = \frac{\delta_{tot} - \delta o}{\delta_0} \times 100$$

Where δ_{tot} is the deflection at the total time t=2188 hrs and δo is the initial deflection. The RCD values are given in Table. 8.

6.2 Creep Characterization

Since the service life of composite applications runs to years, it is impractical (and expensive) to do testing over that period [27]. Therefore some form of characterization is required to predict the long term properties of the material. Since the design usually is based on stiffness, the technique should be able to predict the long term modulus of the specimen. A visco-elastic material can be characterized in two ways, linear and non-linear, depending upon which dominates. In linear characterization, the constitutive equations are functions of time only, while in the case of non-linear characterization the constitutive equations are functions of time and stress. In linear behavior, the isochronous curves (stress-strain curves at a particular time) are straight lines. The isochronous curves for different times (t=1 min., 28 days and 120

days) are shown for chopped strand mat (Fig. 86-88) and for glass fabric (Fig. 89-90). These show that chopped strand mat composites behave in a non-linear way at all three times, especially at high stresses; the non-linearity increases with increasing rubber content and time. The woven fabric composites behave in a linear way, at low stresses and times (It is common to observe linear visco-elastic behavior in short term tests, but the behavior may become non-linear for longer times at the same stress levels [18]. The larger the deformation or stress to which a visco-elastic material is subjected, the larger is the non-linearity [28]). As is clear from the isochronous curves, and from other considerations, the non-linear characterization is more appropriate for the creep of the MNS composites.

Several different techniques are used for non-linear creep characterization: the Multiple integral equation-a rational mechanics approach; the Findlay procedure-a semi-empirical technique; the Schapery equation-an irreversible thermodynamics approach; and the modified superposition principle [28]. The Multiple integral representation is impractical if strong non-linearities are present, while the modified superposition principle and the Findlay procedure are completely empirical. On the other hand the Schapery constitutive equation is based on principles of thermodynamics and is most used for composites so this is the approach taken in our study. A shortcoming is that it does not provide any physical insight into the behavior observed. Its general form is:

$$\varepsilon(t) = g_0 A_0 \sigma(t) + g_1 \int_0^t \Delta A(\Psi - \Psi') \frac{dg_2[\sigma(t)]}{d\tau} d\tau \qquad (1)$$

where $\Psi = \psi(t) = \int_0^t \frac{d\tau}{a\sigma}$

and $$\psi' = \psi(\tau) = \int_0^{\tau} \frac{d\tau}{a\sigma}$$

where A_0 is the immediate elastic response while ΔA is the delayed response or creep compliance and g_0, g_1, g_2 and $a\sigma$ are functions of stress. These stress dependent properties have specific thermodynamic significance. Changes in g_0, g_1 and g_2 reflect third and higher order dependence of Gibb's free energy on the applied stress and $a\sigma$ arises from similar high order effects in both entropy production and free energy [29]. Creep characterization using the Schapery equation usually requires creep and recovery tests. Since in our study only creep tests have been performed, we cannot compute g_1 and g_2 individually; instead we compute the product of the two. Thus six parameters are required instead of seven to characterize the visco-elastic response. The creep compliance, ΔA, of the composites is often approximated by using a power law of the form:

$$\Delta A(\psi) = A \times \psi^n$$

Where n is a material constant and g_0, g_1, g_2 and $a\sigma$ are approximated by the following expression.:

$$g' = \frac{\mathrm{Sinh}\,\sigma/\sigma_c}{\sigma/\sigma_c} \quad \text{or} \quad \frac{\sigma/\sigma_c}{\mathrm{Sinh}\,\sigma/\sigma_c}$$

Where σ_c is a material constant and g' represent all of the functions of stress. Since in our tests a constant load was applied in a single step, eq. (1) can be integrated to yield:

$$D(t) = \frac{\varepsilon(t)}{\sigma} = g_0 A_0 + \frac{g_1 g_2 A t^n}{a_\sigma^n} \qquad (2)$$

At low stresses the material behaves linearly and all the functions of stress are equal to one, i.e. , $g_0 = g_1 \times g_2 = a\sigma = 1$ thus Eq. (2) reduces to a linear form:

$$D(t) = \frac{\varepsilon(t)}{\sigma} = A_0 + A \times t^n \qquad (3)$$

In our study the low stress level was 16.7% of the ultimate strength and the constants A_0, A and n are calculated through a least squares fit between the experimental data (at 16.7%) and equation (3) using the software "MinSquare" and then the average values of the constants are calculated. Assuming that A_0, A and n are the same at the high stresses (30%, 45% and 60%), the other constants g_0, g_1, g_2 and $a\sigma$ are calculated by fitting equation (2) by the least square method to the experimental data. The stress dependence of these quantities is then calculated for each composite. The values of the terms in eq. (2) [g_0, g_1, g_2, $a\sigma$, A_0, A and n] for different composites are shown in Table 9.

The fitted curves and the experimental points for creep strain vs. time are compared, for chopped strand mat, in Fig. 91-93, and for glass fabric, in Fig. 94-95. These show reasonable congruence, so the analytical expressions could be used for the predictive purpose; the largest error or difference is about 9%. While it would be tempting to extrapolate the predictions to a longer time periods, there is no demonstrated justification for doing so. This reservation

becomes even more important when it is recognized that no consideration of failure or fracture is implicit in the predictions.

6.3 Discussion of results

Two variables were used in the creep tests: rubber content and stress level. The following observations can be made about the effect of these two on the RCD values [Table. 8]. For both composites the RCD values are fairly independent of the stress level [Fig. 96]. Up to 45% of ultimate strength the RCD is independent of rubber content [Fig. 97], but at higher stresses the chopped strand mat shows a higher RCD with increasing rubber content, as also shown by the breaking of the specimens. This observation is consistent with that by Hertzberg [8]: the creep rate increases in direct proportion to the volume of rubber present in a neat resin. The RCD values for the glass fabric composites are smaller than the chopped strand mat composites, because of the presence of continuous fibers in the direction of the load. Overall both the chopped strand mat and the glass fabric composites do not creep excessively, which confirms that the MNS composites can be used safely in structural applications for long service periods.

The creep in a composite arises from two processes: viscoelastic deformation of the matrix, which may be reversible, and damage, which is irreversible. The damage is due to matrix cracking, interfacial separation and fiber fracture. At high stresses these can be expected to be prevalent. That is why the RCD values sharply increase at 60% of ultimate strength [Fig. 96], leading to failure in some cases (Since the chopped strand mat with 17.5% rubber has the lowest strength it is expected to have the highest amount of damage, hence its failure after 400 hours).

The isochronous curves [Fig. 86-90] show the laminates behave in a non-linear viscoelasitc manner. Usually the long time response is more non-linear than the short time behavior, thus the non-linear characterization is used in this study.

Chapter : 7

Conclusions

7.1 Fatigue

(1) The static tests (at 5.08 mm/min) show that when the rubber content in MNS is increased from 7.5% to 17.5%, the modulus decreases 11%-37% and the strength decreases 12%-44%. The yield strain of the MNS composites is larger, compared to the unmodified polyester (32%-60%), but it does not change appreciably with increasing rubber content. The static tests at the stress rate at which the fatigue tests are performed (3378 MPa/sec) show higher modulus and strength; the average increase in strength (50%-110%) depends on the type of reinforcement.

(2) The slope of the S-N curves change around 10^4 cycles for chopped strand mat composites and around 10^5 cycles for woven fabric composites. The damage zone, which is evident by the whitening of the specimens in the glass composites, increases as the cycles increase, reaches a maximum, and then decreases as the cycles increase further. The maximum occurs at about 10^4 cycles for the chopped strand mat and at about 10^5 cycles for the glass fabric. This suggests the change in slope is due to a change in damage mechanism. It is proposed that in the low cycle range the damage is dominated by fiber breakage but with an increasing number of cycles, matrix cracking becomes more dominant, causing the maxima in the damage zones. With further cycles, interfacial damage becomes dominant, causing the decrease in damage zone.

(3) Generally the damage progression is similar for all the composites studied except for glass fabric with unmodified polyester. Usually it starts on the

surface with debonding along the transverse fibers. Matrix cracking then develops, and as the cycling continues, debonding and matrix cracking develop in the strands oriented in the stress direction, and the damage moves to the center of the thickness, causing some fiber breakage along its way. The Talrega diagram also shows the damage mechanisms are matrix cracking and debonding. In the case of the glass cloth with the unmodified polyester, the failure is mainly due to shear delamination in the center. The reason for this may be that the fibers are Volan coated, which is more compatible with the unmodified polyester, and thus they adhere better, so the matrix breaks.

(4) Although the S-N curves are not linear, when the data are plotted on a Log-Log plot the curves become so. Then the data are characterized by the value of m, where 1/m represents the slope of the linear (Log-Log) plot, ($S/S_o = N^{-1/m}$). The values of m for the different composites show that the fatigue performance improves with increasing rubber. For chopped strand mat the increase is in the range of 6.7%-9% when the rubber content is increased from 7.5% to 17.5%; for glass fabric the increase is 13%-18% when the rubber content is increased from 7.5% to 17.5% and for carbon fabric the increase is in the range of -8% to 40% when the rubber content is increased from 7.5% to 17.5%.

(5) Since all the normalized S-N curves for the glass composites overlap, it appears the fatigue behavior is fiber dominated. In the carbon composites the behavior is matrix dominated, which is obvious from the trends in the normalized S-N curves for the different matrices. This is consistent with the fact that carbon fibers are more fatigue resistant than glass.

(6) Generally with off-axis laminates and when the loading has a compressive component, both carbon and glass composites perform similarly. Because of this, and because of fiber misalignment, weave distortion and yarn

crossovers, the performance of the carbon and glass composites was expected to be similar. However, with the MNS matrix, due to its increased strain to failure and a modest decrease in modulus, the performance of the carbon composite was better than glass.

(7) With the chopped strand mat the change in slope after 10^4 cycles is large and it may represent an approaching endurance limit.

(8) The initial strain-N curves show the fatigue performance improves with increasing rubber content for any reinforcement.

(9) The stiffness loss, represented by deflection vs. number of cycles, is divided into three stages. In the first, there is rapid decrease in stiffness; in the second it remains nearly unchanged; in the final stage, again it drops rapidly, and the 40% loss in modulus (our fracture criterion) and complete failure occur at approximately the same number of cycles.

7.2 Creep

(1) Flexural creep tests were performed only on chopped strand mat and glass fabric composites, with two variables: rubber content and stress level. The comparison of relative creep deflection shows the values are independent of the stress level in most cases. Increasing the rubber content in the woven fabric composites shows the RCD values are independent of rubber content, while the same is true with the chopped strand mat composite at low stress levels, but at higher stress the chopped strand mat with 17.5% rubber has a higher RCD value.

(2) The isochronous curves show that the laminates exhibit non-linear viscoelastic behavior.

(3) The Schapery constitutive equation represents the time-dependent creep behavior of these composites quite well; relatively small divergencies are apparent after about 1000 hours of creep.

Chapter : 8

Suggestions For Future Work

(1) Fatigue testing of the unreinforced MNS matrix with different rubber contents.

(2) Testing the composite specimens to higher (10^7) cycles to confirm the presence or absence of an endurance limit.

(3) Testing MNS composites in fatigue with a variety of different rubber compositions.

(6) Testing the composites in creep at more stress levels to find more accurate functions for the stress dependent parameters in Schapery's equation.

(7) Creep recovery tests should be performed to find all the parameters in Schapery's equation and to provide further information about the damage accumulation in creep.

Appendix : I

Composition	Pure Polyester	MNS 0%	MNS 7.5%	MNS 12.5%	MNS 17.5%
Resin [1]					
Polyester	60.44 %	51.2%	47.33 %	44.77 %	42.21 %
Epoxy	0 %	15.3%	14 %	13.43 %	12.66 %
Styrene	39.6 %	33.5%	31 %	29.3 %	27.63 %
Rubber (ATBN)	0 %	0%	7.5 %	12.5 %	17.5 %
Glass Content[2]					
Chopped strand mat	51.90%	51.99%	46.89 %	47.71 %	43.58 %
Glass Fabric	60.09%	60.76%	62.04 %	63.57%	55.18%

1. Weight percent based on the total weight of resin.

2. Weight percent based on total weight of composite.

Table : 1 :- Composition of resin and Glass content in the composite

Specimen	Flexural Modulus E MPa	Yield Stress σ MPa	Yield Strain ε m/m
Chopped Strand mat			
Pure Polyester	9336(±615)	256.31(±35.79)	.0303(±.0036)
MNS 0% Rubber	9491(±325)	268.21(±19.79)	.0308(±.0022)
MNS 7.5% Rubber	11031 (±386)	293.52 (±9.90)	.0363 (±.0005)
MNS 12.5% Rubber	9688 (±275)	256.46 (±13.22)	.0357 (±.0008)
MNS 17.5% Rubber	7358 (±589)	200.23 (±26.76)	.0345 (±.0016)
Glass Fabric			
Pure Polyester	16148 (±355)	278.55 (±25.80)	.0195 (±.0031)
MNS 0% Rubber	14979(±1322)	366.22(±23.42)	.0284(±.004)
MNS 7.5% Rubber	18318 (±515)	422.07 (±14.26)	.0277 (±.0012)
MNS 12.5% Rubber	16354 (±184)	371.40 (±17.40)	.0286 (±.0018)
MNS 17.5% Rubber	11576(±269)	234.84(±1.96)	.0227(±.002)
Carbon Fabric			
Pure Polyester	39452 (±2546)	365.84 (±29.58)	.0096 (±.001)
MNS 0% Rubber	43803(±222)	650.87(±33.18)	.0150(±.0008)
MNS 7.5% Rubber	35515 (±1655)	529.45 (±60.04)	.0154 (±.0024)
MNS 12.5% Rubber	49014 (±547)	582.74 (±13.02)	.0127 (±.0006)
MNS 17.5% Rubber	30999 (±4071)	422.51 (±87.49)	.0145 (±.0004)

Table : 2 :- Mechanical properties of all the composites tested in three point bending at a rate of 5.08 mm/min. Numbers in parenthesis are standard deviations.

Specimen	Initial Modulus E MPa	Flexural Strength σ MPa	Strain to failure ε m/m
Chopped Strand mat			
Pure Polyester	13362	488.06	.0365
MNS 0% Rubber	13881	503.88	.0363
MNS 7.5% Rubber	15679	572.56	.0365
MNS 12.5% Rubber	13645	572.19	.0419
MNS 17.5% Rubber	11011	518.06	.0471
Glass Fabric			
Pure Polyester	23469	564.74	.0241
MNS 0% Rubber	21975	672.88	.0306
MNS 7.5% Rubber	27248	730.53	.0268
MNS 12.5% Rubber	22960	649.91	.0283
MNS 17.5% Rubber	14927	408.56	.0274
Carbon Fabric			
Pure Polyester	44616	643.67	.0144
MNS 0% Rubber	47847	820.82	.0172
MNS 7.5% Rubber	49518	840.33	.0170
MNS 12.5% Rubber	54241	867.59	.0160
MNS 17.5% Rubber	40217	532.76	.0133

Table : 3 :- Mechanical properties of all the composites tested in three point bending at a loading rate of 3378 MPa/Sec (Loading rate on which fatigue specimen are tested).

Specimen	$b = \frac{S/S_o - 1}{\log N}$			$m = -\frac{Log(N)}{Log(S/S_0)}$
	for whole life, %	upto 10^4 cycles, %	after 10^4 cycles, %	for whole life, %
Chopped Strand mat				
Pure Polyester	14.74	17.22	6.25	7.86
MNS 0% Rubber	15.36	18.83	5.93	7.44
MNS 7.5% Rubber	13.27	19.46	4.97	6.96
MNS 12.5% Rubber	13.58	18.89	5.14	7.43
MNS 17.5% Rubber	13.67	21.39	4.31	7.59
	for whole life, %	upto 10^5 cycles, %	after 10^5 cycles, %	
Glass Fabric				
Pure Polyester	13.49	15.67	7.61	9.03
MNS 0% Rubber	13.21	15.23	6.29	8.77
MNS 7.5% Rubber	13.94	15.01	7.13	8.09
MNS 12.5% Rubber	12.99	14.65	6.69	9.14
MNS 17.5% Rubber	13.59	14.93	3.20	9.55
Carbon Fabric				
Pure Polyester	12.23	15.00		11.37
MNS 0% Rubber	12.22	12.908		11.07
MNS 7.5% Rubber	11.35	12.24		12.69
MNS 12.5% Rubber	12.38	13.45		11.66
MNS 17.5% Rubber	9.18	9.97		17.79

Table : 7 :- Value of fatigue characterizing parameters, b and m for different composites.

Specimen	RCD % 16.7% of σ_f	RCD % 30% of σ_f	RCD % 45% of σ_f	RCD % 60% of σ_f
Chopped Strand mat				
MNS 7.5% Rubber	27.80	26.32	27.52	t_f=1200h
MNS 12.5% Rubber	28.14	26.32	23.55	28.64
MNS 17.5% Rubber	28.80	31.61	28.04	t_f=400h
Glass Fabric				
MNS 7.5% Rubber	16.10	15.52	13.72	13.96
MNS 12.5% Rubber	17.97	17.03	16.17	22.68

Table : 8 :- Relative creep deflection after 120 days at different stress levels. t_f shows the time of failure in hours.

Composite	A_o	A	n	g_o	$g_1 * g_2$	a_σ
Chopped strand mat						
7.5% Rubber	7.5146E-5	2.0580E-5	0.087059	$\frac{\sinh \sigma/227.30}{\sigma/227.30}$	$\frac{\sinh \sigma/198.84}{\sigma/198.84}$	$\frac{\sigma/109.57}{\sinh \sigma/109.57}$
12.5% Rubber	7.2108E-5	2.7202E-5	0.074309	$\frac{\sinh \sigma/133.34}{\sigma/133.34}$	$\frac{\sigma/218.40}{\sinh \sigma/218.40}$	$\frac{\sigma/49.40}{\sinh \sigma/49.40}$
17.5% Rubber	1.0793E-4	2.9203E-5	0.088642	$\frac{\sinh \sigma/140.78}{\sigma/140.78}$	$\frac{\sinh \sigma/120.20}{\sigma/120.20}$	$\frac{\sigma/67.61}{\sinh \sigma/67.61}$
Glass fabric						
7.5% Rubber	4.5350E-5	8.1880E-6	0.072685	$\frac{\sinh \sigma/408.18}{\sigma/408.18}$	$\frac{\sigma/201.32}{\sinh \sigma/201.32}$	$\frac{\sigma/156.91}{\sinh \sigma/156.91}$
12.5% Rubber	4.8976E-5	8.0848E-6	0.086216	$\frac{\sinh \sigma/231}{\sigma/231}$	$\frac{\sinh \sigma/193.74}{\sigma/193.74}$	$\frac{\sigma/87.61}{\sinh \sigma/87.61}$

Table : 9 :- Values of different terms in Schapery's equation.

Appendix : II

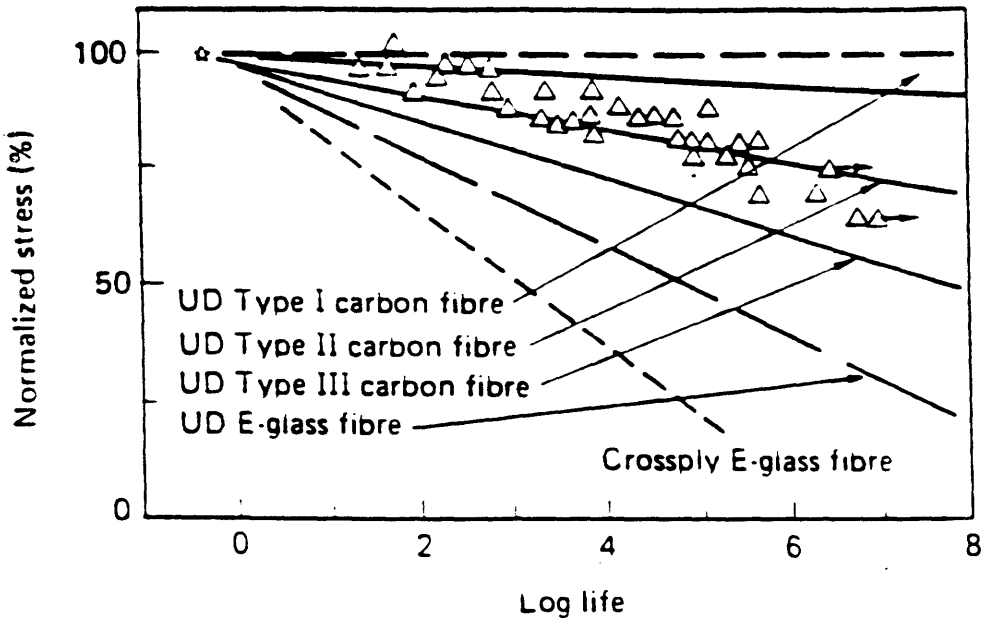

Fig. 1: Normalized S-N curves for unidirectional composites with various types of fibers, tested in longitudinal tensile fatigue [11].

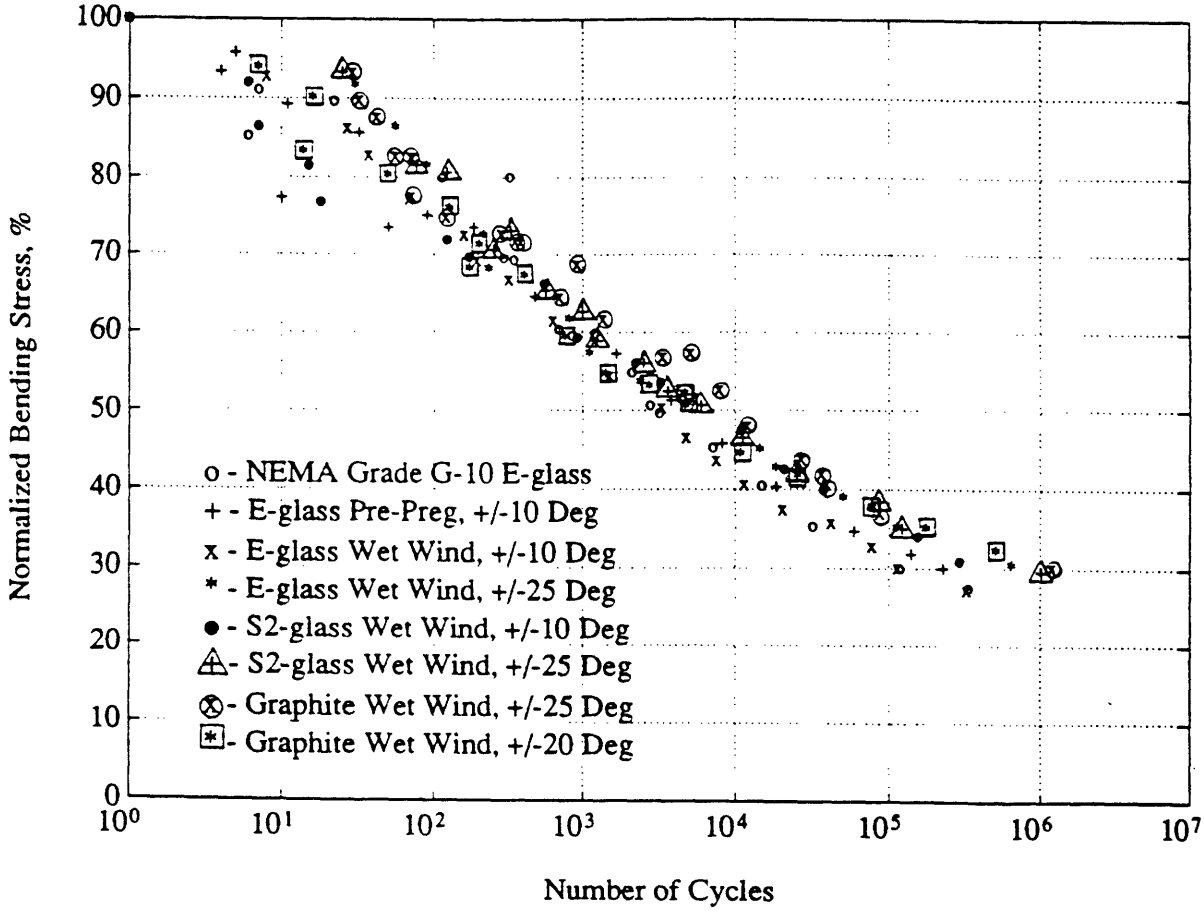

Fig. 2: Normalized S-N curves for cross ply composites with various types of fibers, tested in flexure fatigue [3].

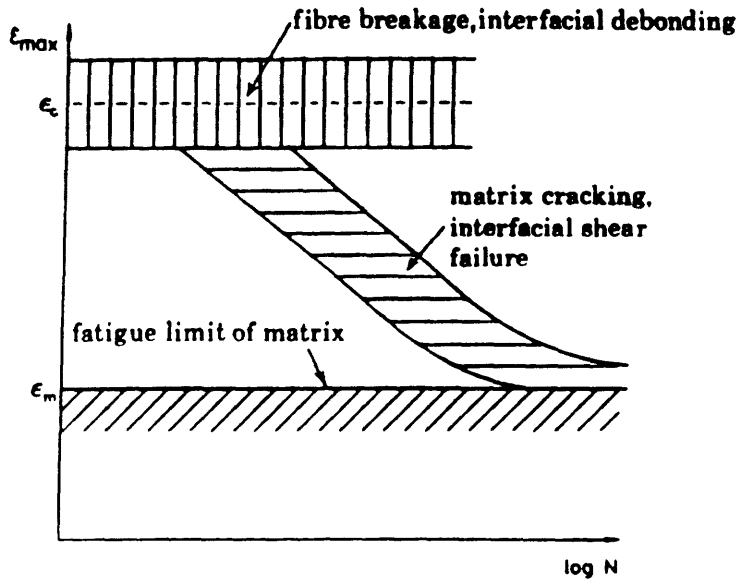

Fig. 3 : Strain -N curve showing regions of different damsge mechanisms, as proposed by Talrega [5].

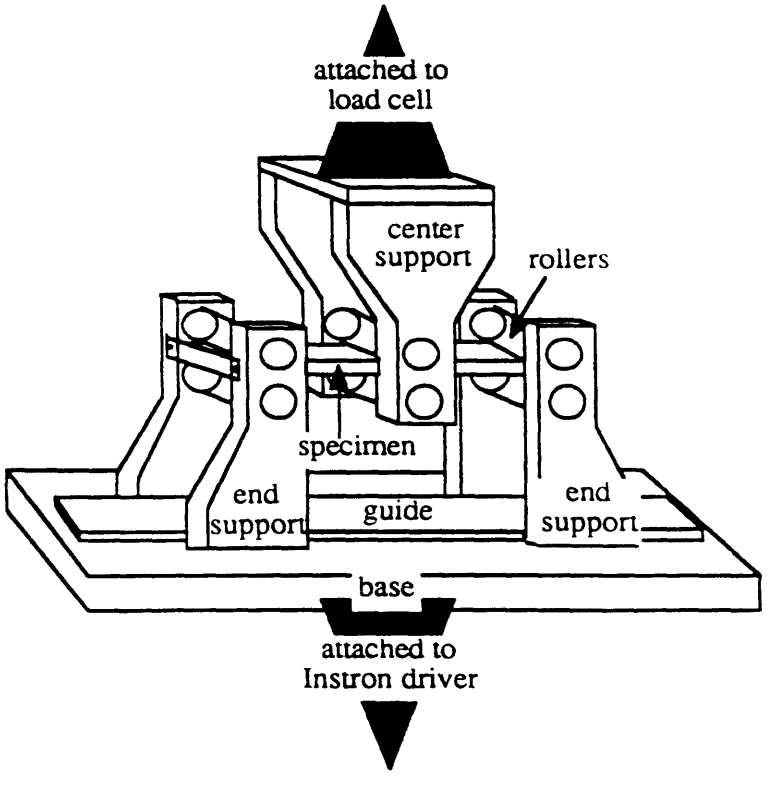

Fig. 5 : Flexural fatigue fixture.

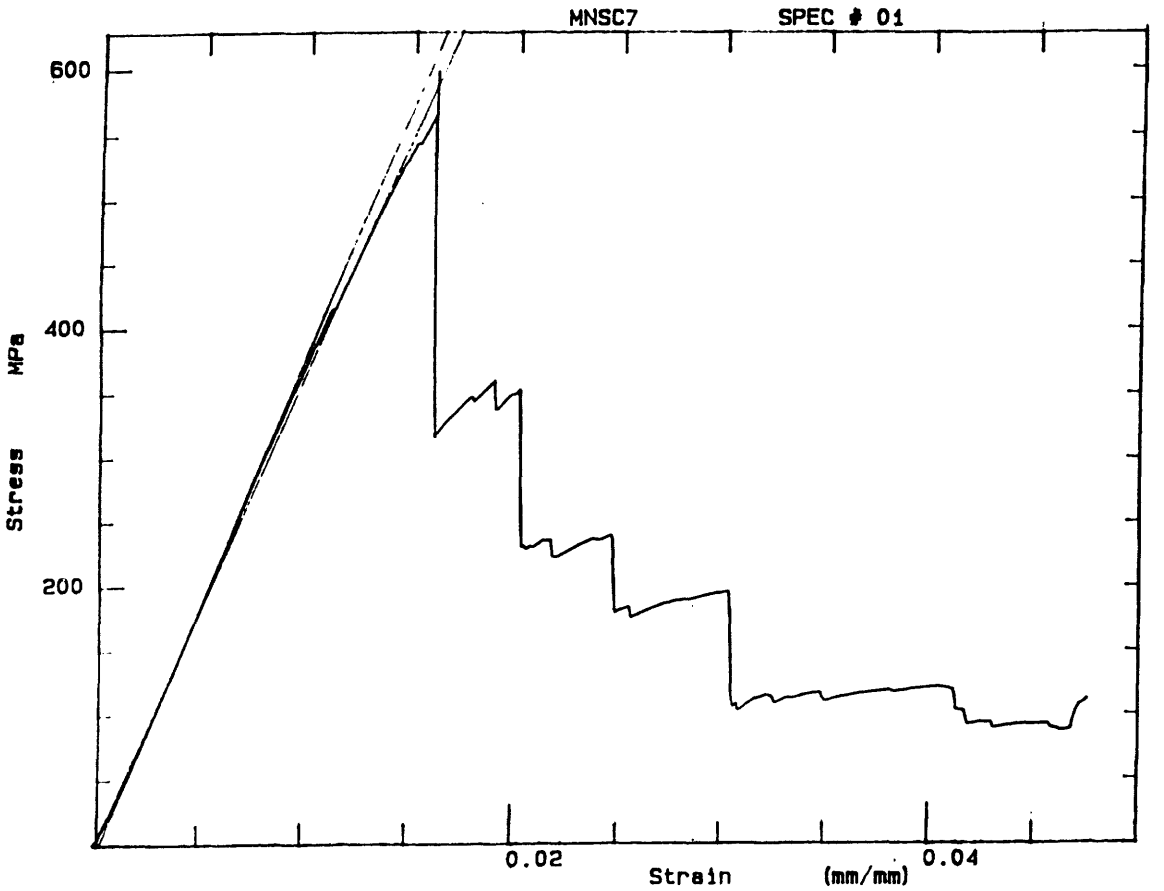

Fig : 6 : A typical stress-strain curve for a composite

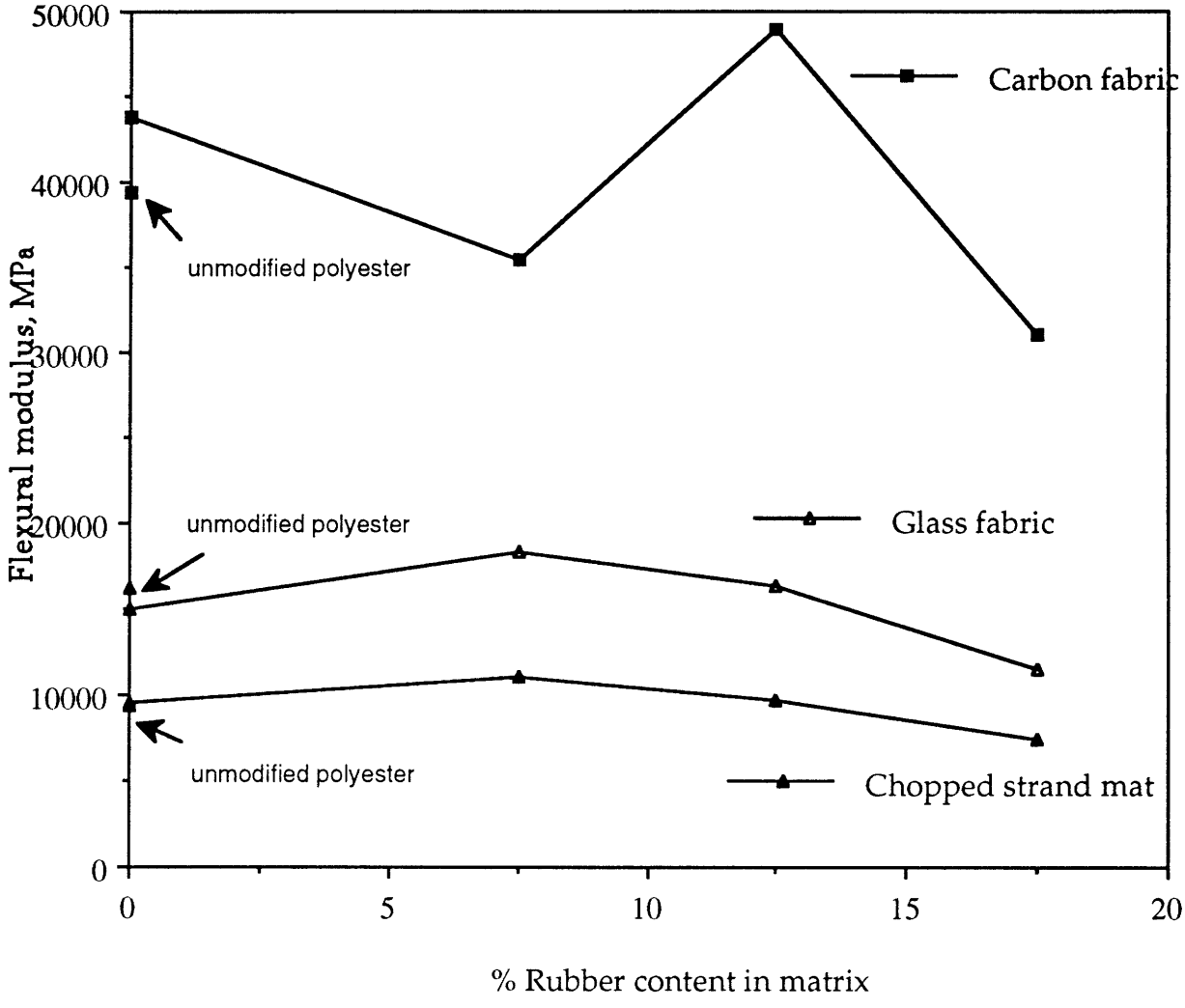

Fig : 7 : Flexural modulus Vs. % rubber content in matrix for different reinforcements (form the static tests performed at a ram speed of 5.08 mm/min).

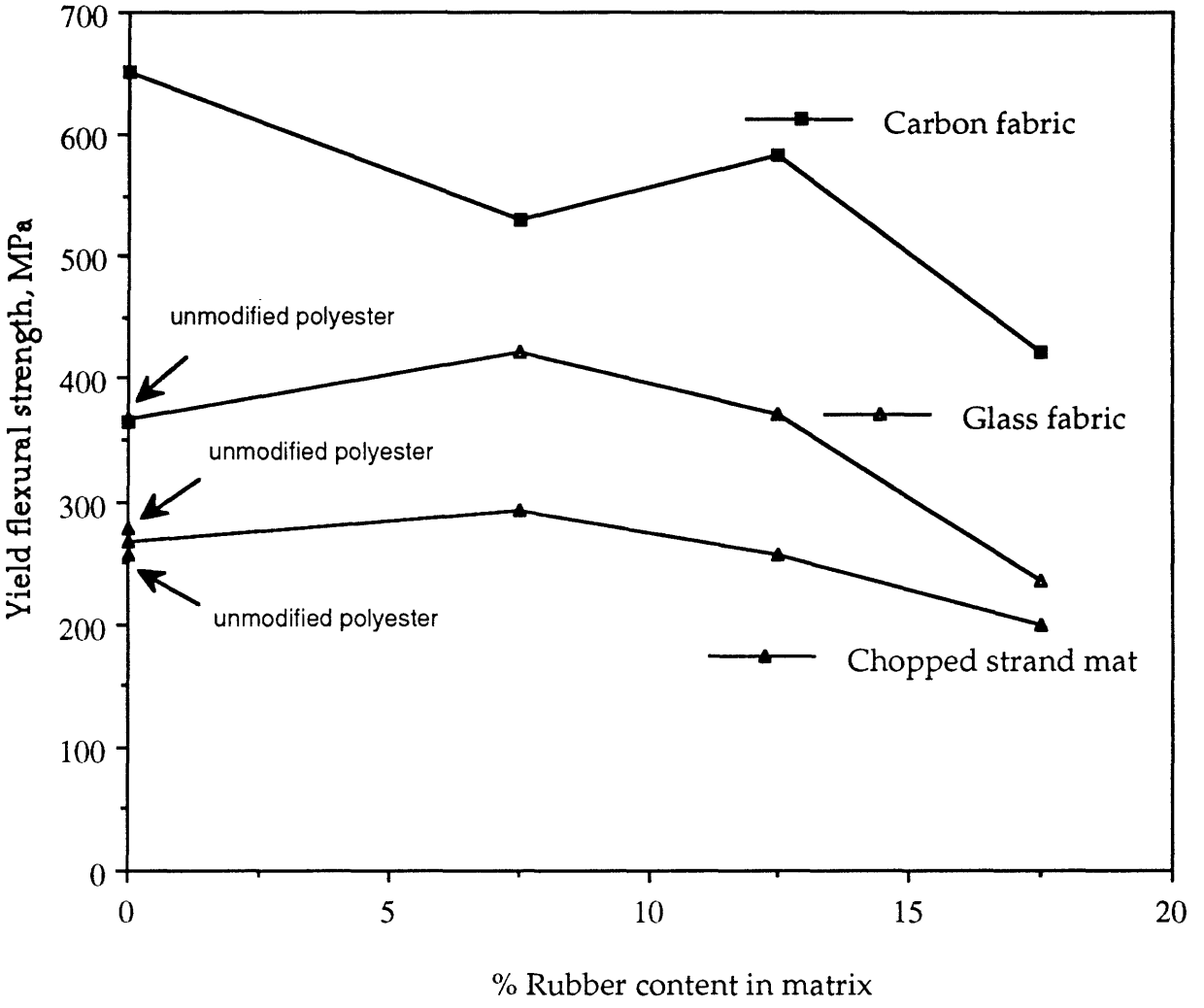

Fig : 8 : Yield strength Vs. % rubber content in matrix for different reinforcements (from the static tests performed at a ram speed of 5.08 mm/min).

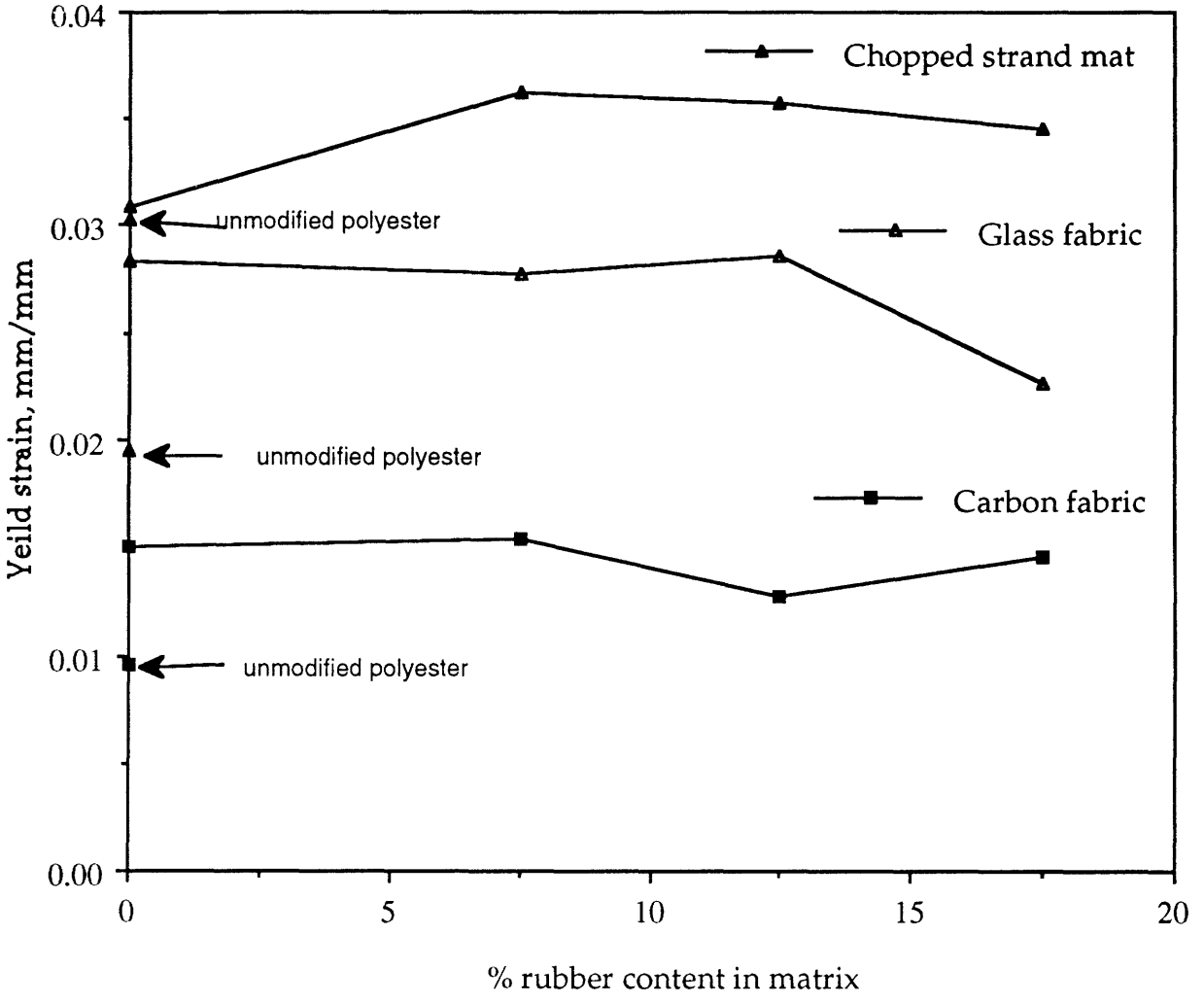

Fig : 9 : Yield strain Vs. % rubber content in matrix for different reinforcements (from the static tests performed at a ram speed of 5.08 mm/min).

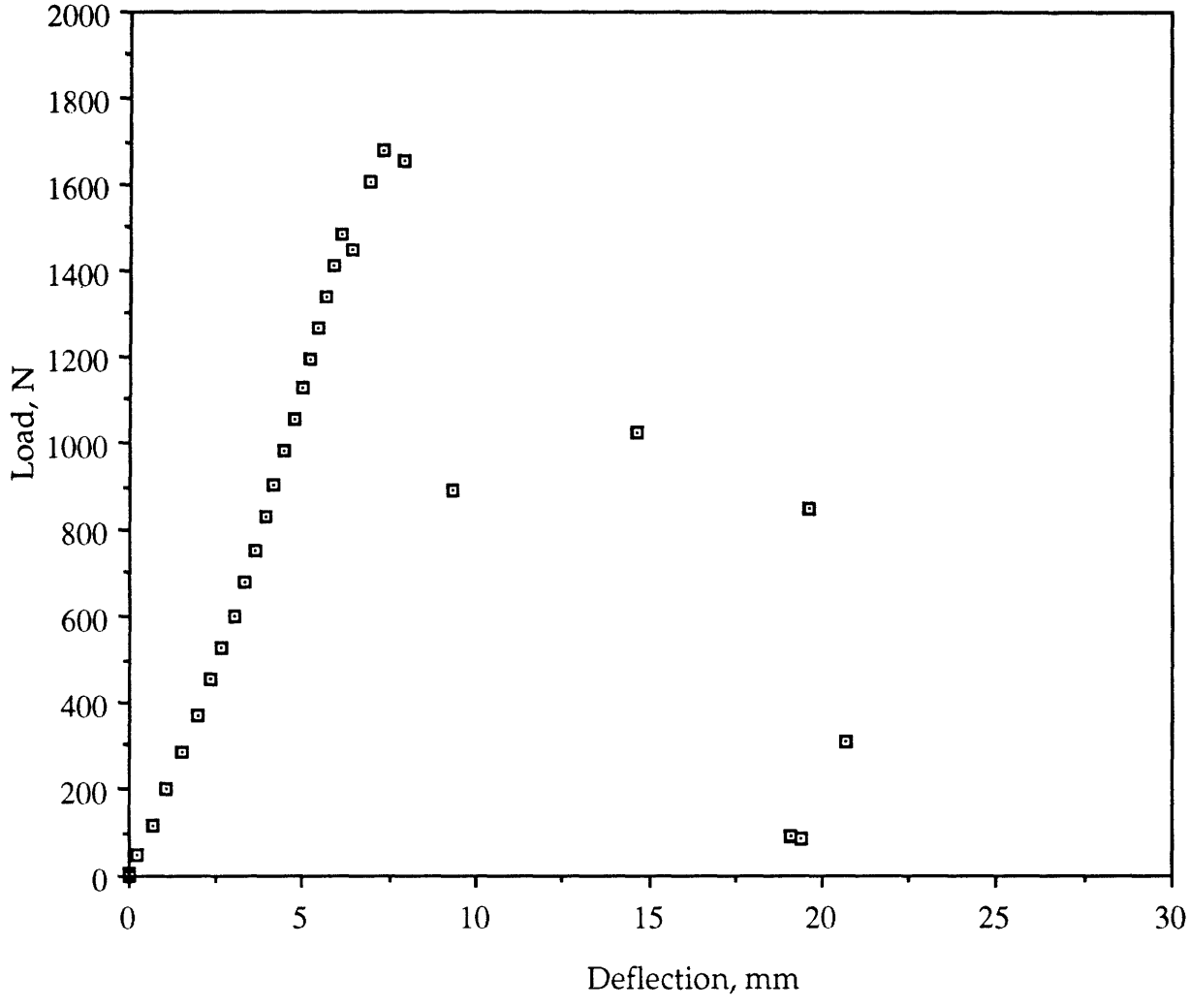

Fig : 10 : A typical load-deflection curve for a composite (carbon fabric/MNS with 7.5% rubber) tested in flexure at a rate of 3378 MPa/sec.

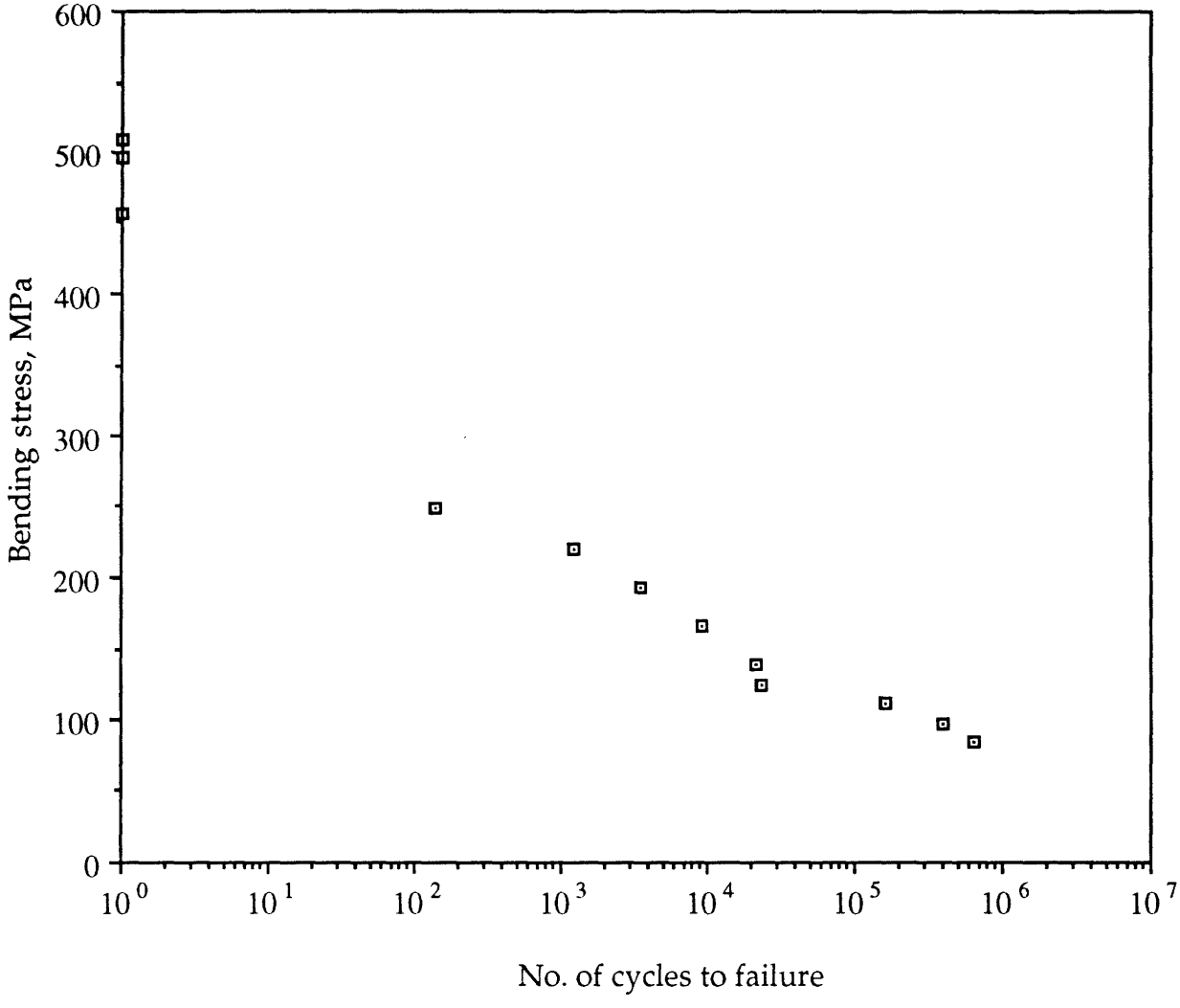

Fig : 11 : S-N curve for chopped strand mat/unmodified polyester, R=-1

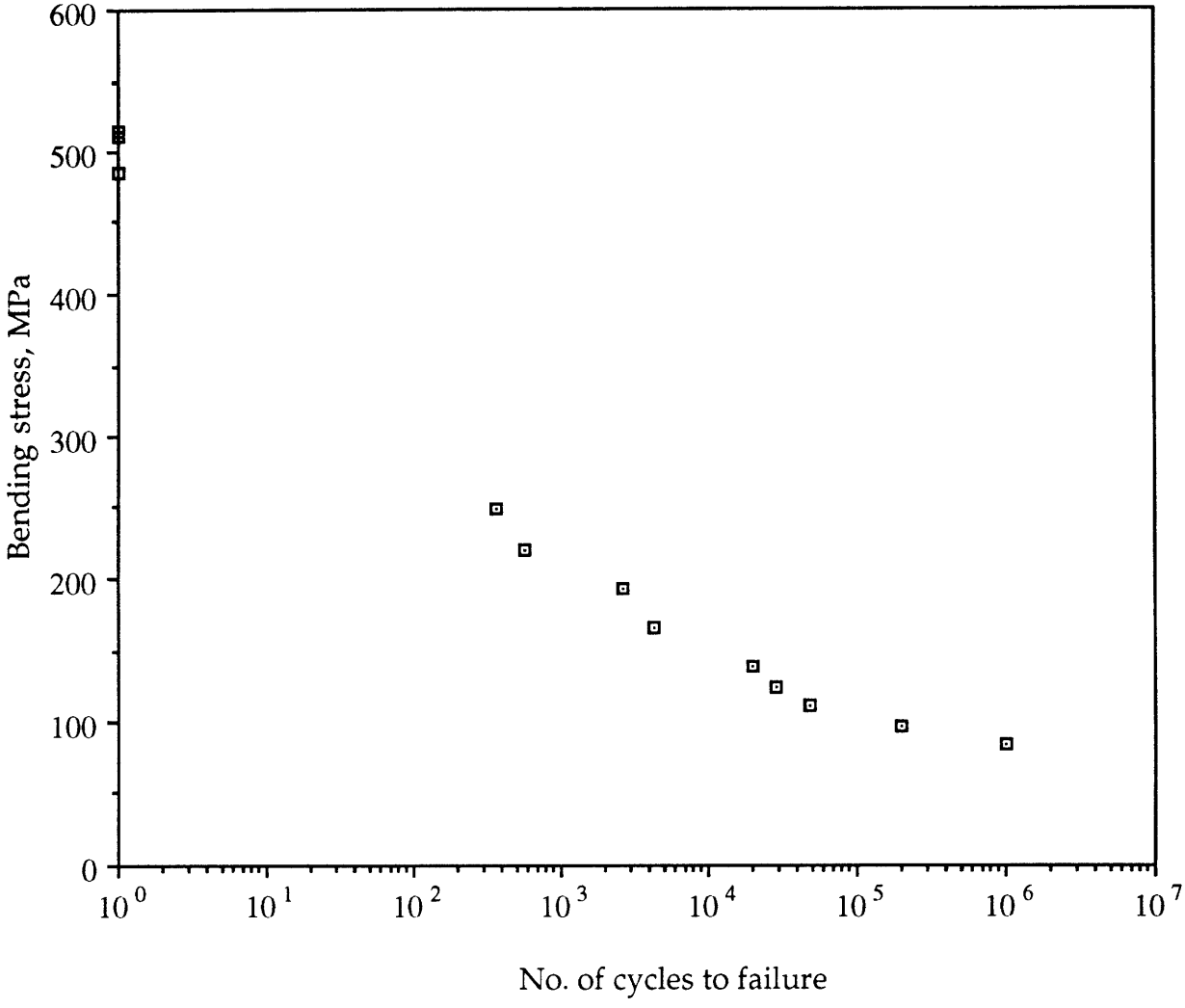

Fig : 12 : S-N curve for chopped strand mat/MNS with 0% rubber, R=-1

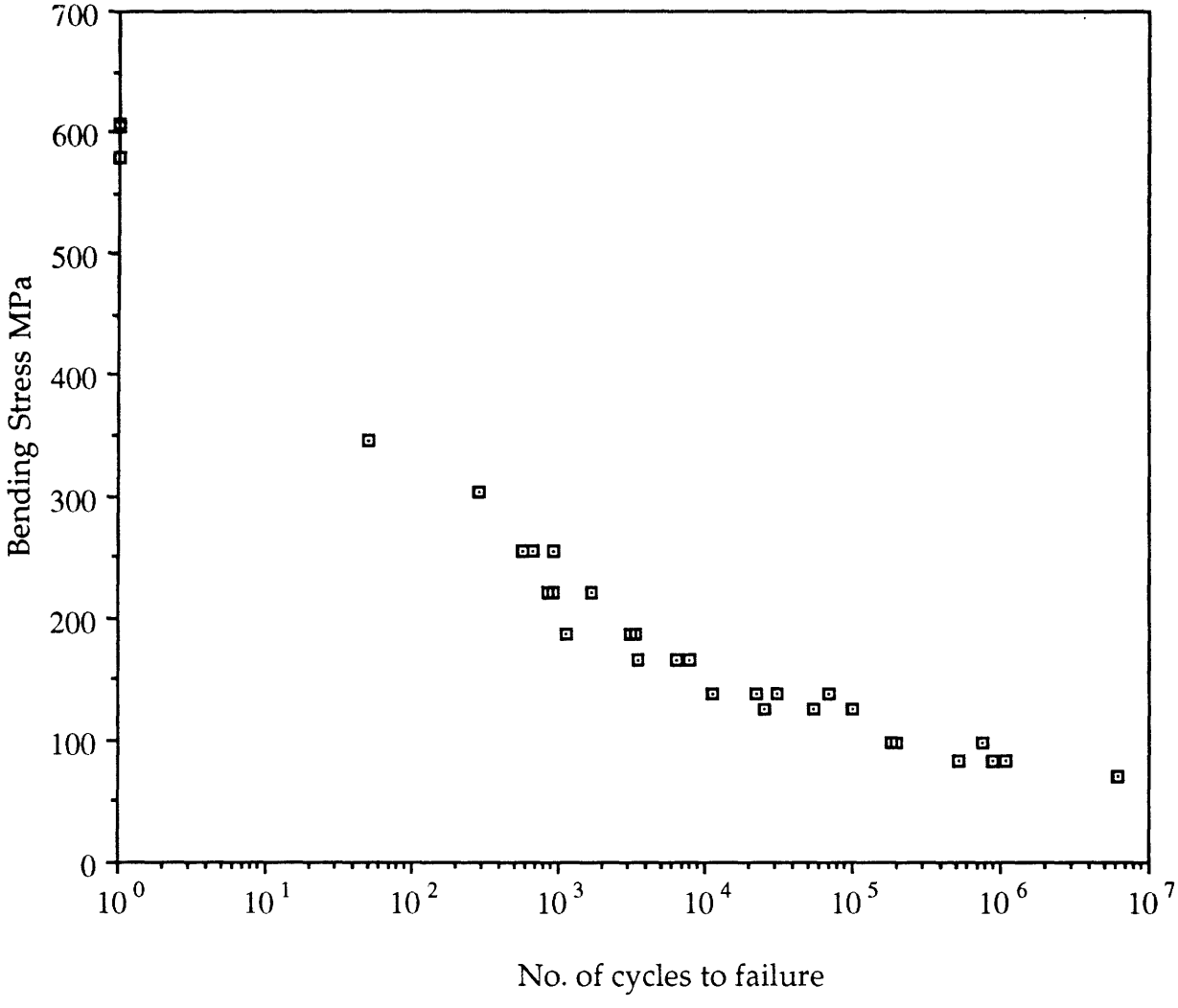

Fig : 13 : S-N curve for chopped strand mat/MNS with 7.5% rubber, R=-1

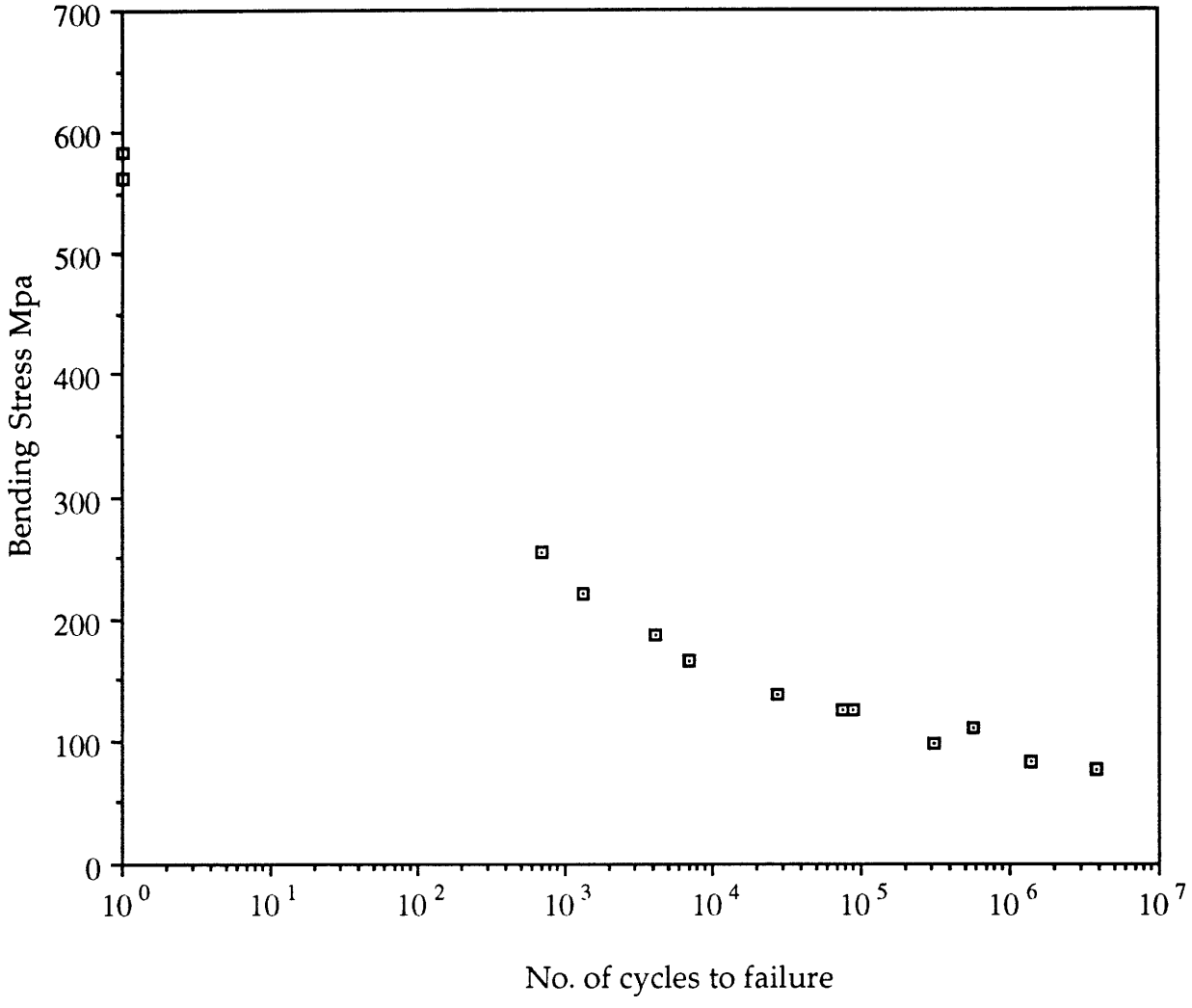

Fig : 14 : S-N curve for chopped strand mat/MNS with 12.5% rubber, R=-1

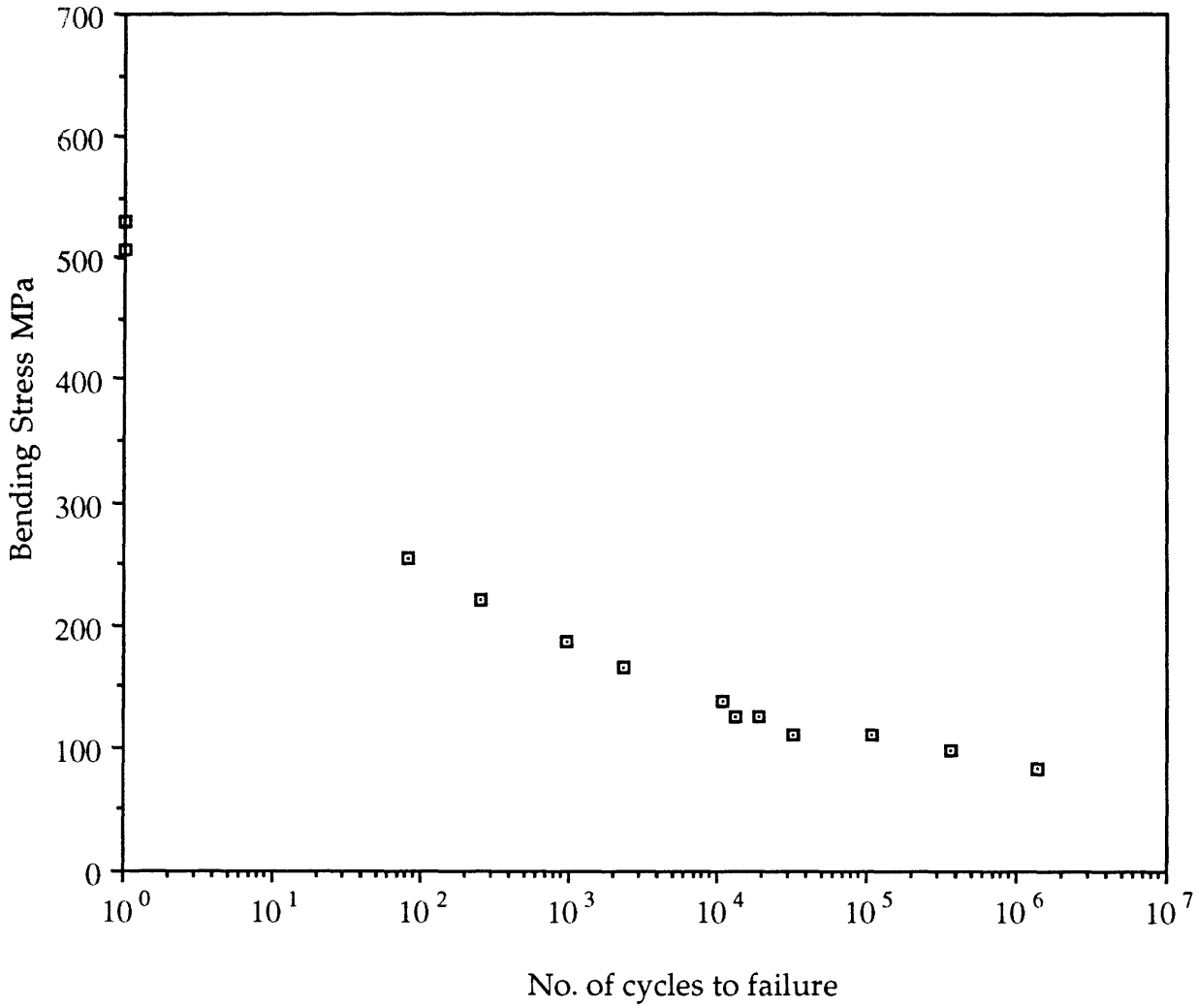

Fig : 15 : S-N curve for chopped strand mat/MNS with 17.5% rubber, R=-1

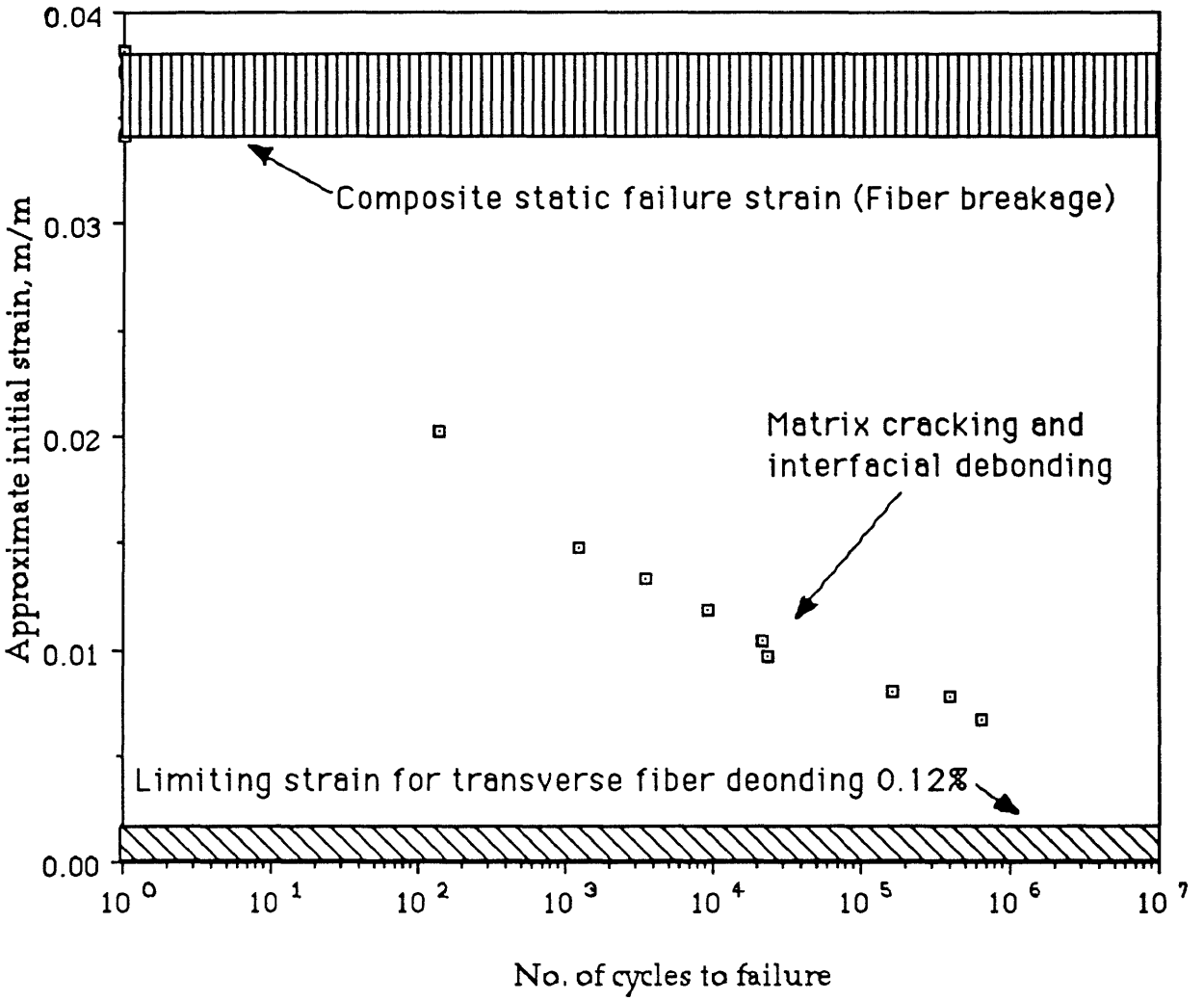

Fig : 16 : Strain-N curve for chopped strand mat/unmodified polyester, R=-1

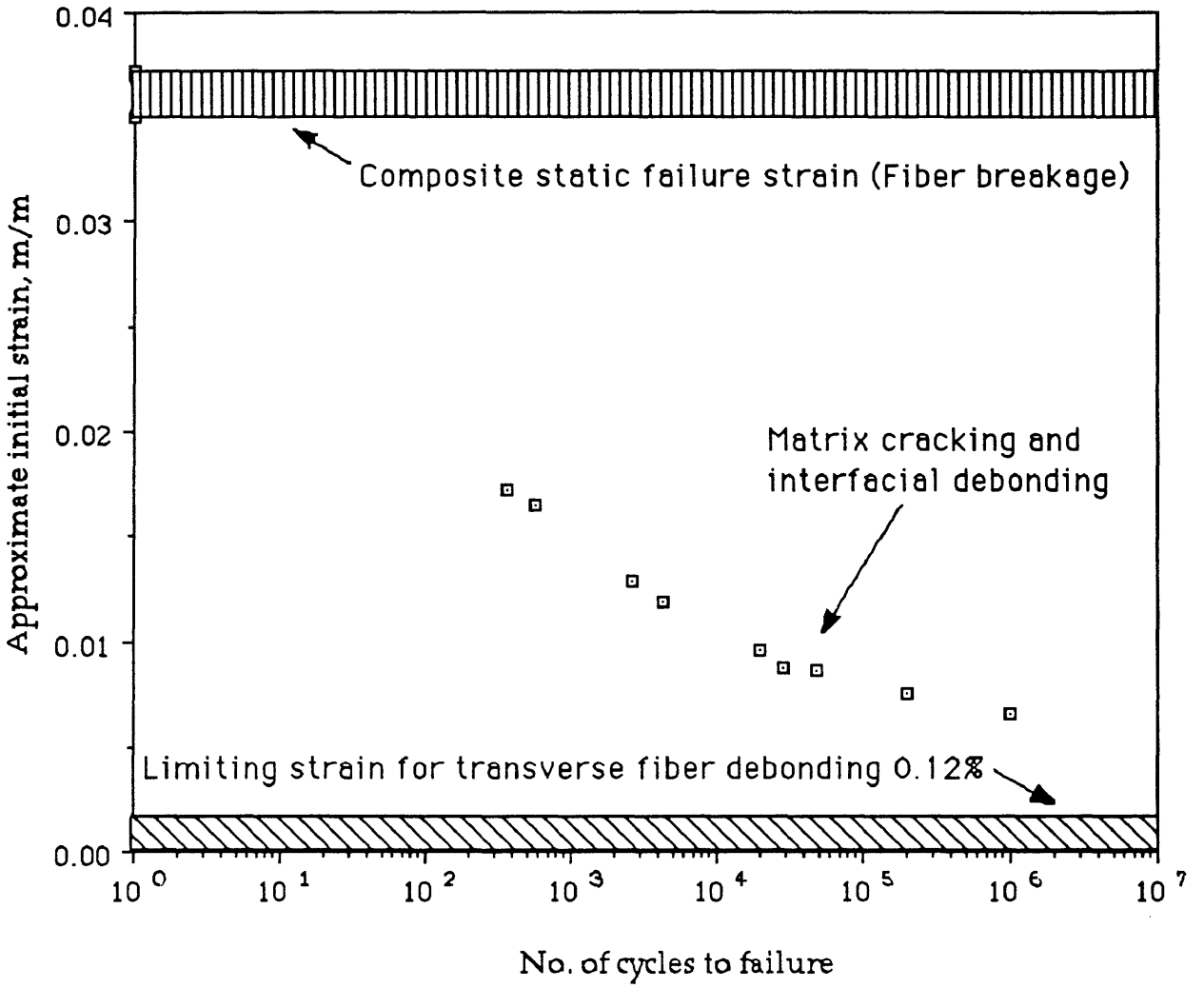

Fig : 17 : Strain-N curve for chopped strand mat/MNS with 0% rubber, R=-1

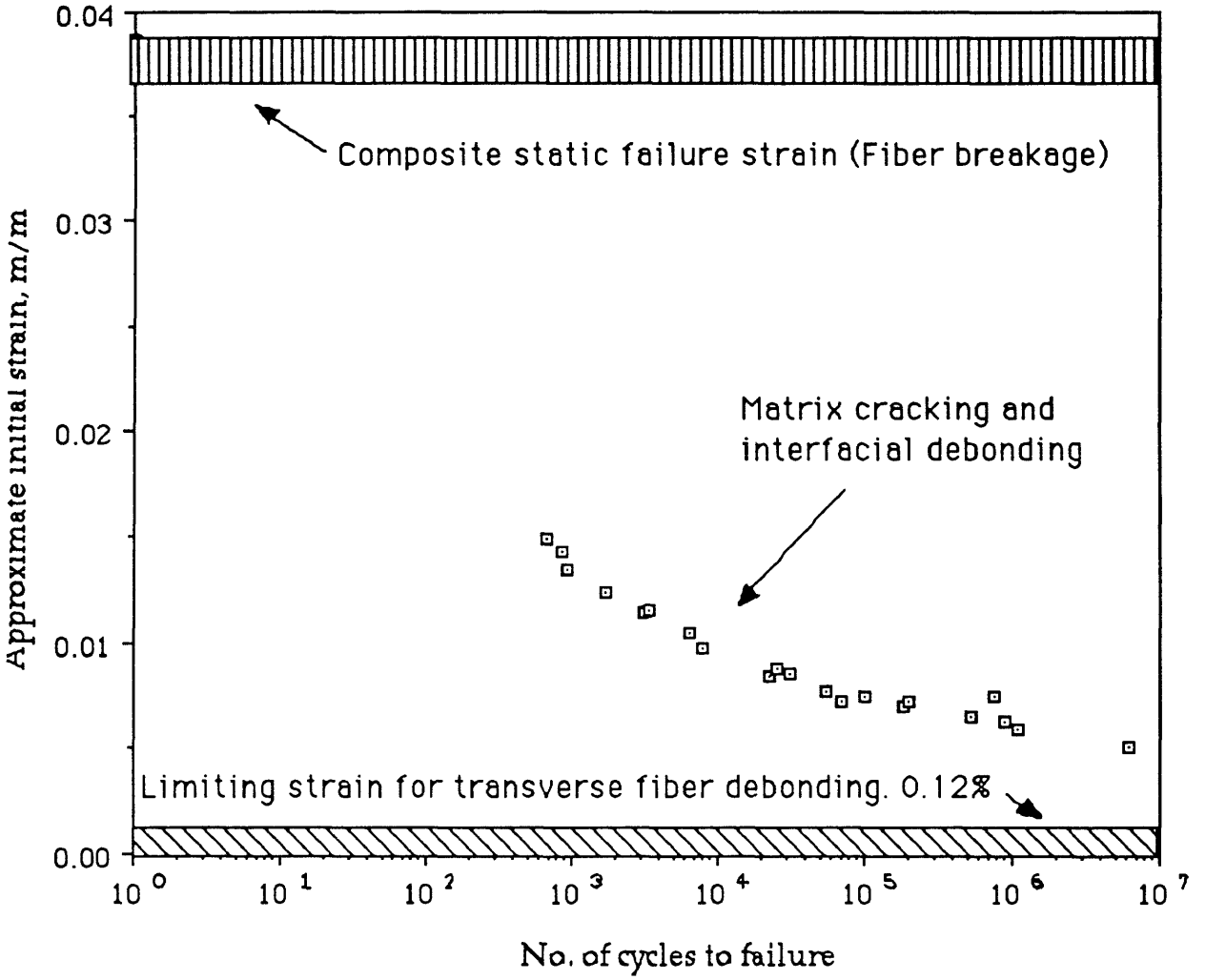

Fig : 18 : Strain-N curve for chopped strand mat/MNS with 7.5% rubber, R=-1

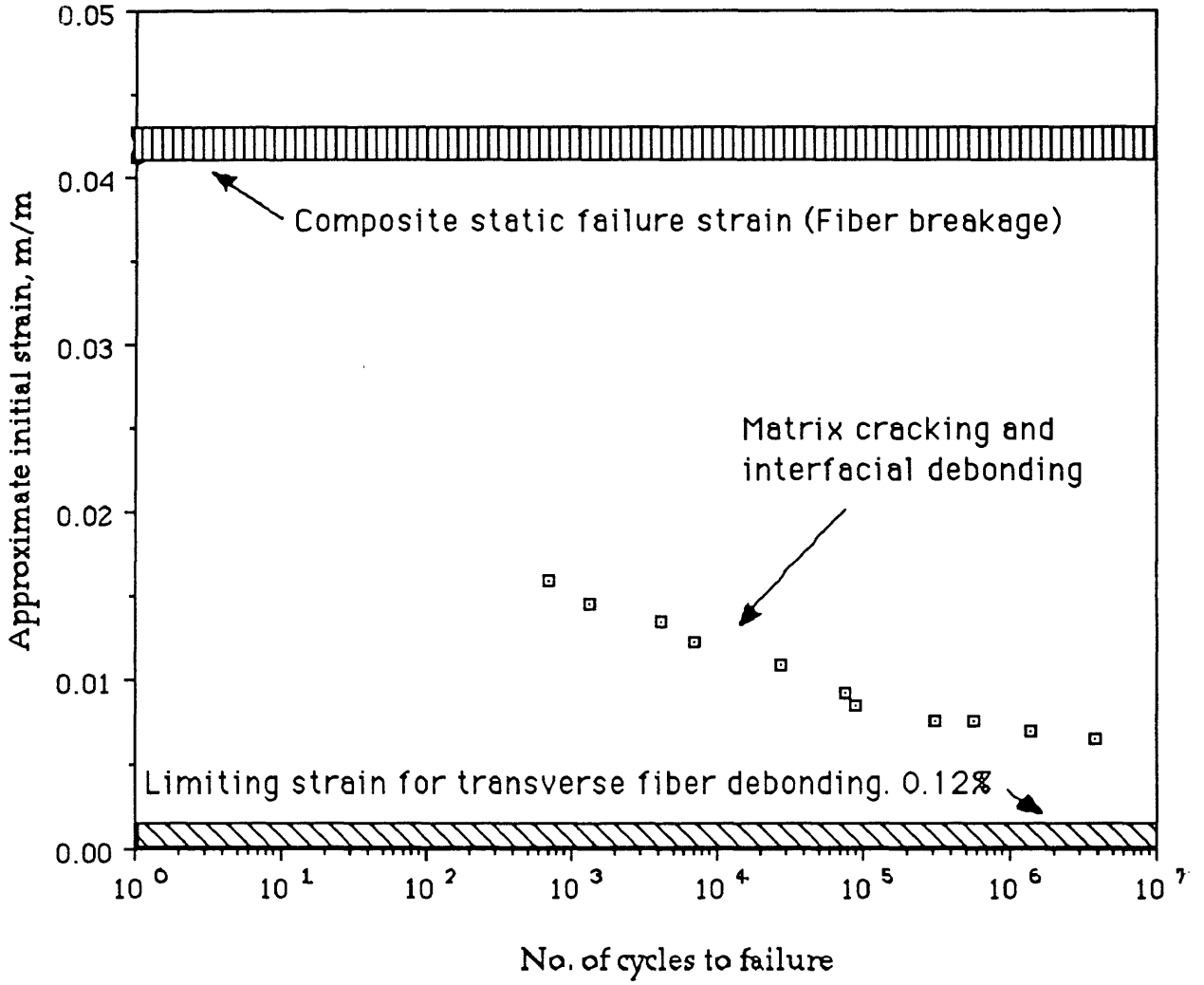

Fig : 19 : Strain-N curve for chopped strand mat/MNS with 12.5% rubber, R=-1

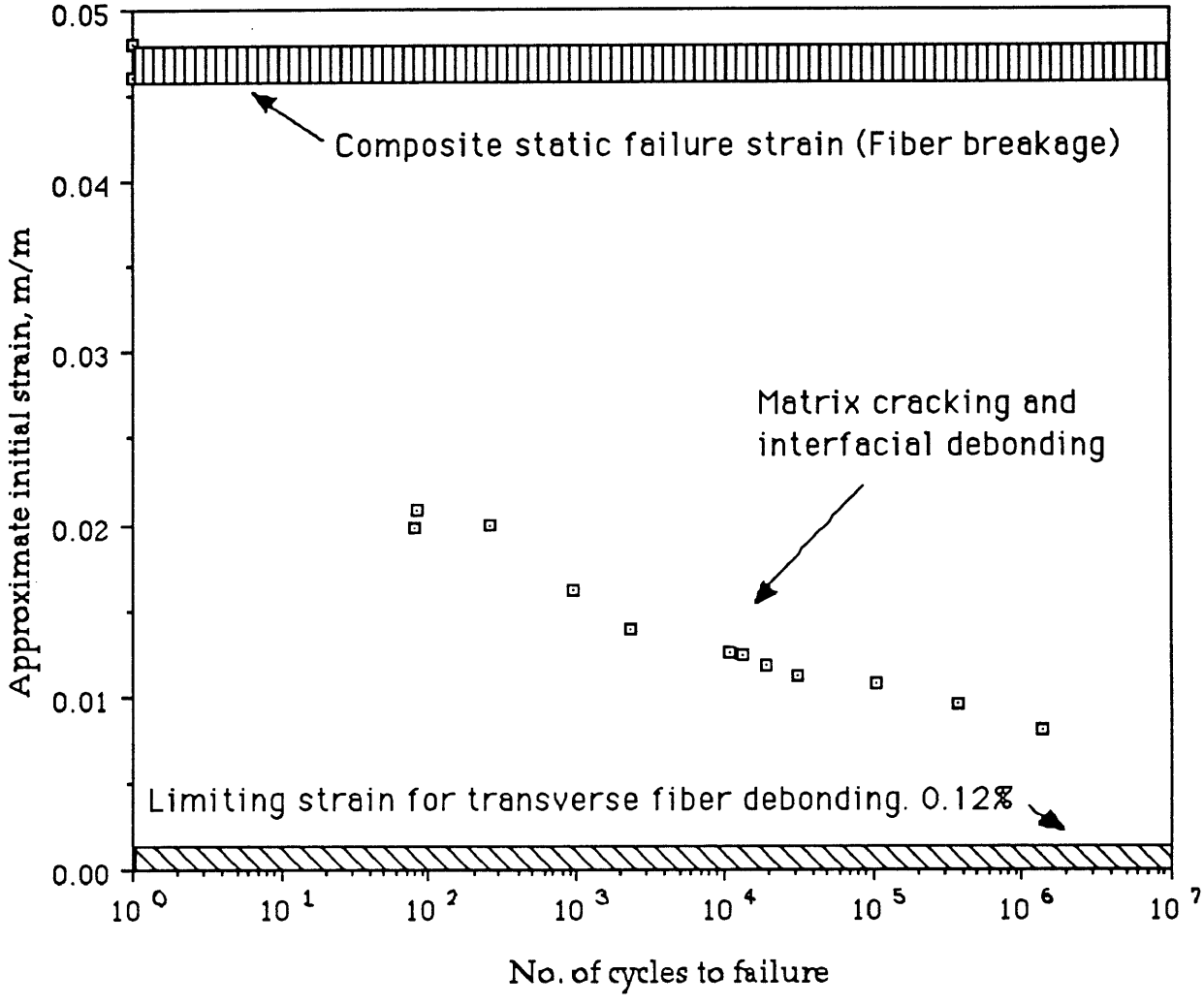

Fig : 20 : Strain-N curve for chopped strand mat/MNS with 17.5% rubber, R=-1

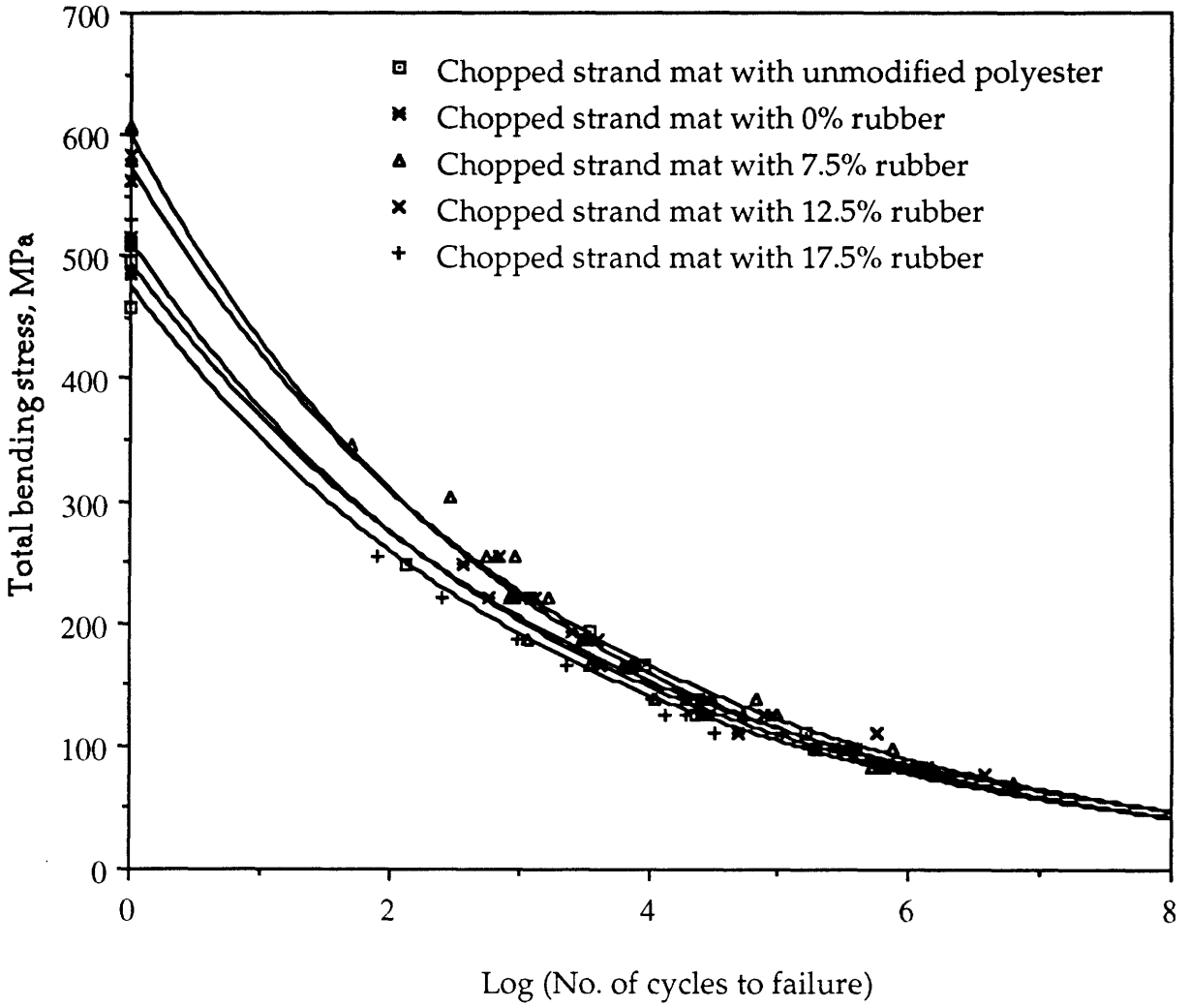

Fig : 21 : Comparison of total stress S-N curves for Chopped strand mat with unmodified polyester, with 0%, 7.5%, 12.5% and 17.5% rubber

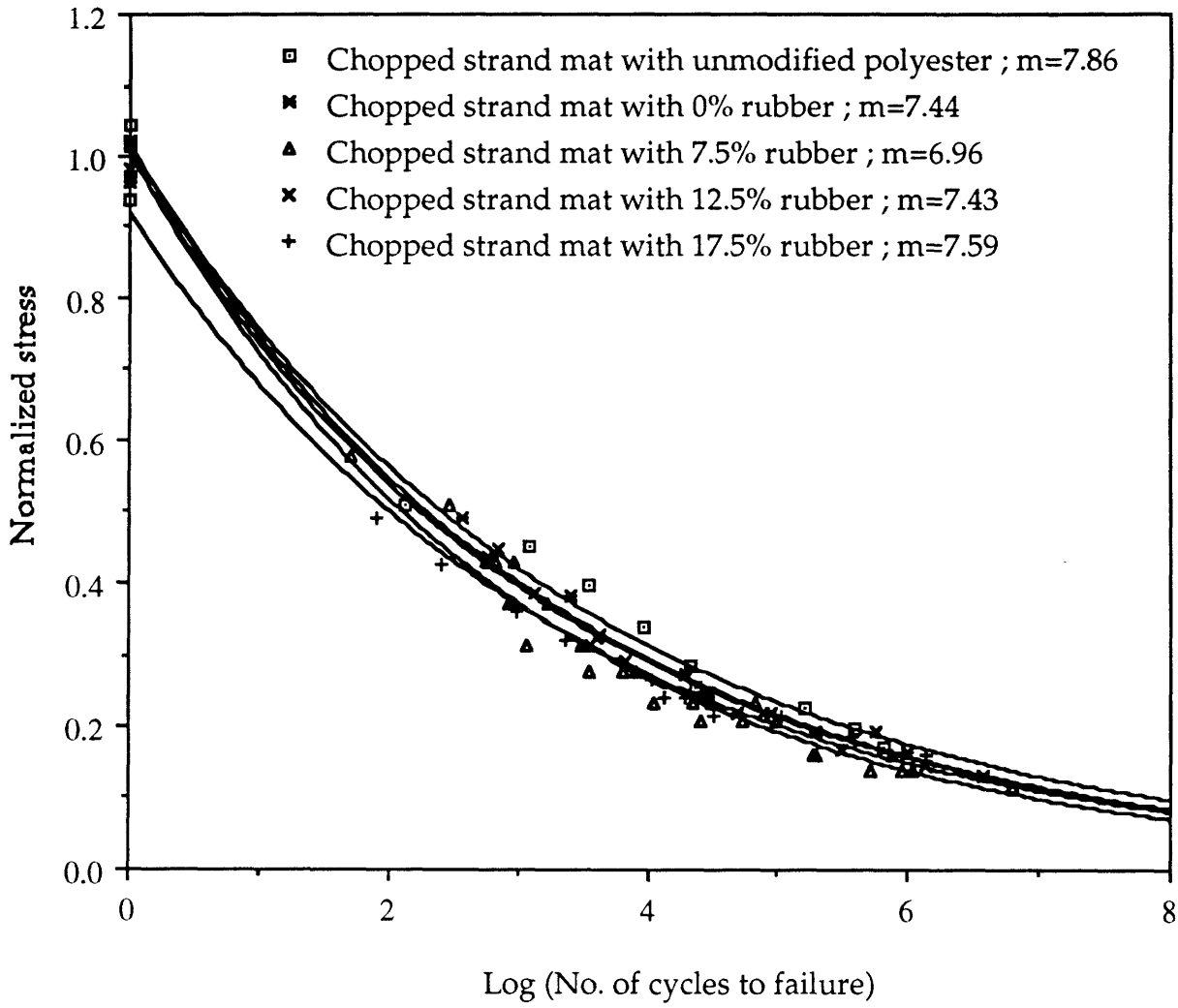

Fig : 22 : Comparison of normalized stress S-N curves for Chopped strand mat with unmodified polyester, with 0%, 7.5%, 12.5% and 17.5% rubber

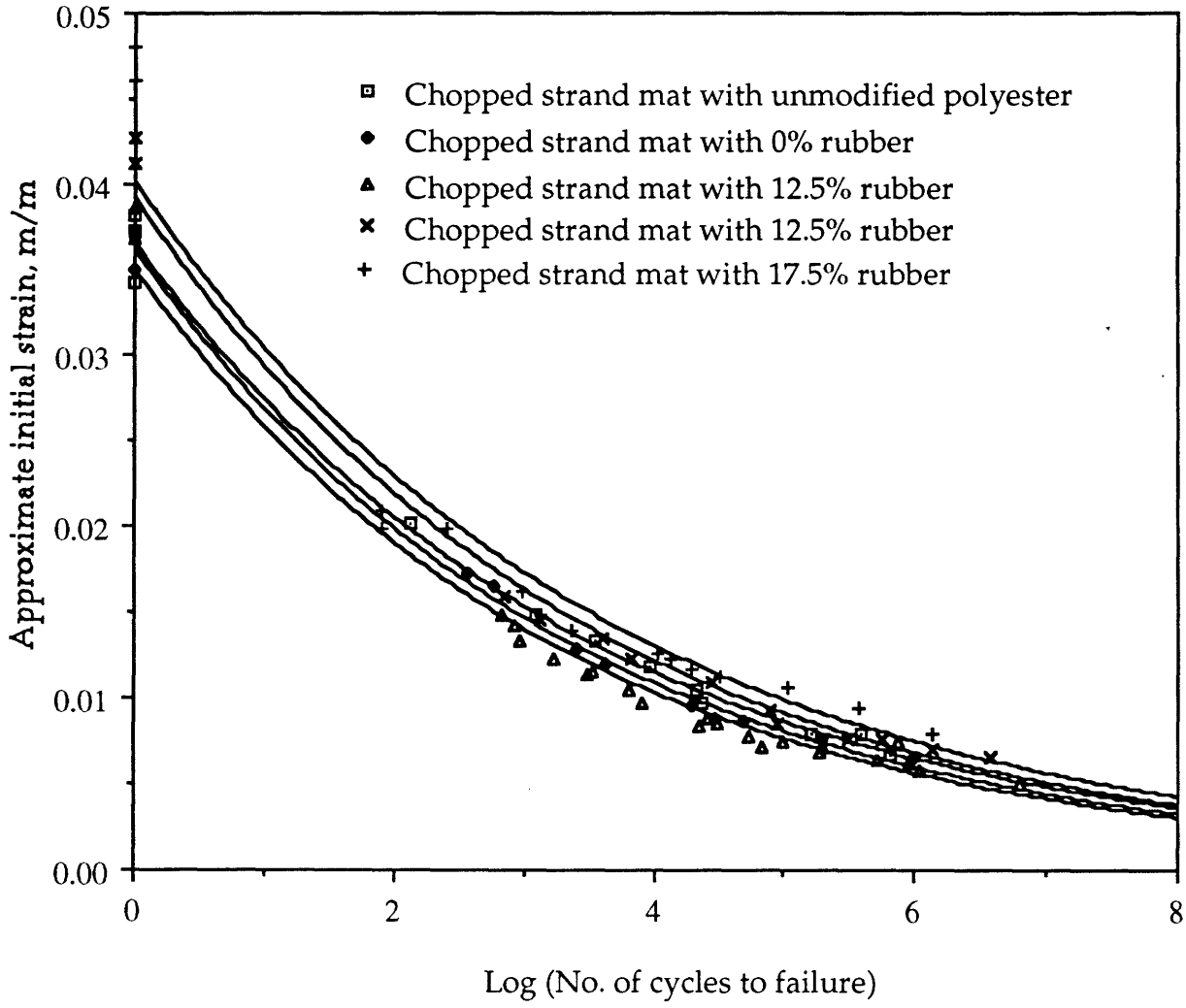

Fig : 23 : Comparison of initial strain-N curves for all Chopped strand mat with unmodified polyester, with 0%, 7.5%, 12.5% and 17.5% rubber.

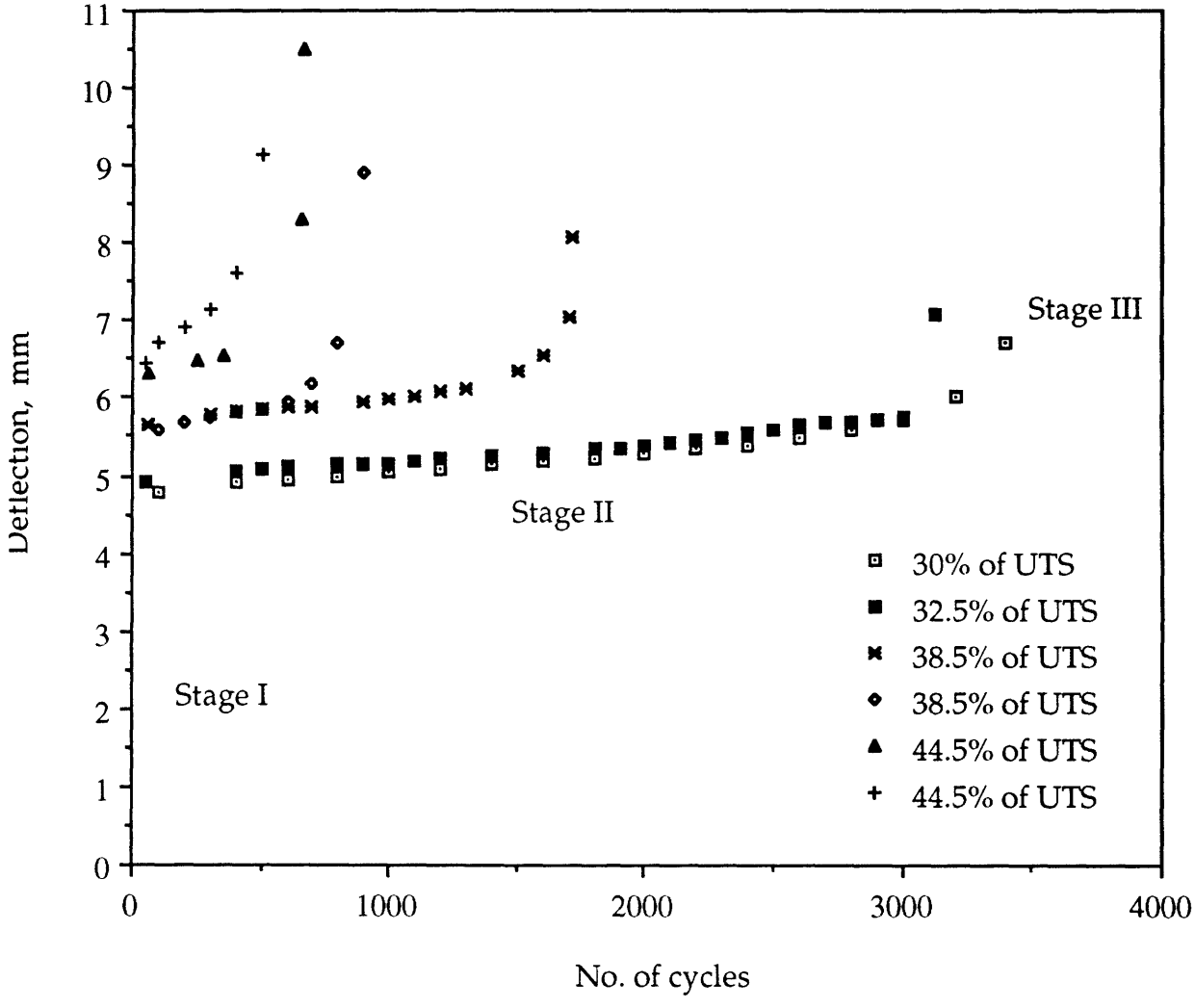

Fig : 24 : Deflection Vs. No. of cycles curve for chopped strand mat/MNS with 7.5% rubber

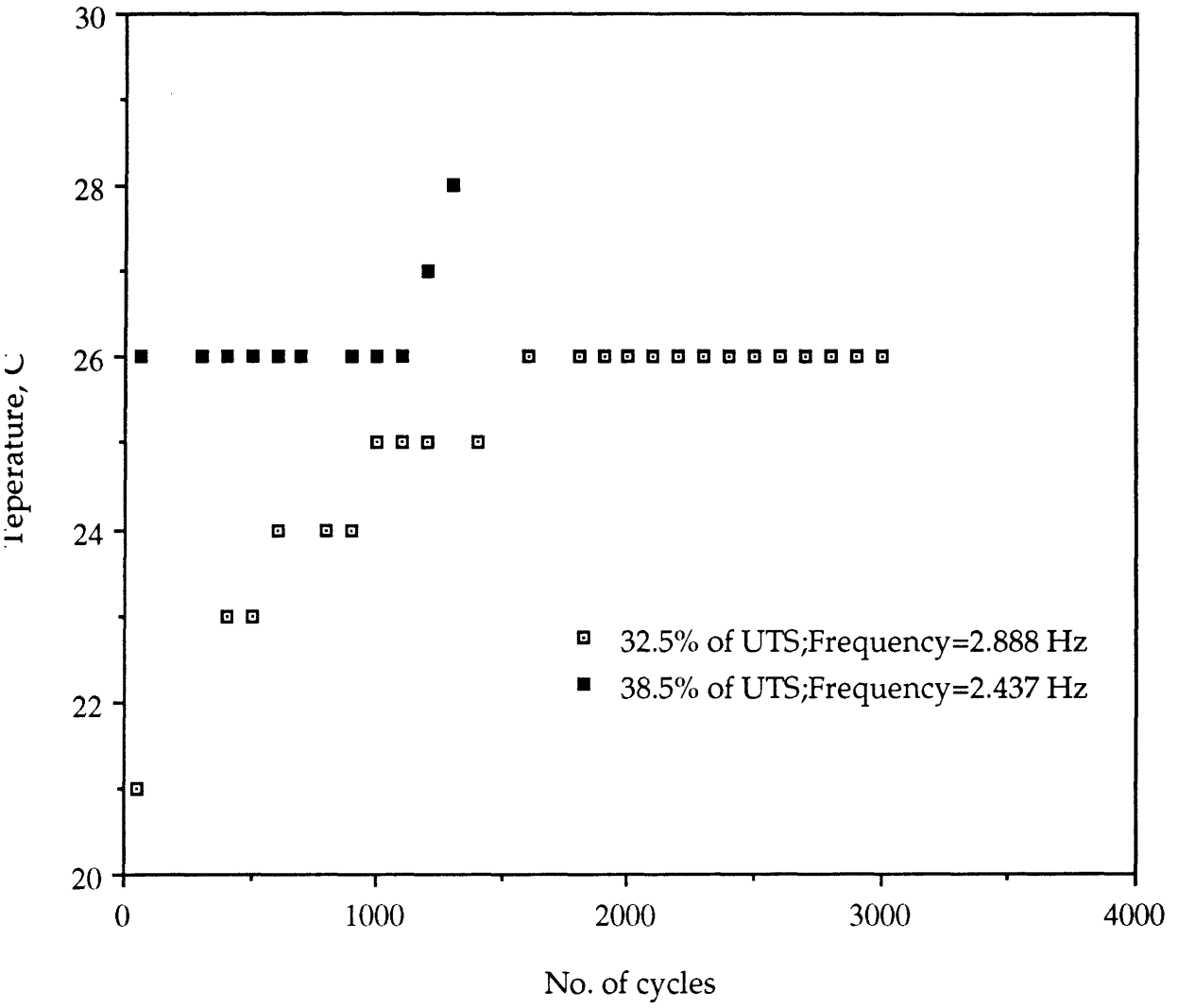

Fig : 25 : Temperature Vs. No. of cycles curve for chopped strand mat/MNS with 7.5% rubber

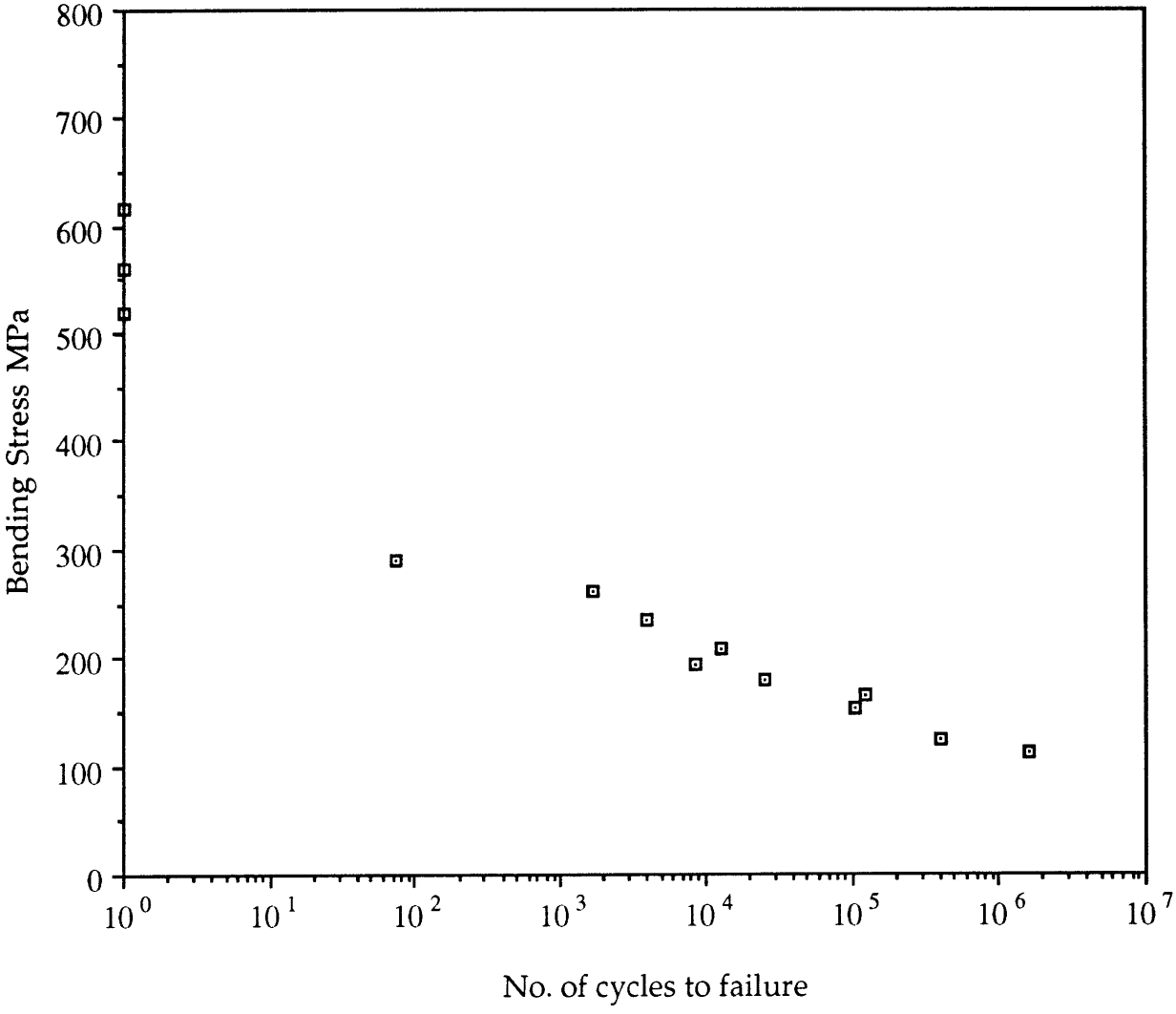

Fig : 26 : S-N curve for glass fabric (181)/unmodified polyester, R=-1

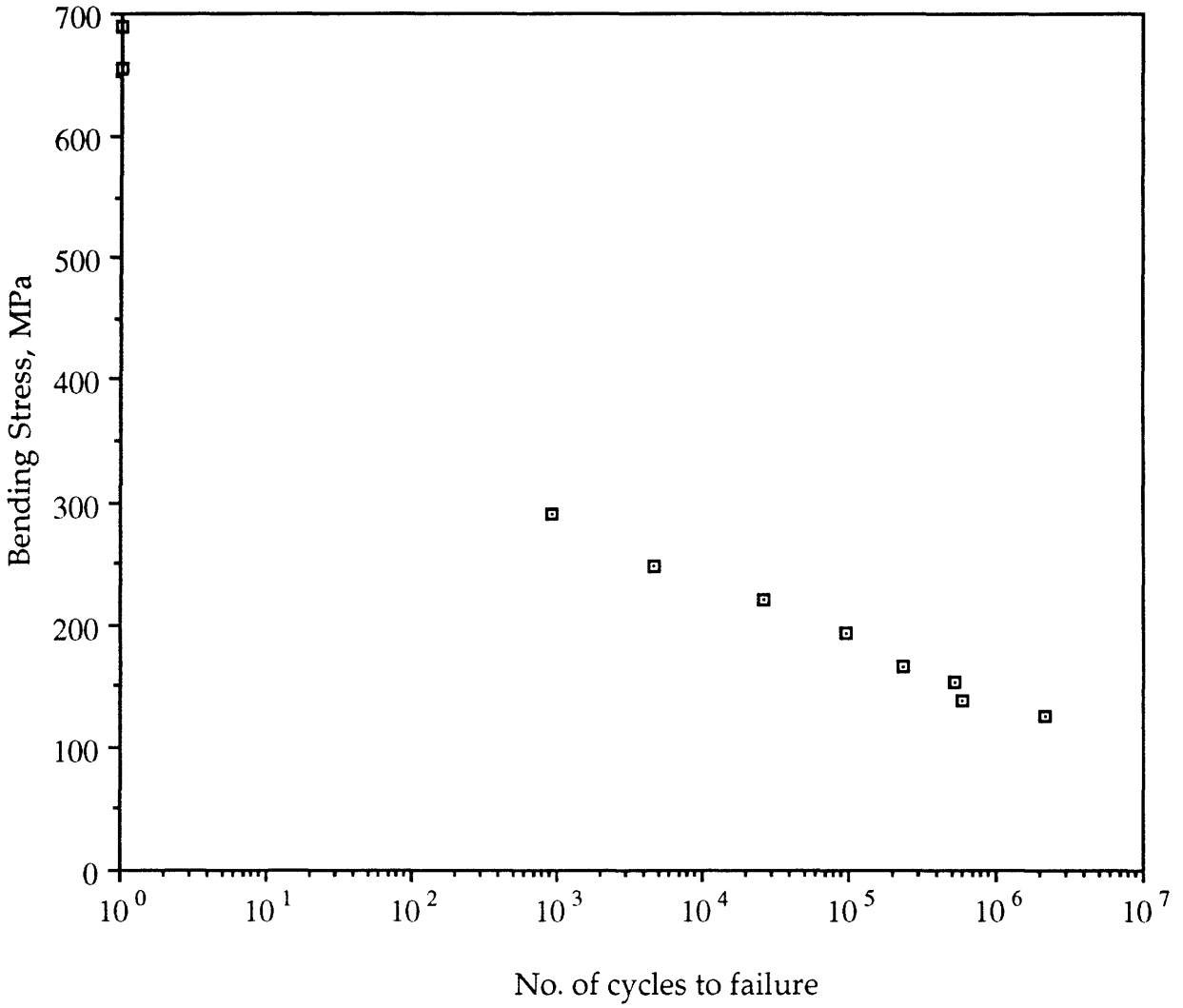

Fig : 27 : S-N curves for glass fabric (181)/MNS with 0% rubber, R=-1

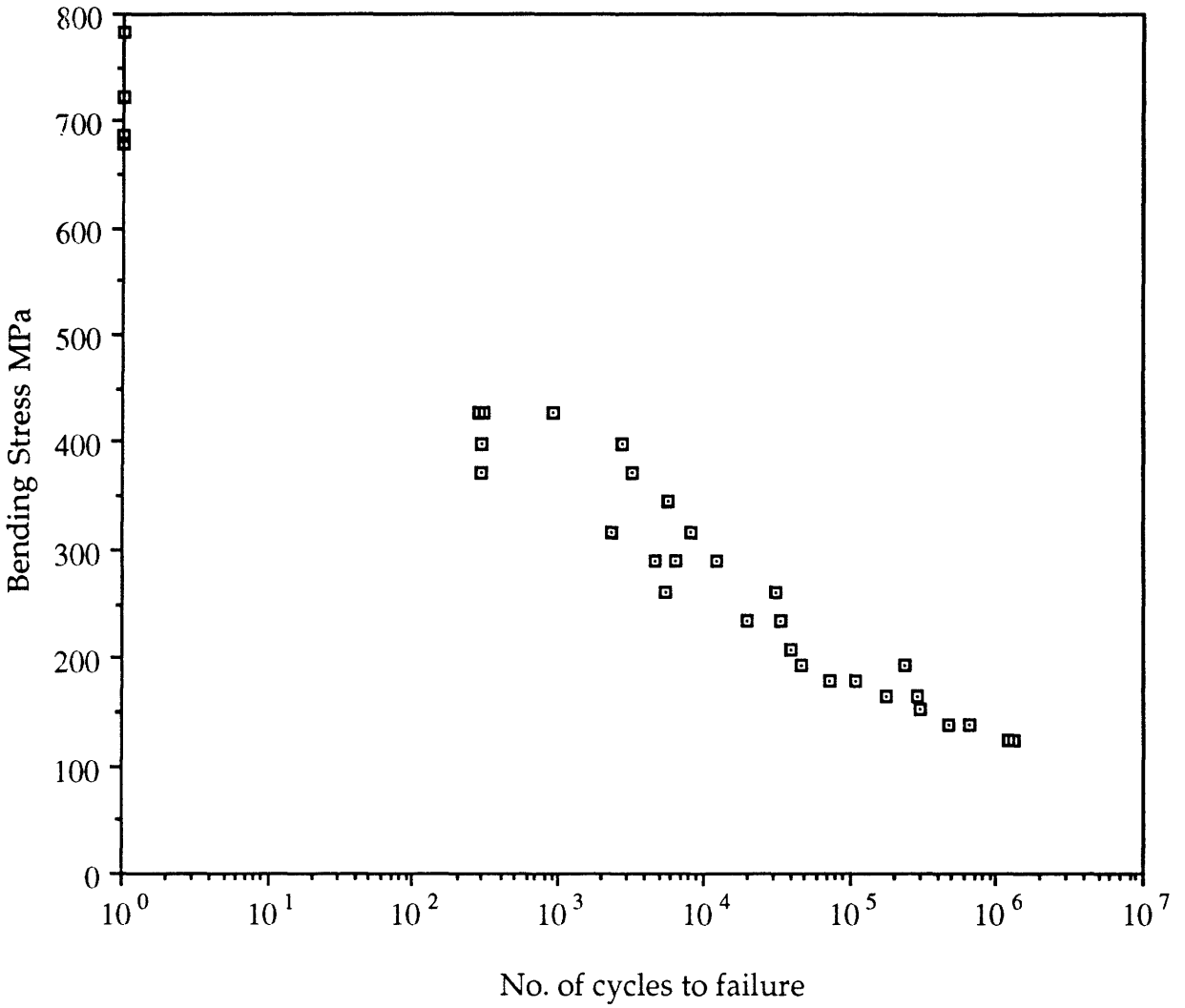

Fig : 28 : S-N curve for glass fabric (181)/MNS with 7.5% rubber, R=-1

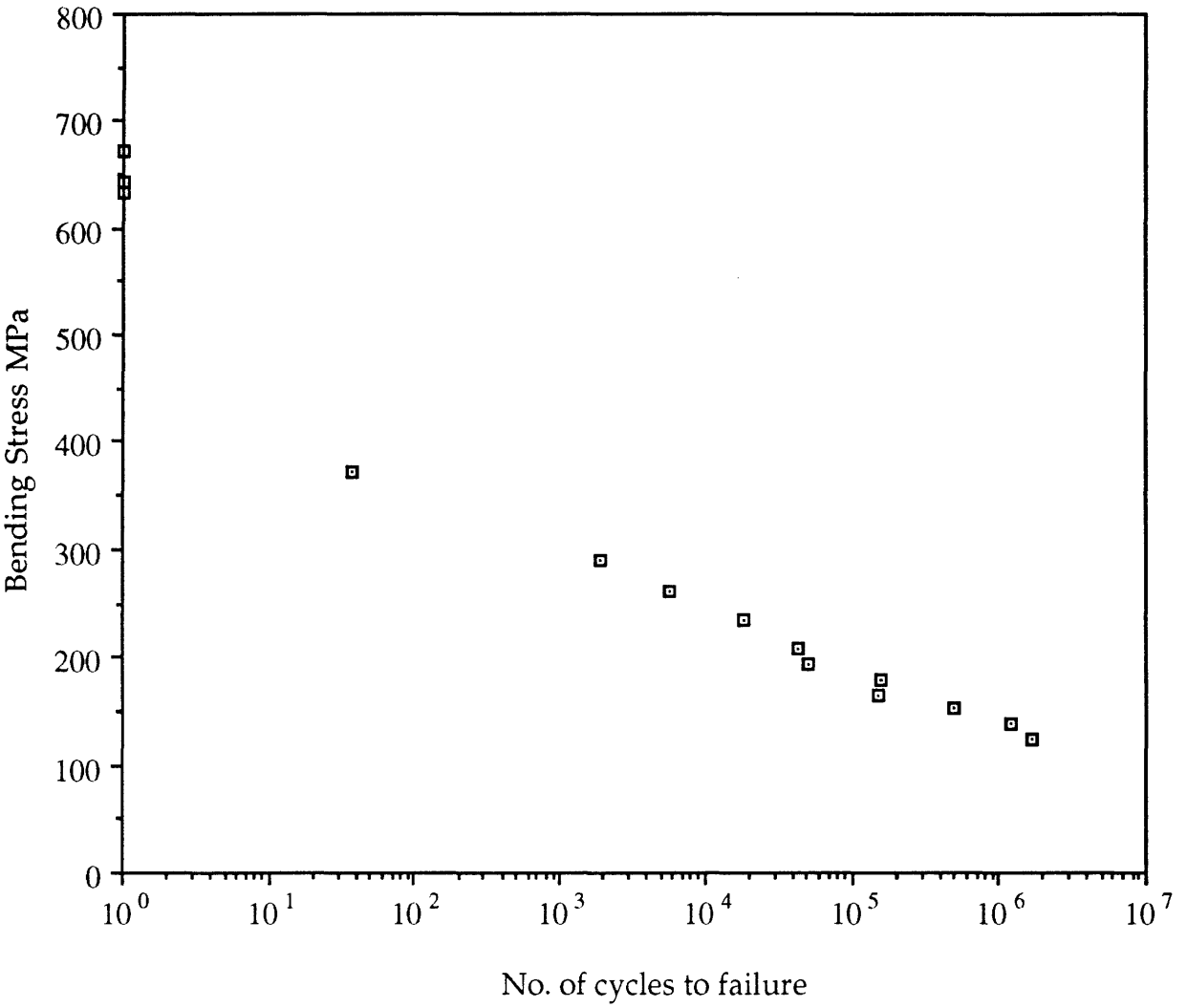

Fig : 29 : S-N curve for glass fabric (181)/MNS with 12.5% rubber, R=-1

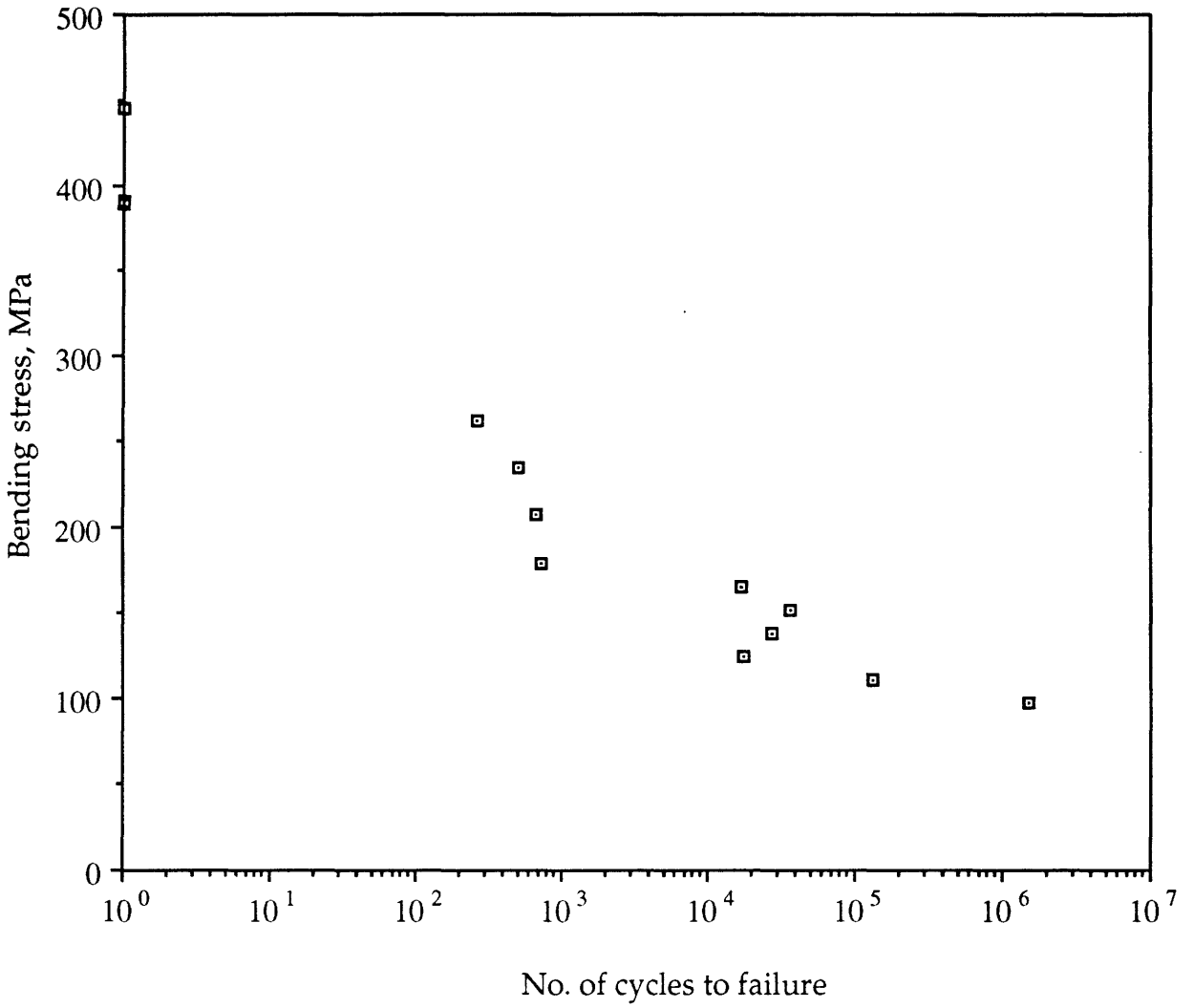

Fig : 30 : S-N curve for glass fabric (181)/MNS with 17.5% rubber, R=-1

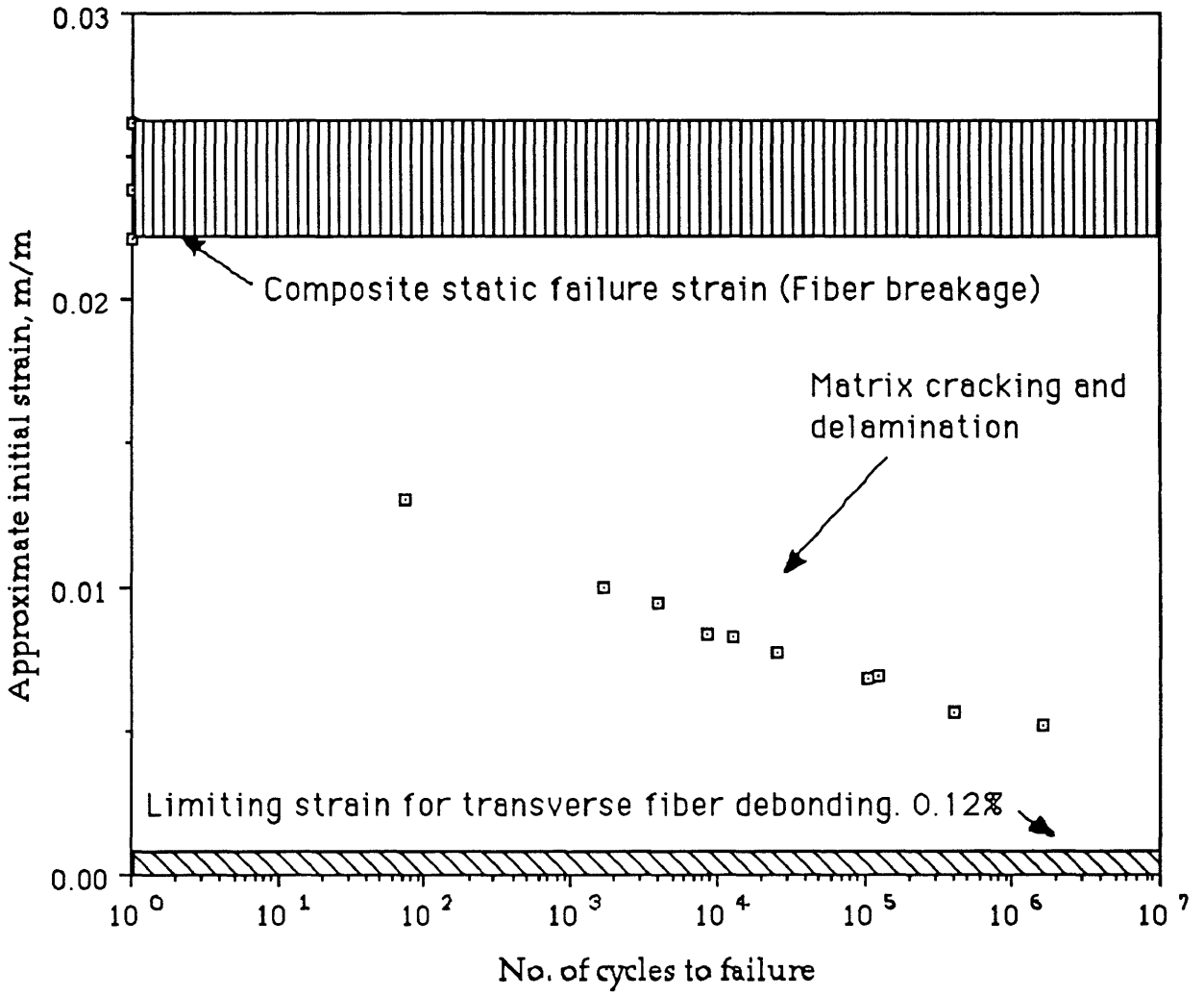

Fig : 31 : Strain-N curve for glass fabric/unmodified polyester, R=-1

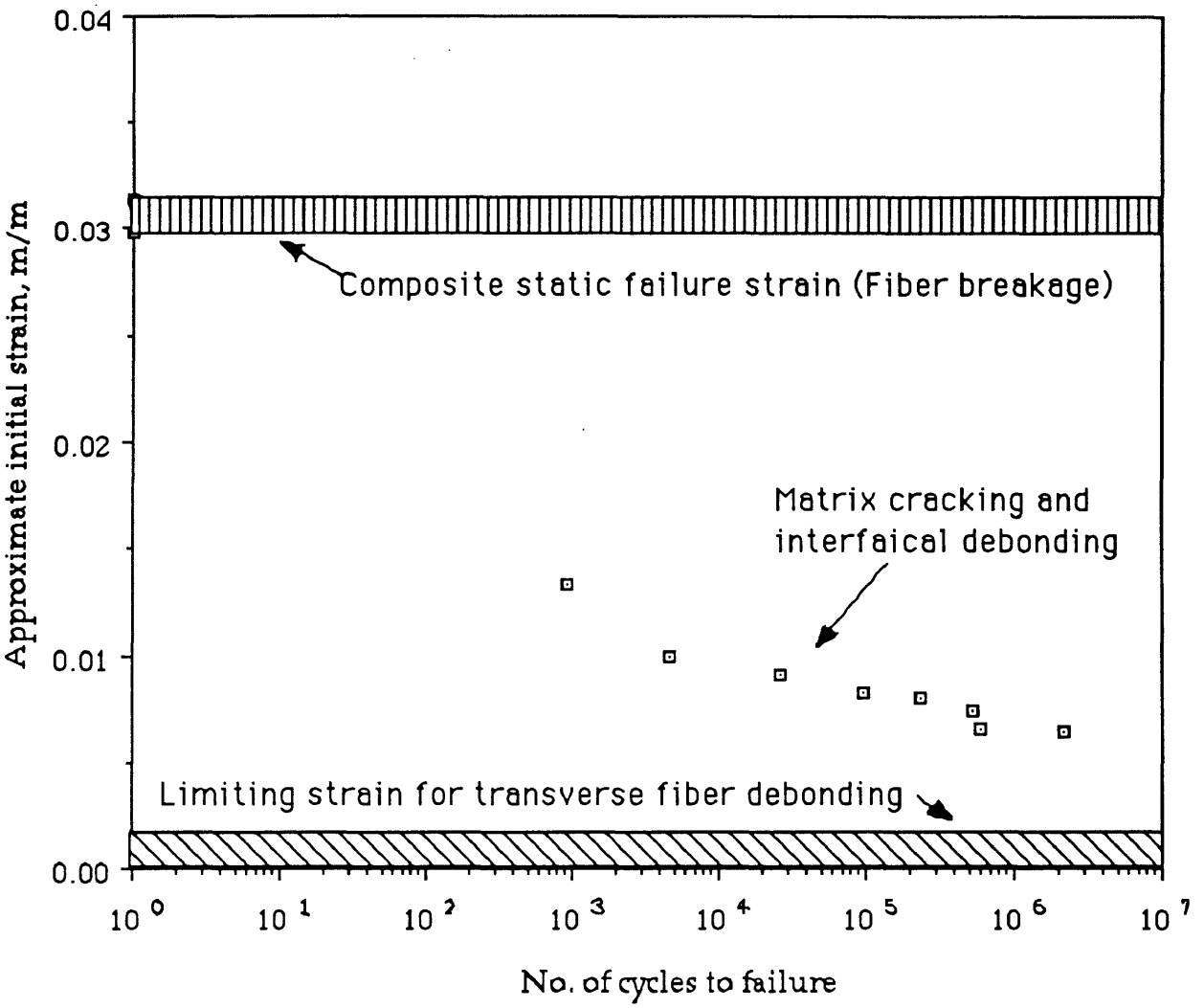

Fig : 32 : Strain-N curve for glass fabric/MNS with 0% rubber, R=-1

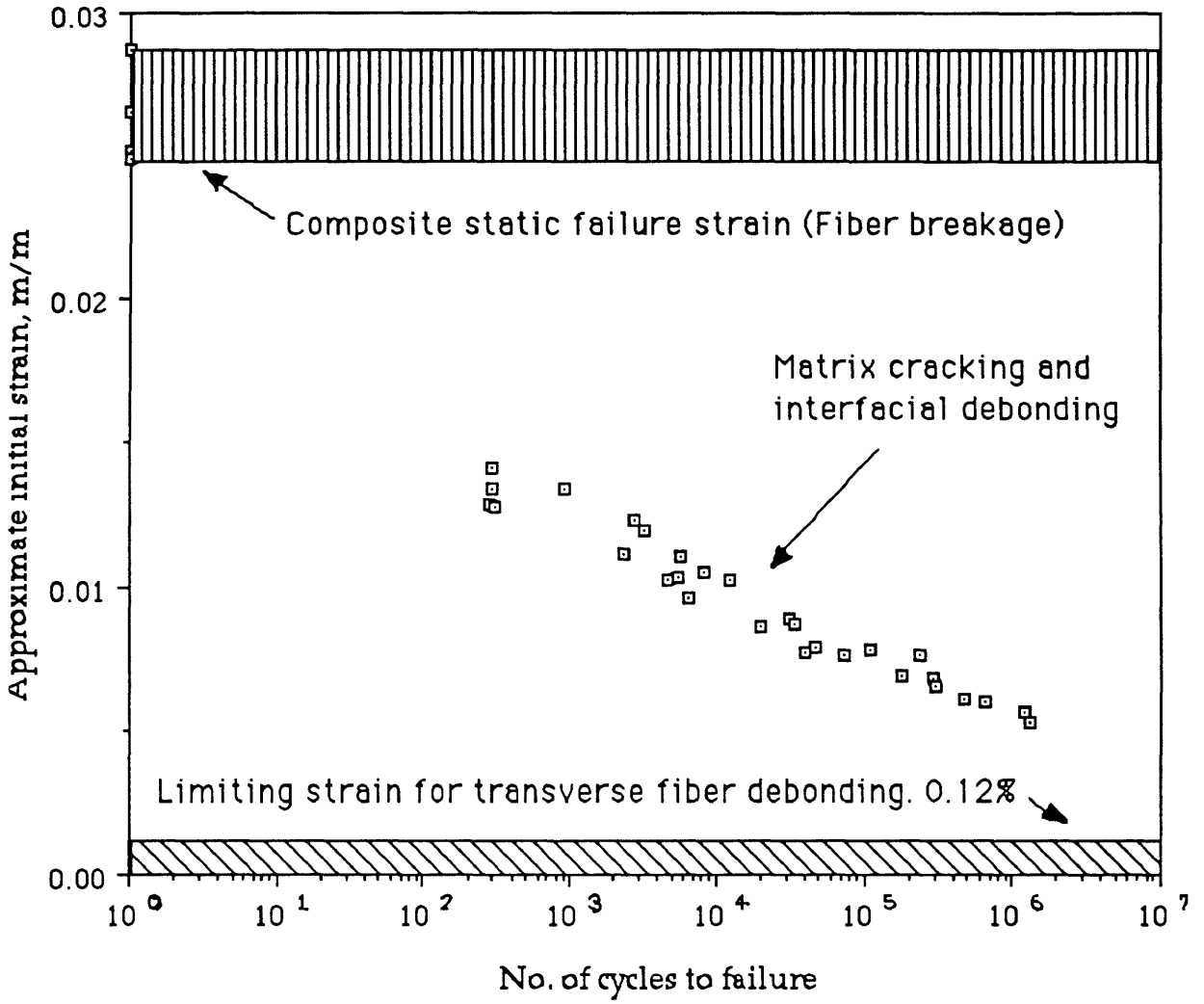

Fig : 33 : Strain-N curve for glass fabric/MNS with 7.5% rubber, R=-1

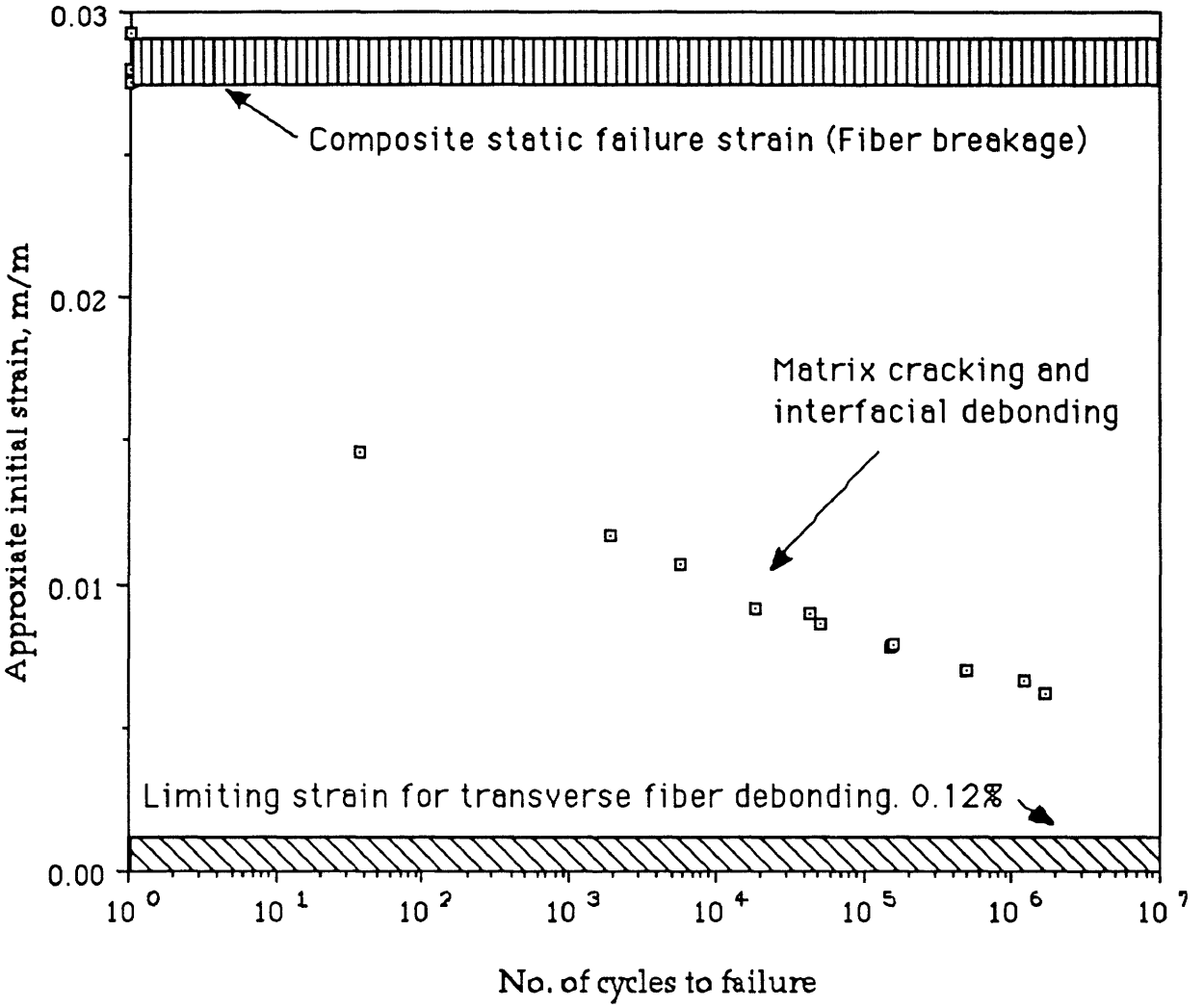

Fig : 34 : Strain-N curve for glass fabric/MNS with 12.5% rubber, R=-1

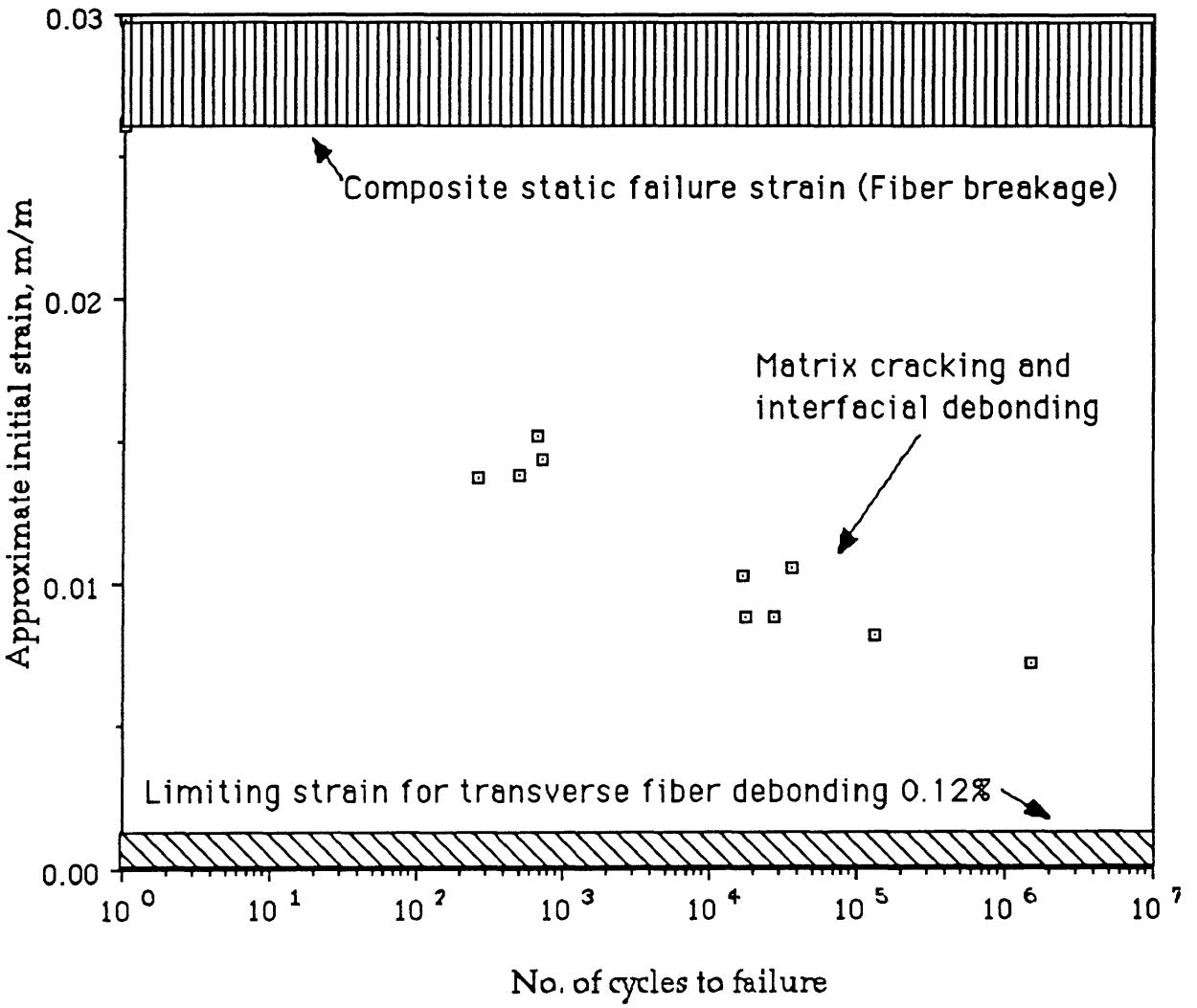

Fig : 35 : Strain-N curve for glass fabric (181)/MNS with 17.5% rubber, R=-1

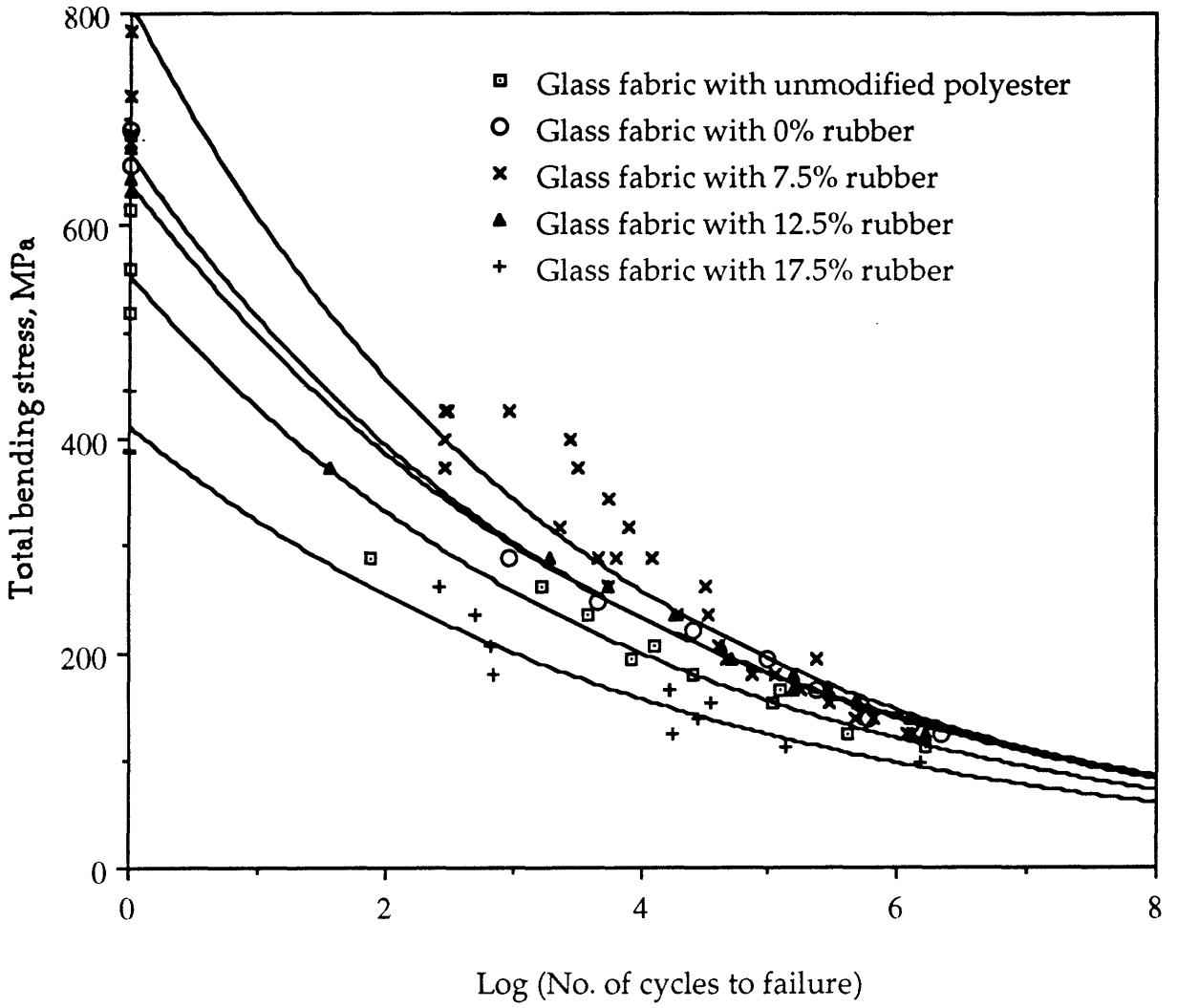

Fig : 36 : Comparison of total stress S-N curves for glass fabric with unmodified polyester, MNS with 0%, 7.5%, 12.5% and 17.5% rubber, R=-1

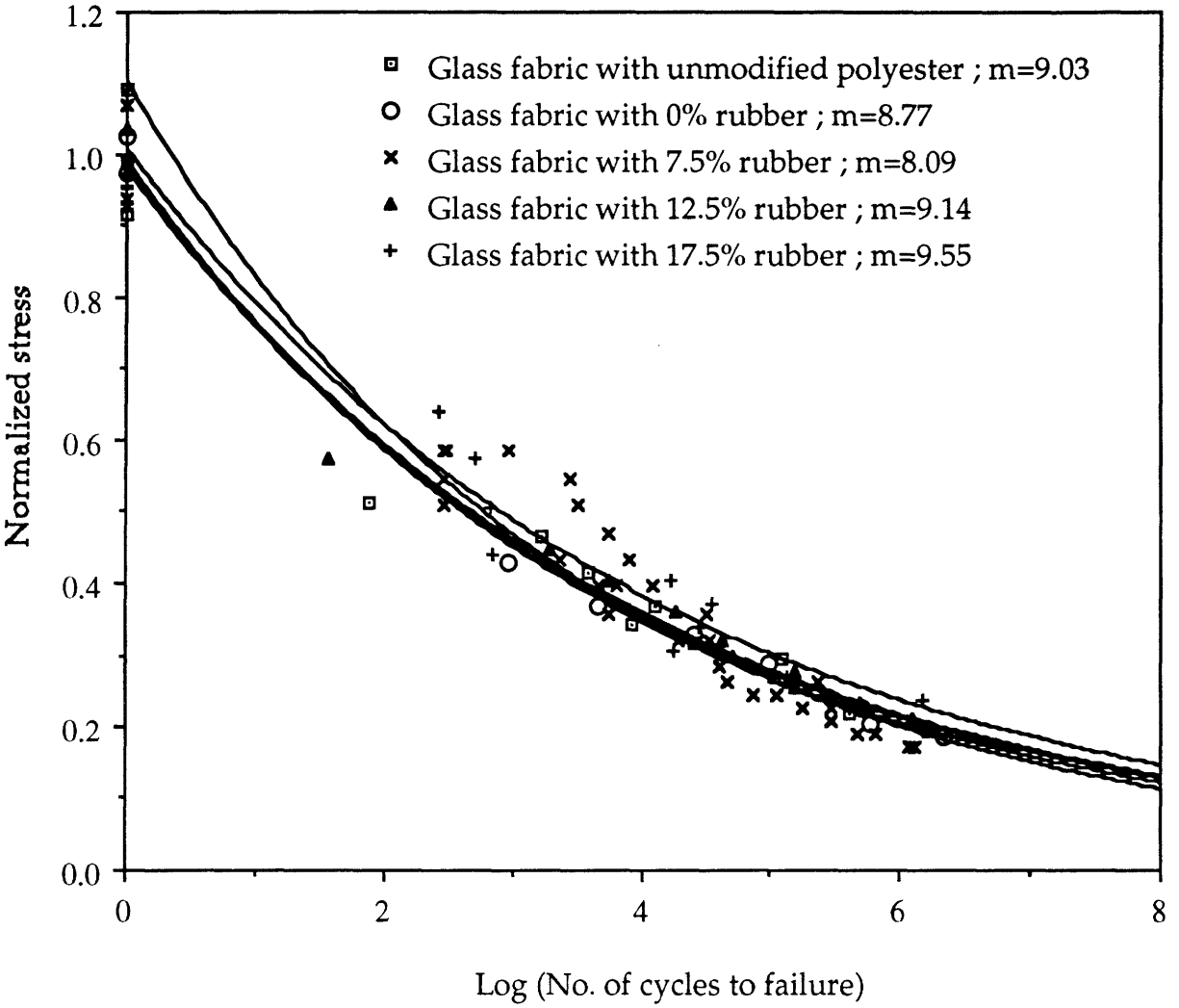

Fig : 37 : Comparison of normalized stress S-N curves for glass faric with un-modified polyester, MNS with 0%, 7.5%, 12.5% and 17.5% rubber, R=-1

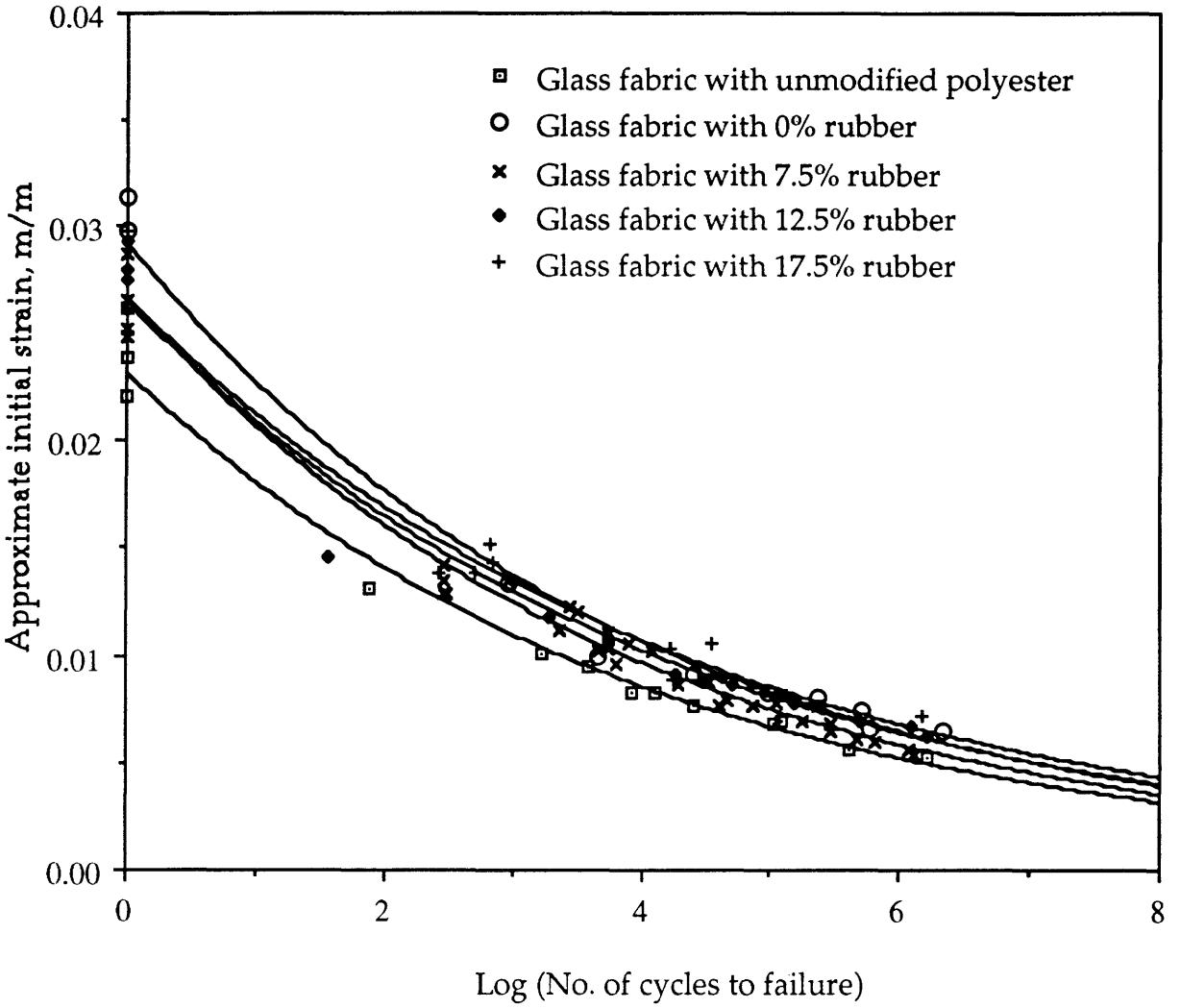

Fig : 38 : Comparison of initial strain-N curves for glass fabric with un-modified polyester, MNS with 0%, 7.5%, 12.5% and 17.5% rubber, R=-1

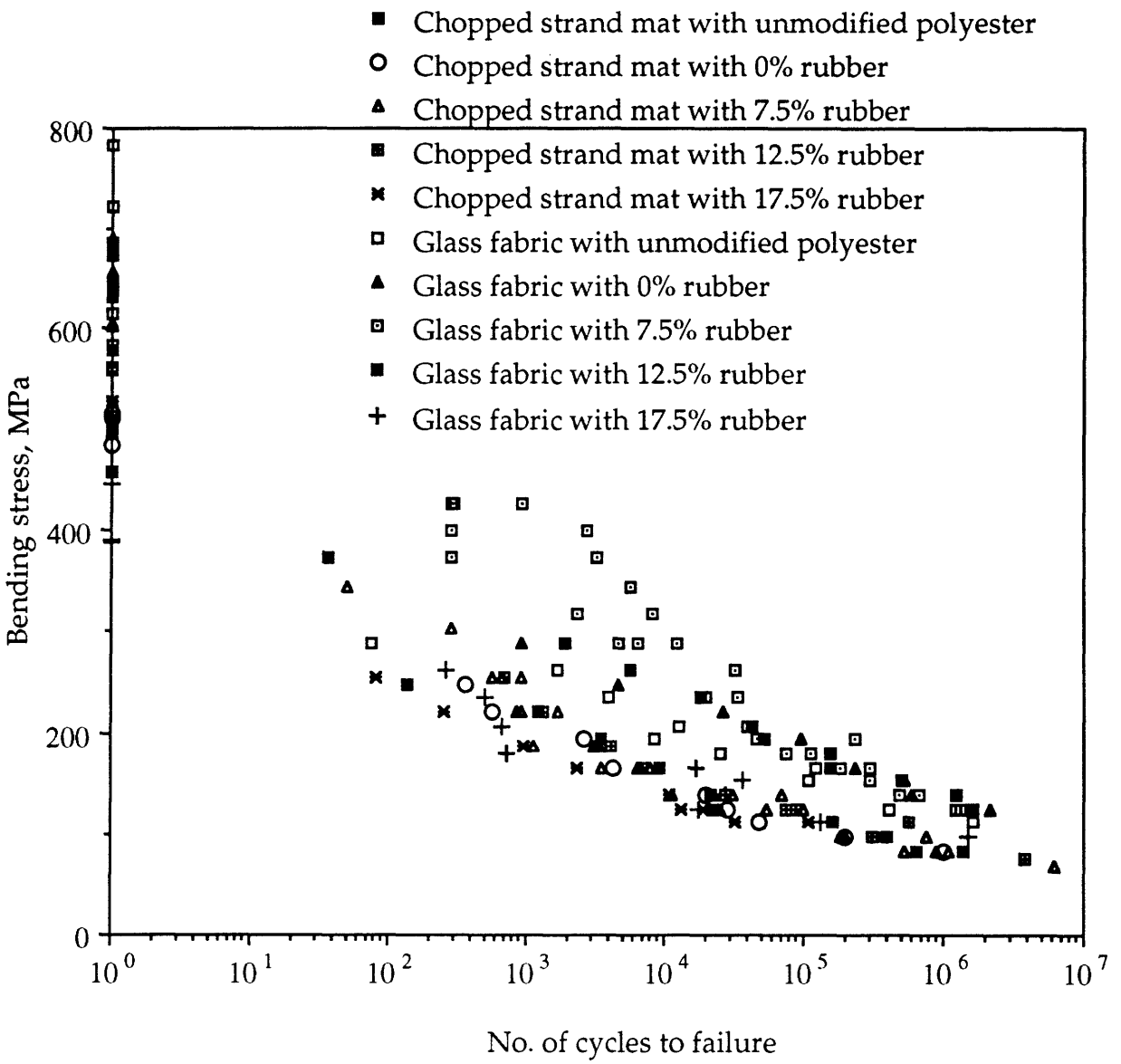

Fig : 39 : Comparison of total stress S-N curves for all Chopped strand mat composites and Glass fabric composites

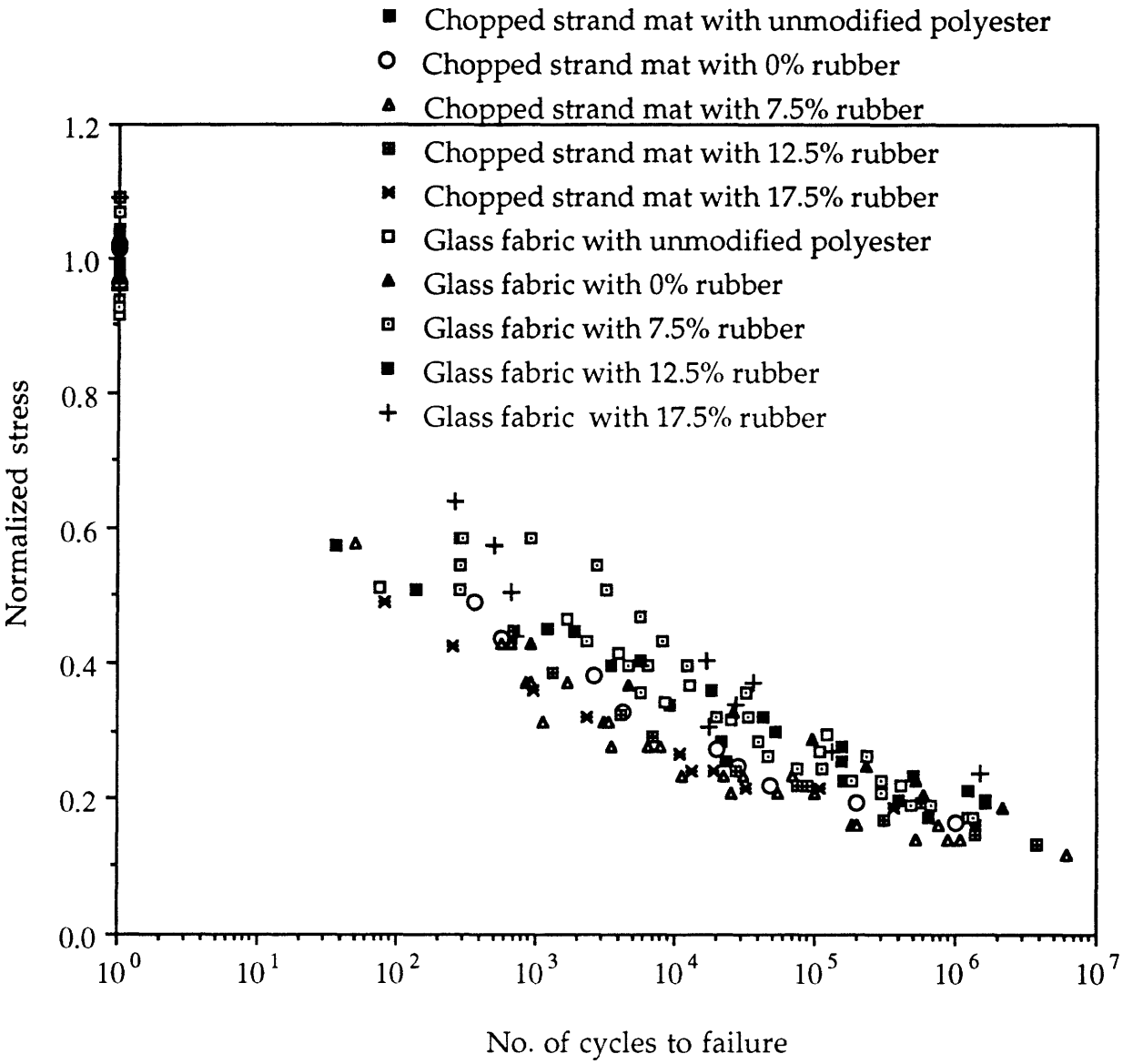

Fig : 40 : Comparison of normalized stress S-N curves for all Chopped strand mat composites and Glass fabric composites

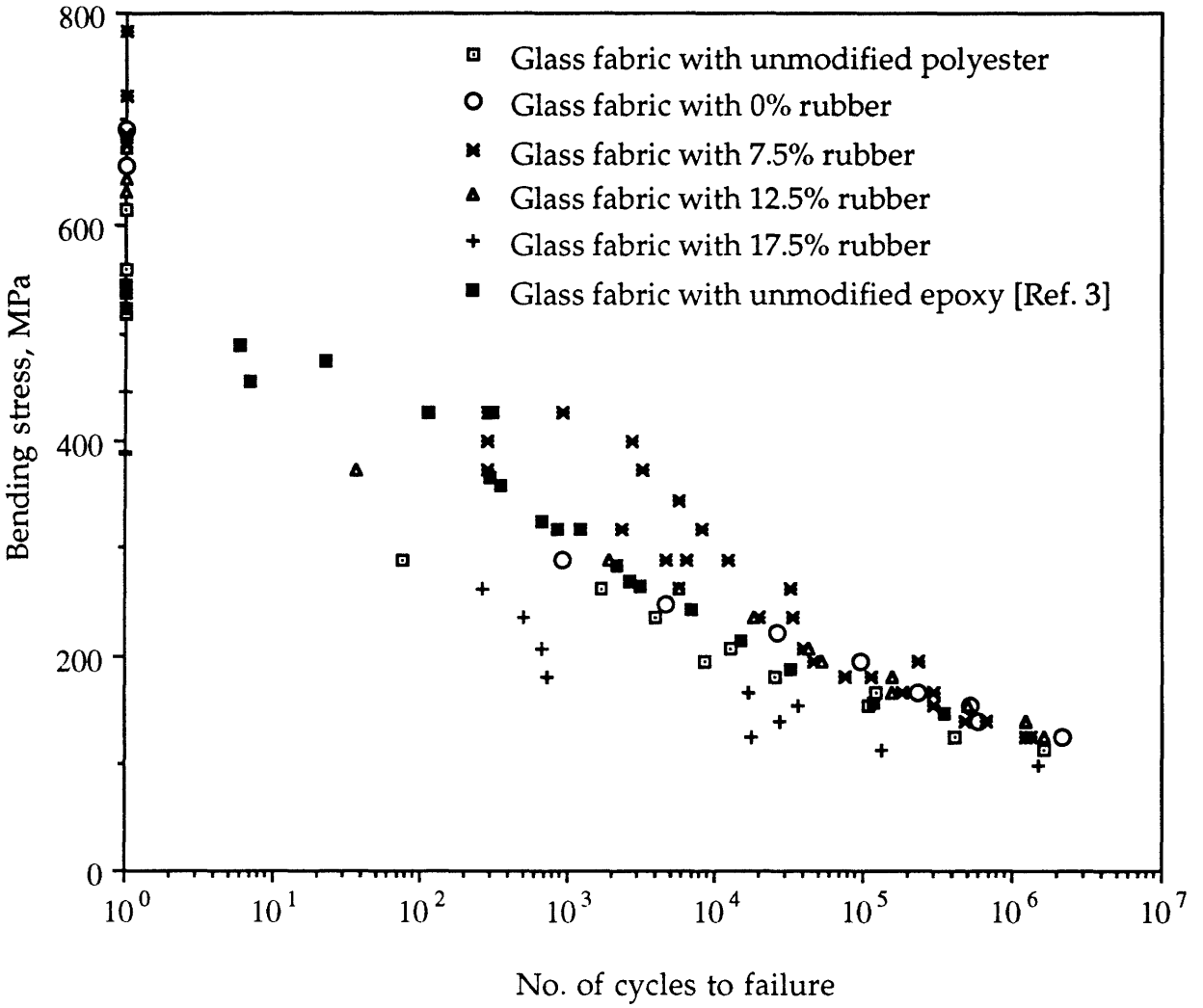

Fig : 41 : Comparison of total stress S-N curve for glass fabric (7688) with epoxy [Ref. 3] to the S-N curves for glass fabric (181) with unmodified polyester, MNS with 0%, 7.5%, 12.5% and 17.5% rubber, R=-1

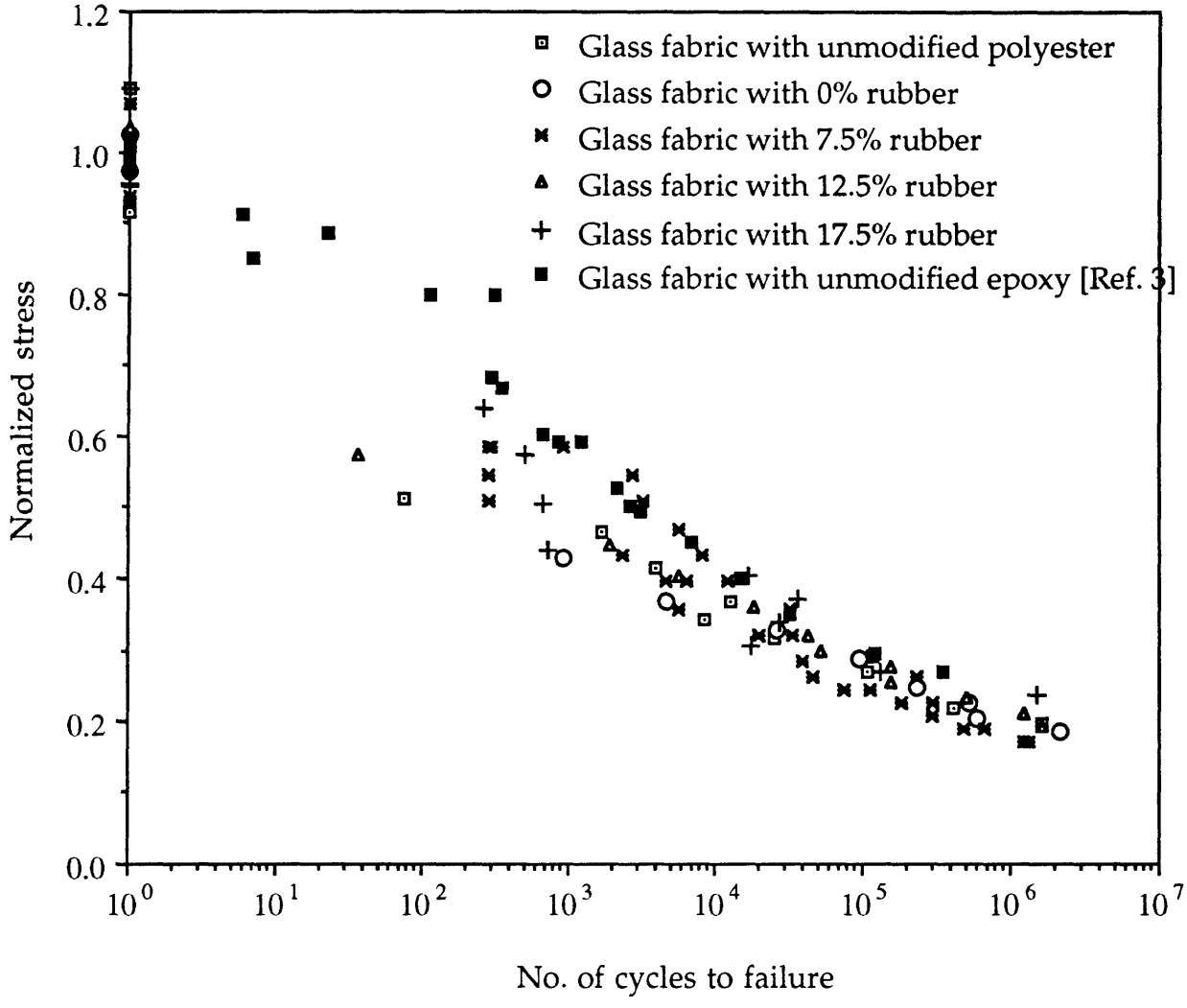

Fig : 42 : Comparison of normalized stress S-N curve for glass fabric (7688) with epoxy [Ref. 3] to the S-N curves for glass fabric (181) with unmodified polyester, MNS with 0%, 7.5%, 12.5% and 17.5% rubber, R=-1.

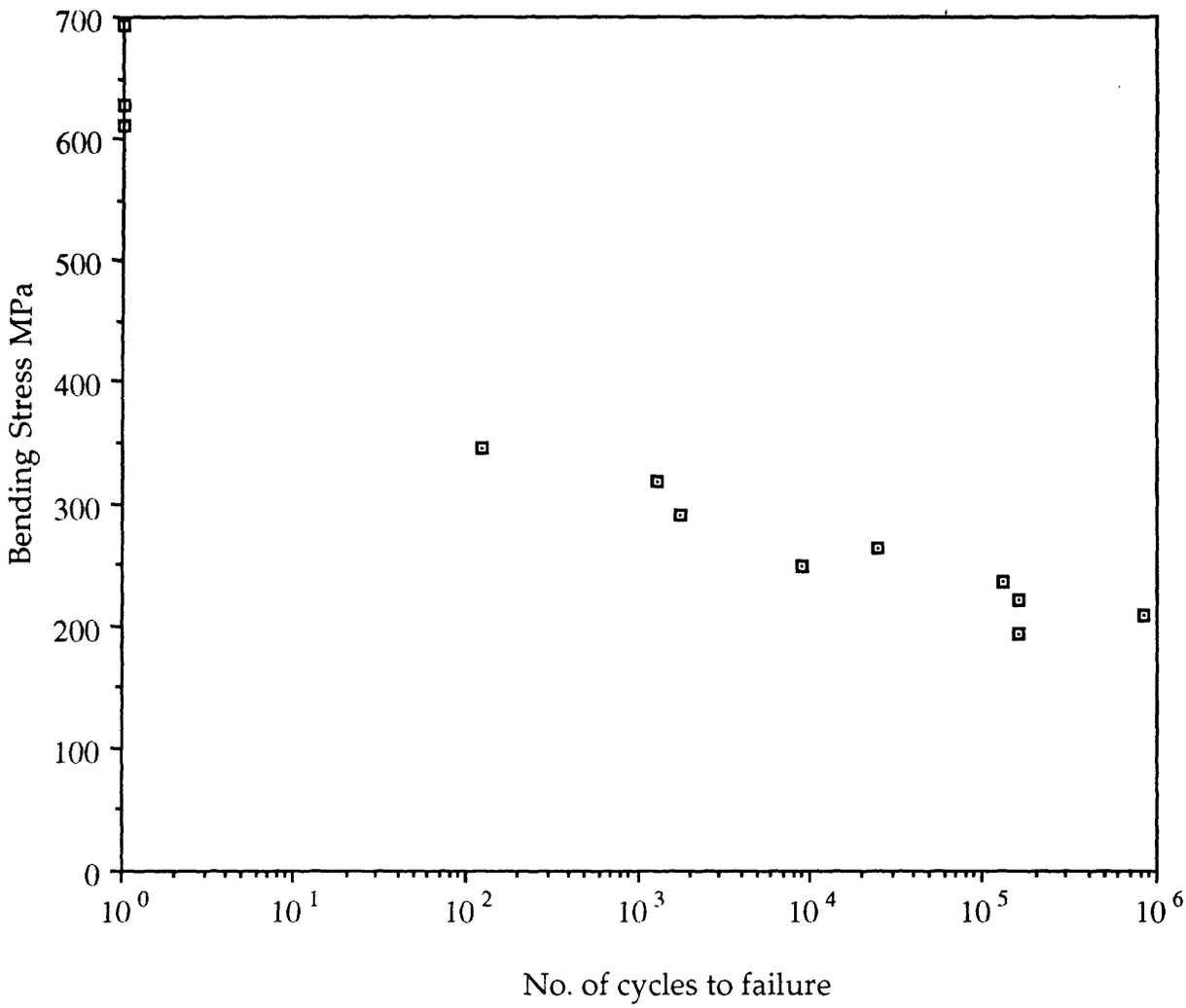

Fig : 43 : S-N curve for carbon fabric/unmodified polyester, R=-1

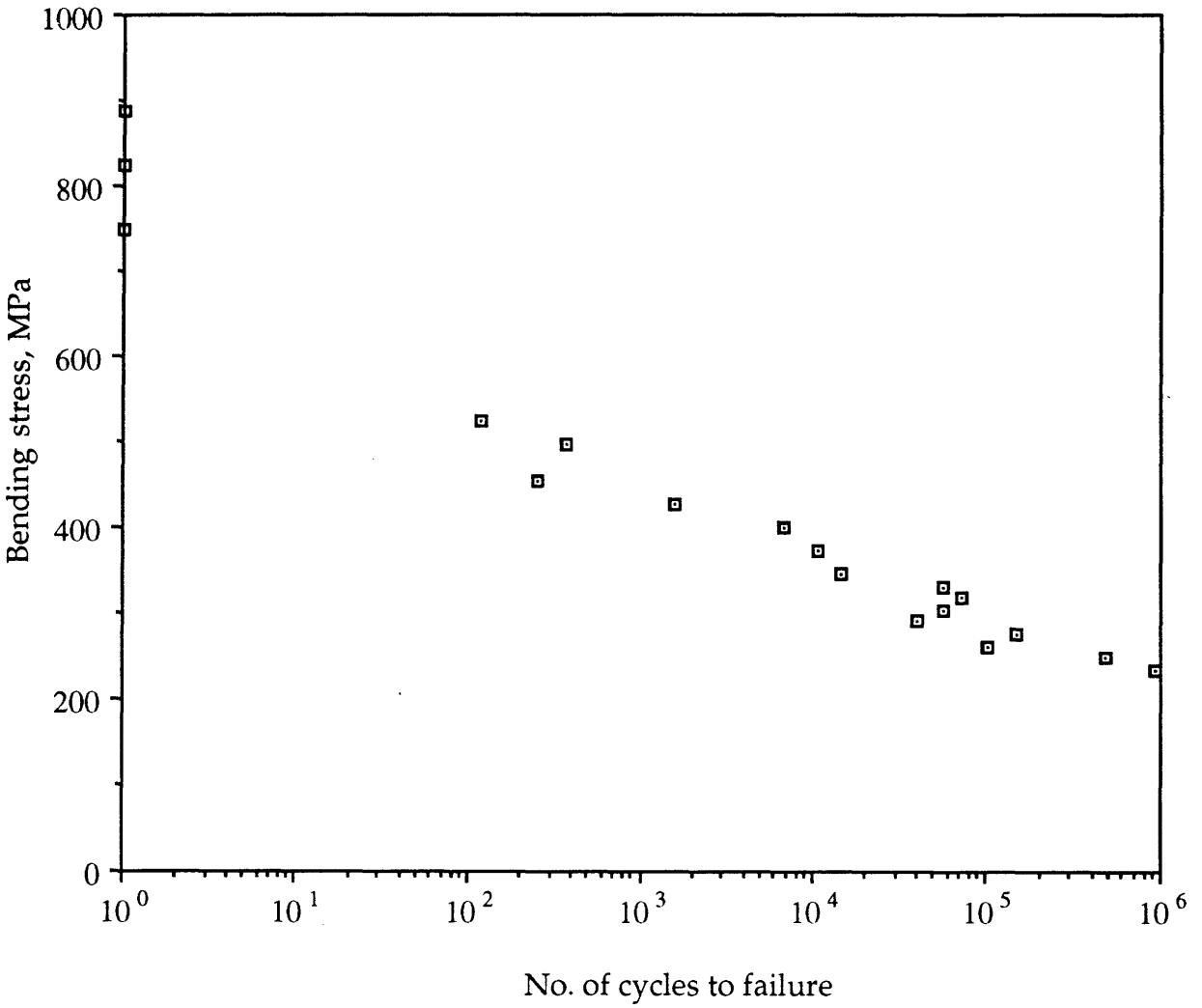

Fig : 44 : S-N curve for carbon fabric/MNS with 0% rubber, R=-1

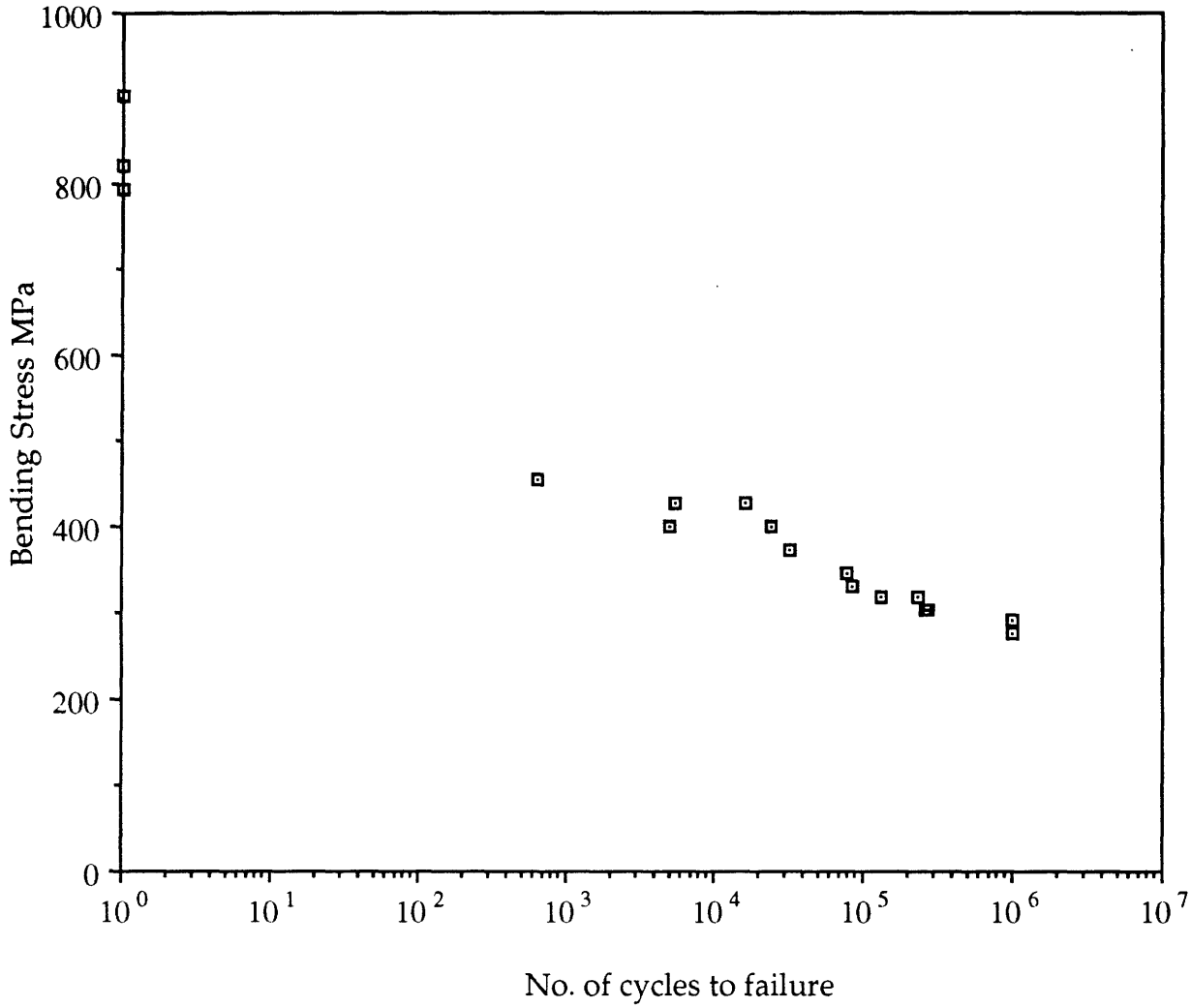

Fig : 45 : S-N curves for carbon fabric/MNS with 7.5% rubber, R=-1

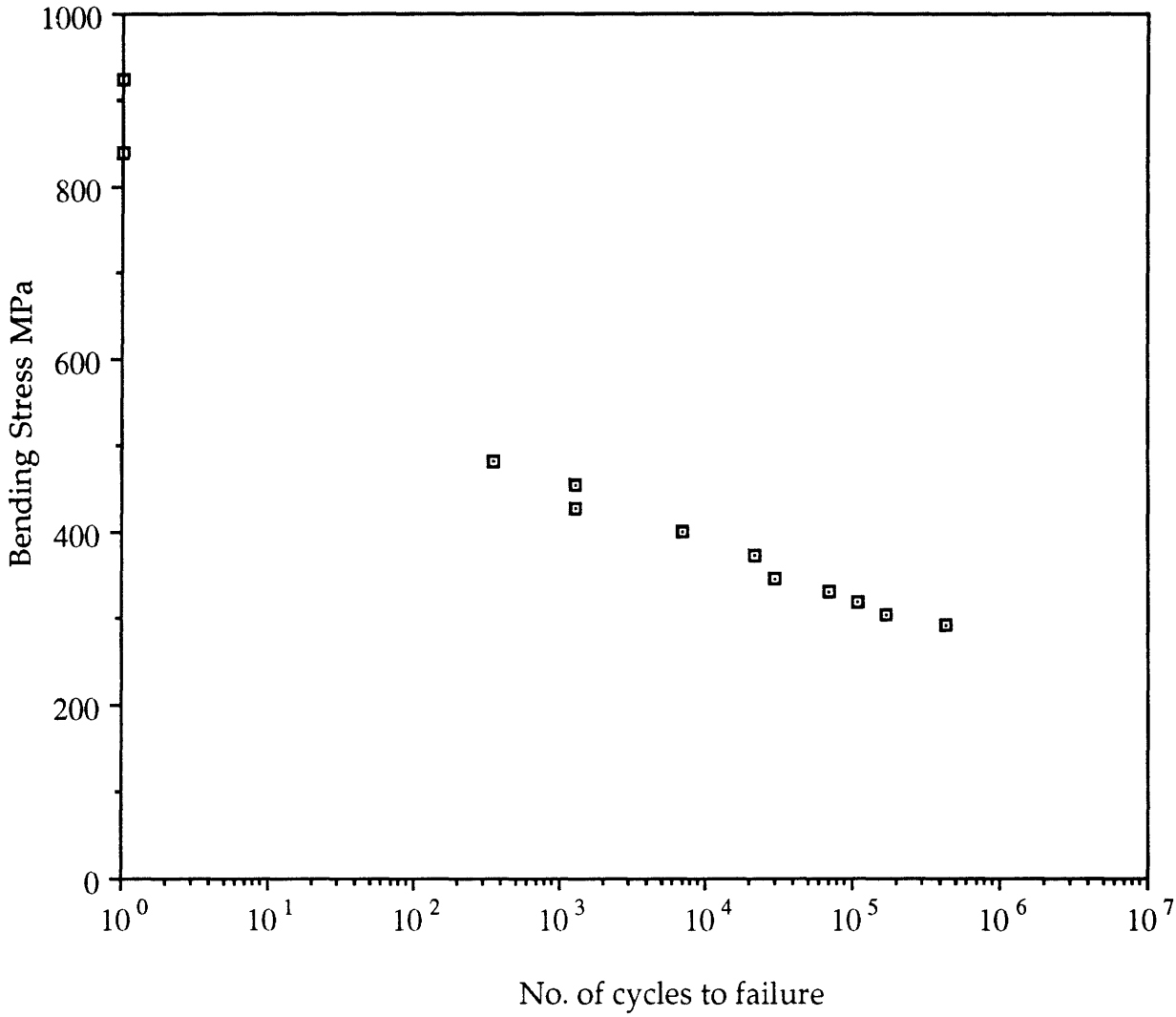

Fig : 46 : S-N curve for carbon fabric/MNS with 12.5% rubber, R=-1

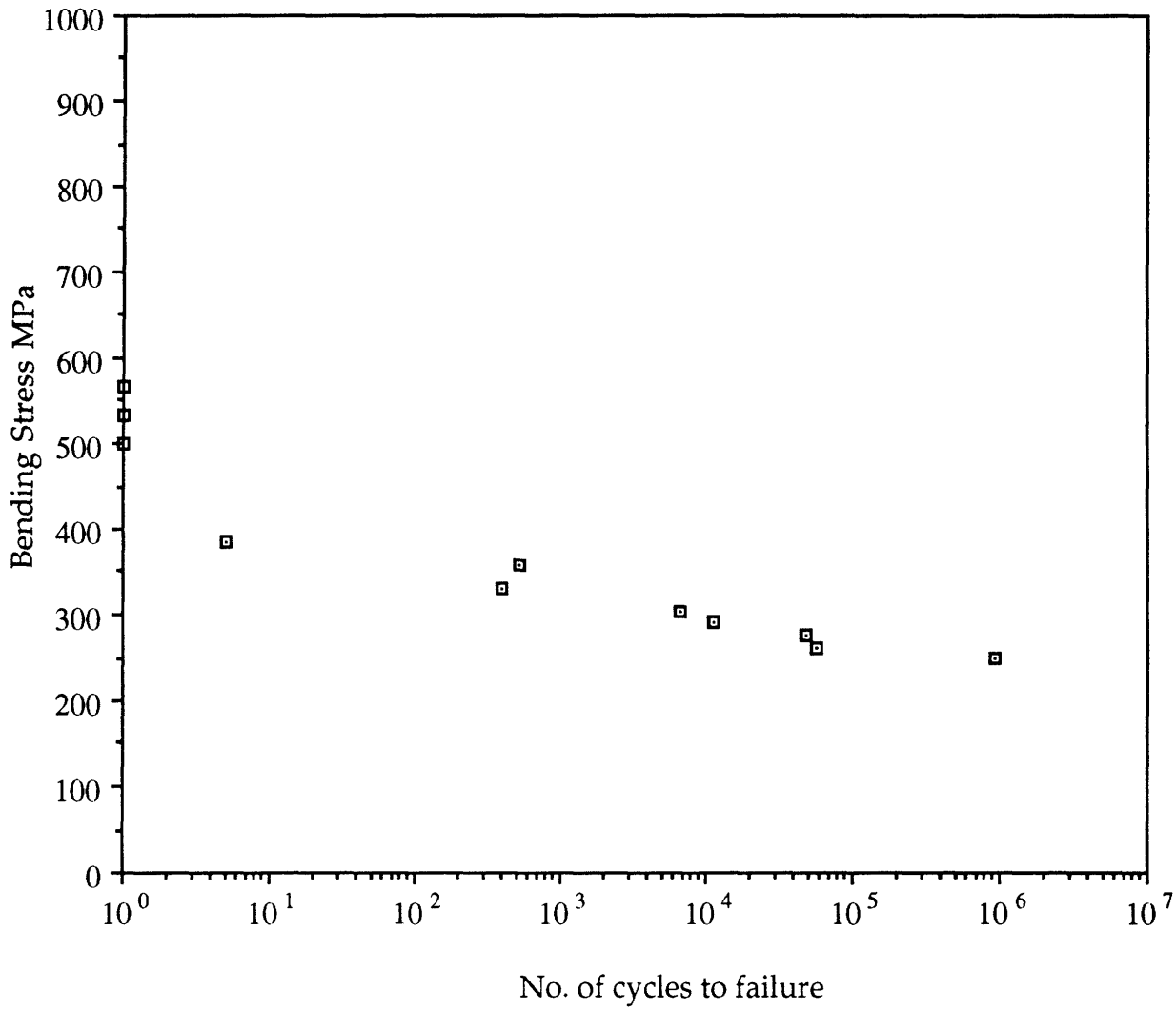

Fig : 47 : S-N curve for carbon fabric/MNS with 17.5% rubber, R=-1

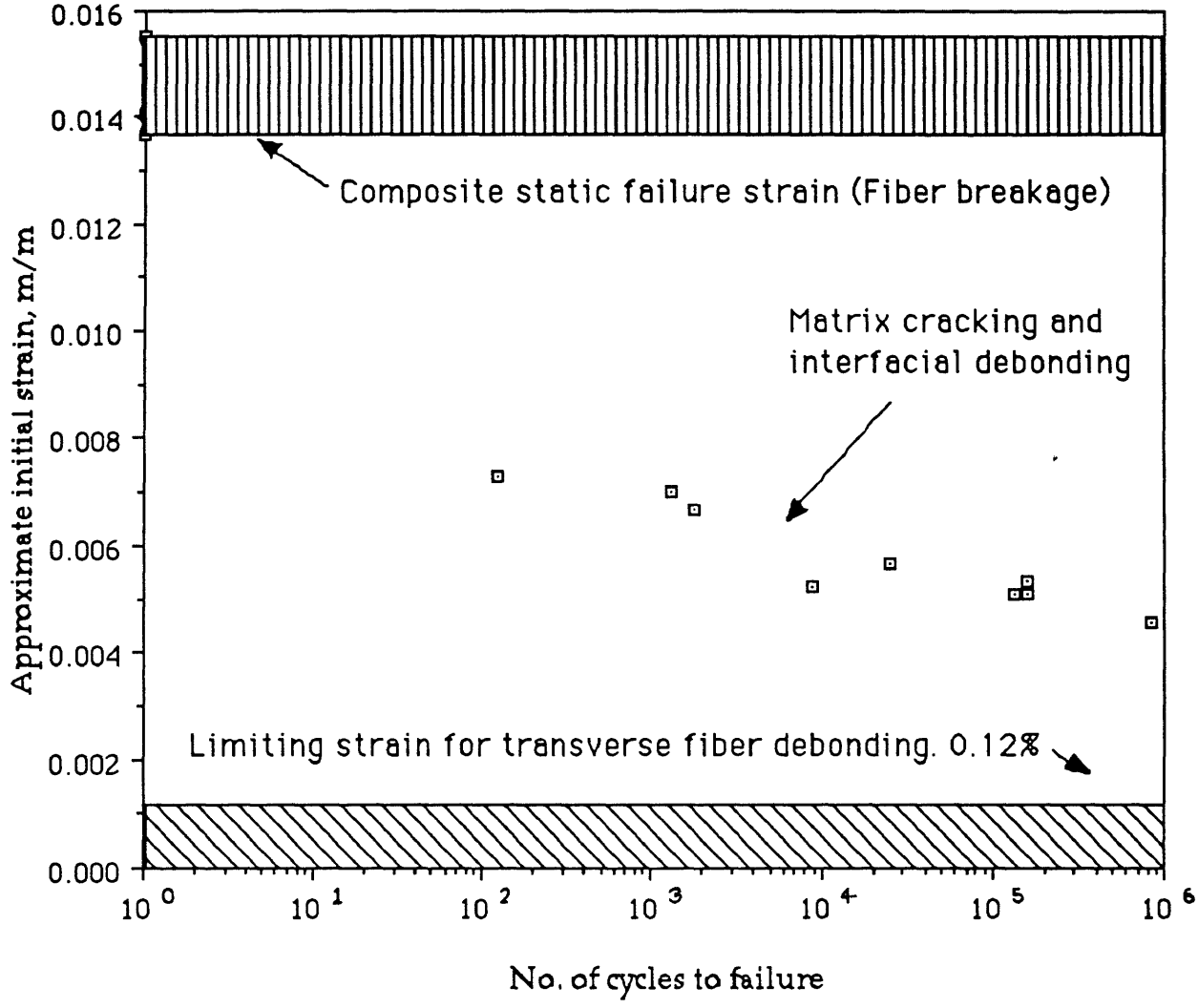

Fig : 48 : Strain-N curve for carbon fabric/unmodified polyester, R=-1

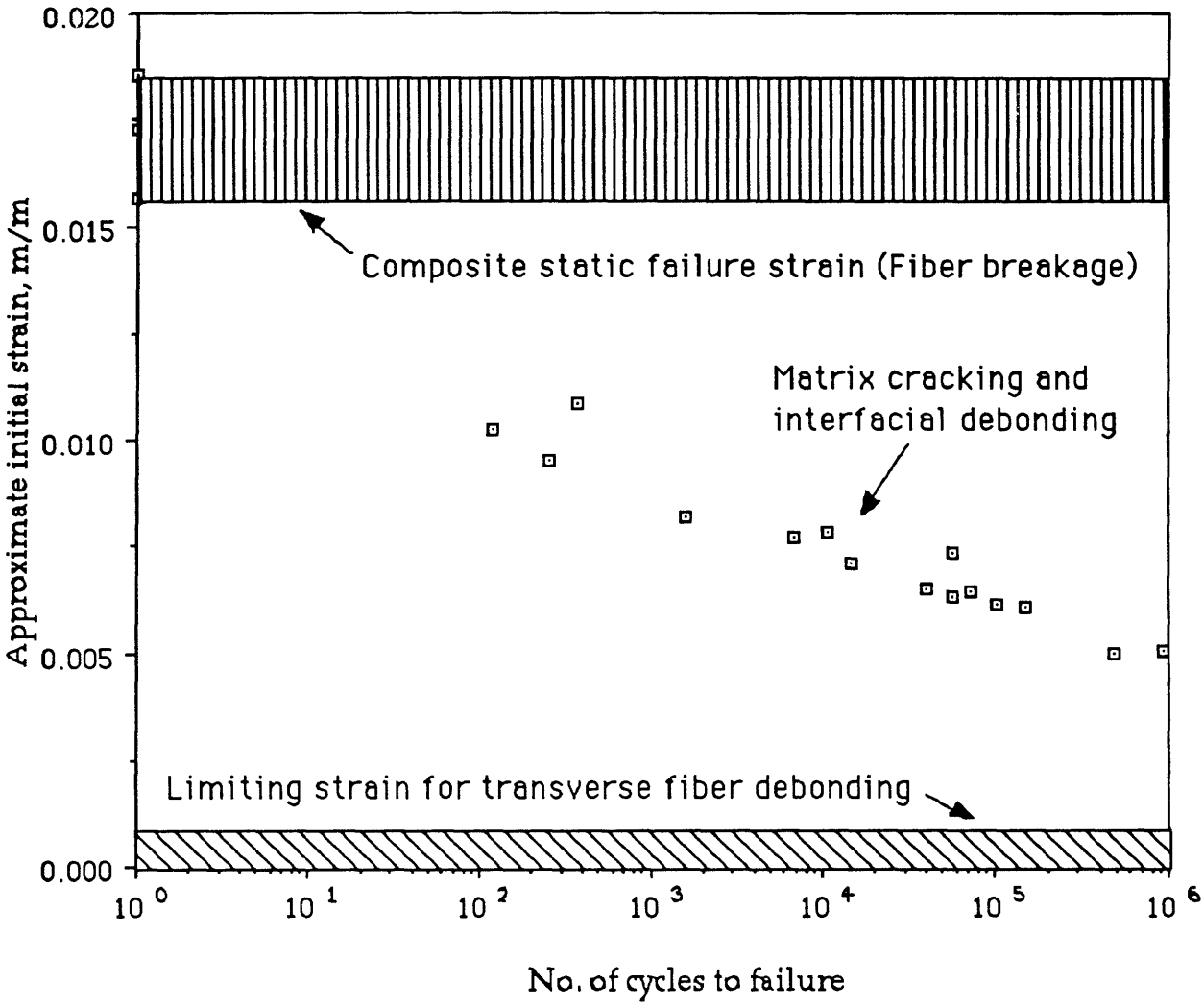

Fig : 49 : Strain-N curve for carbon fabric/MNS with 0% rubber, R=-1

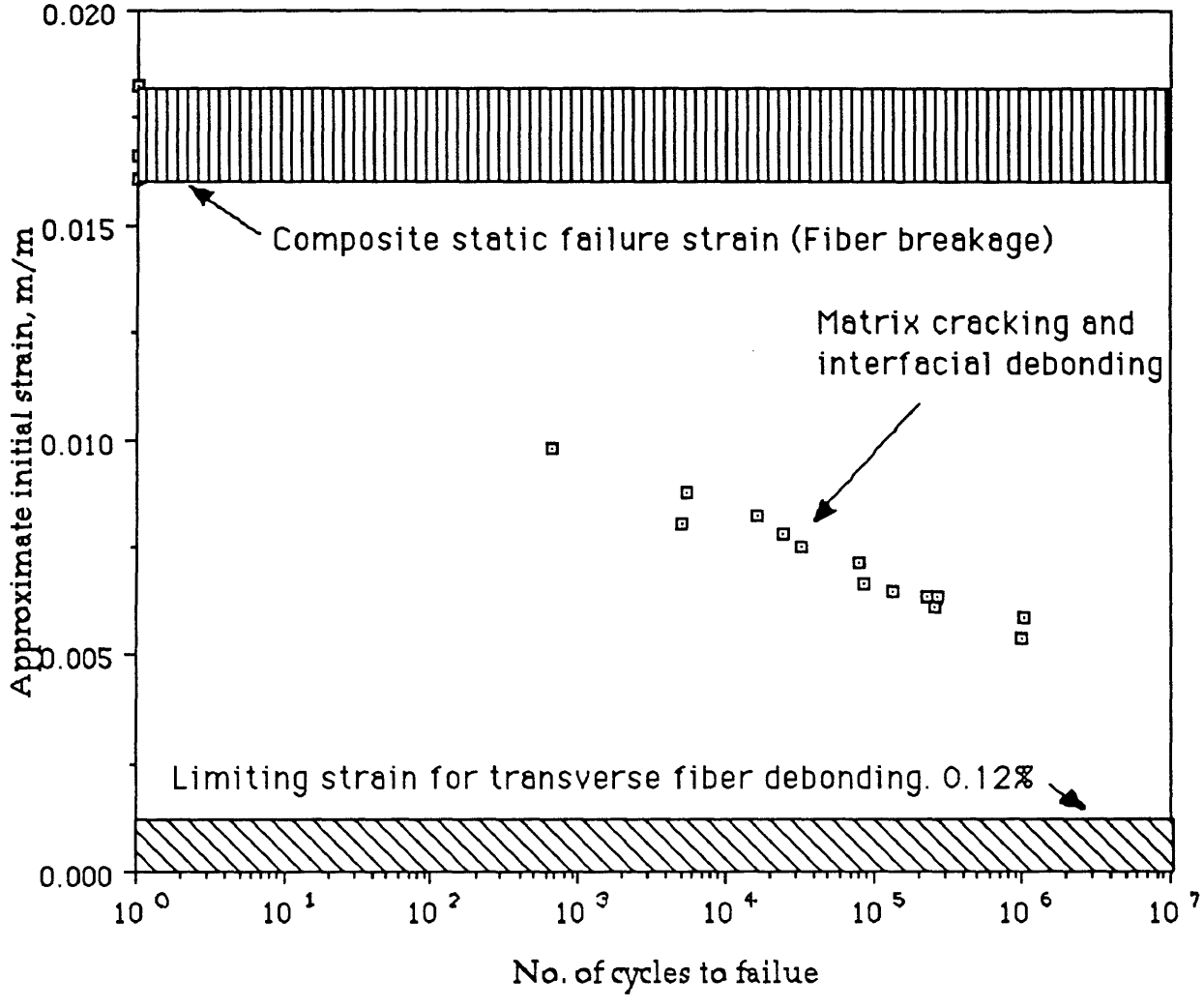

Fig : 50 : Strain-N curve for carbon fabric/MNS with 7.5% rubber, R=-1

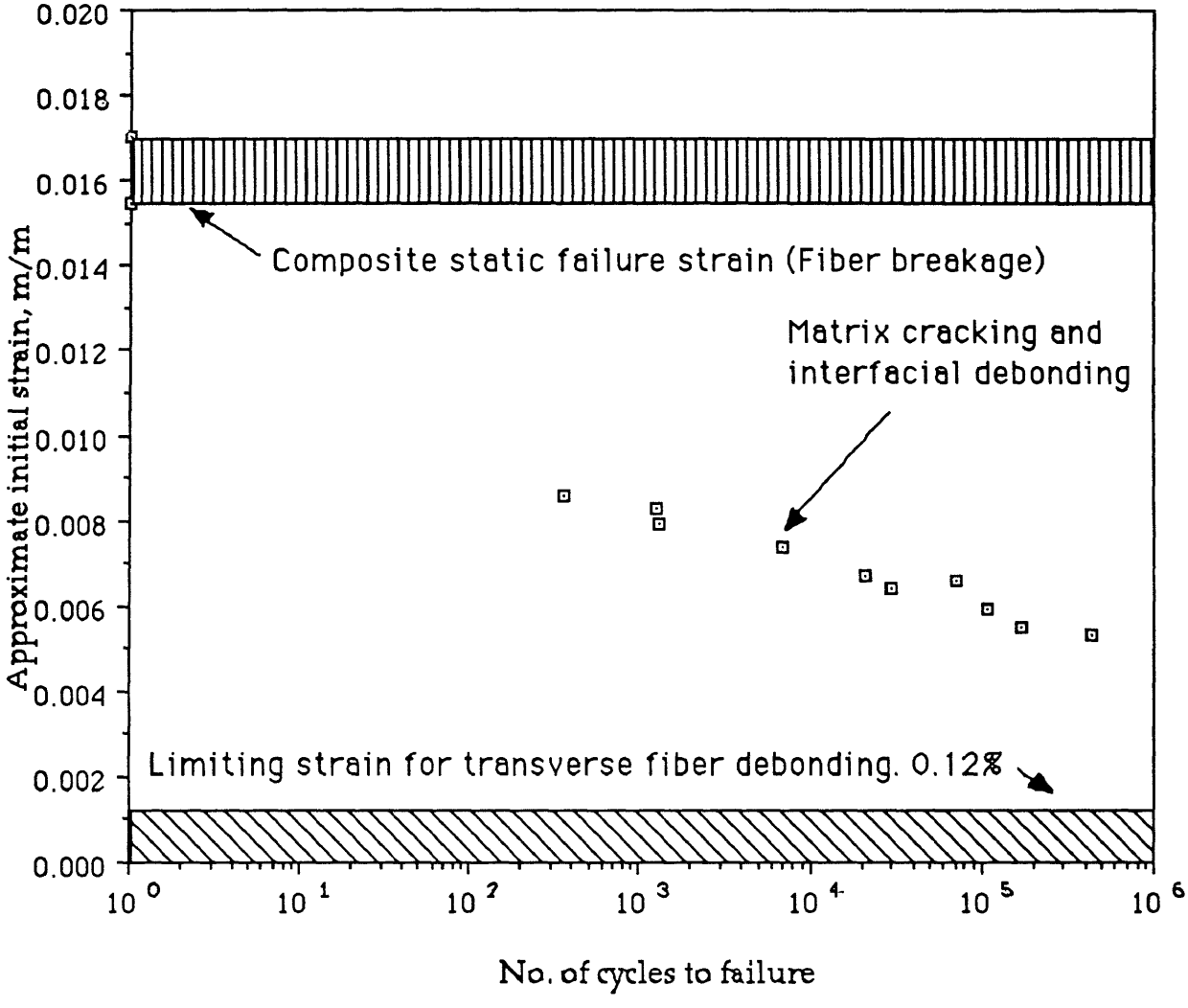

Fig : 51 : Strain-N curve for carbon fabric/MNS with 12.5%rubber, R=-1

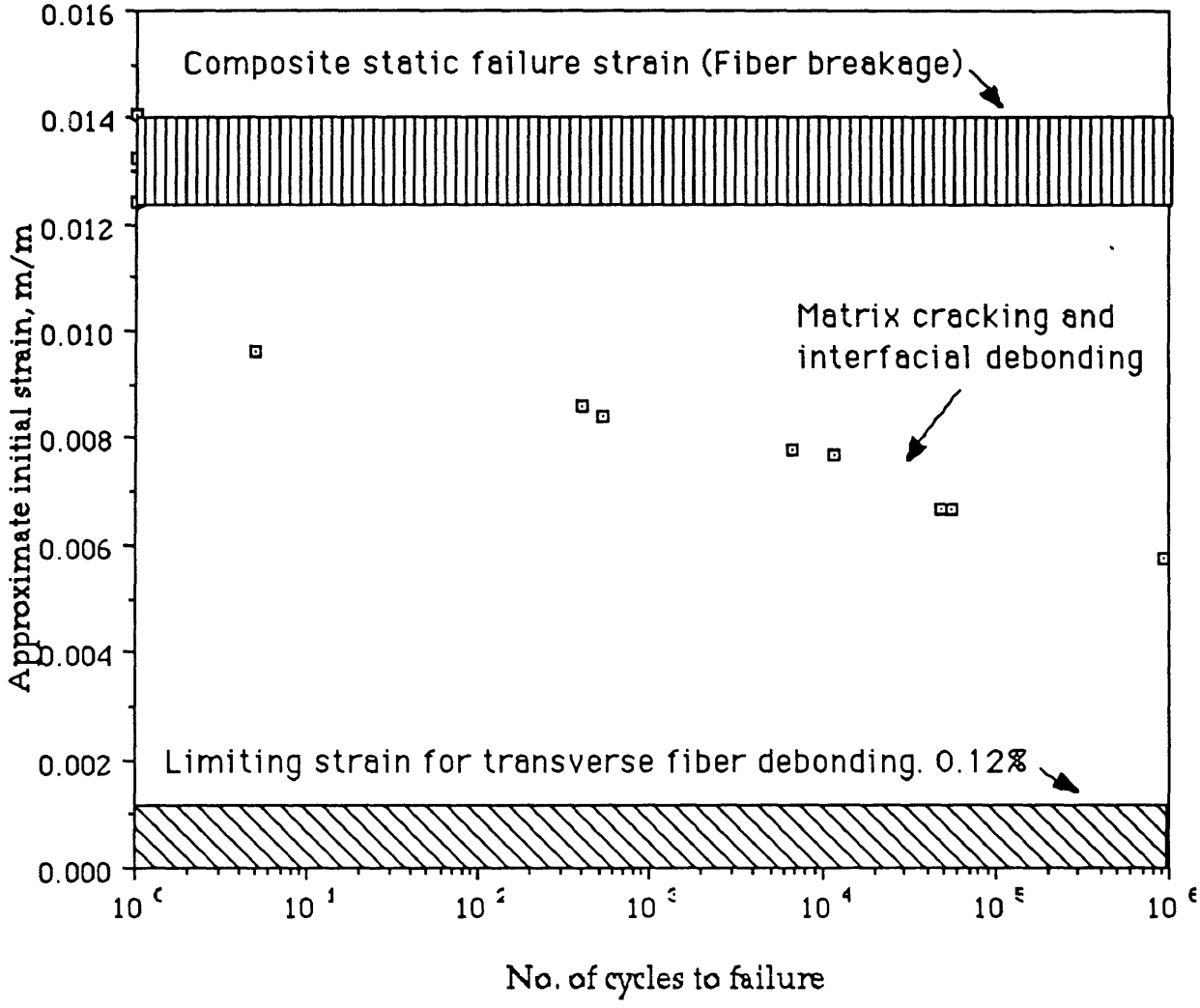

Fig : 52 : Strain-N curve for carbon fabric/MNS with 17.5% rubber, R=-1

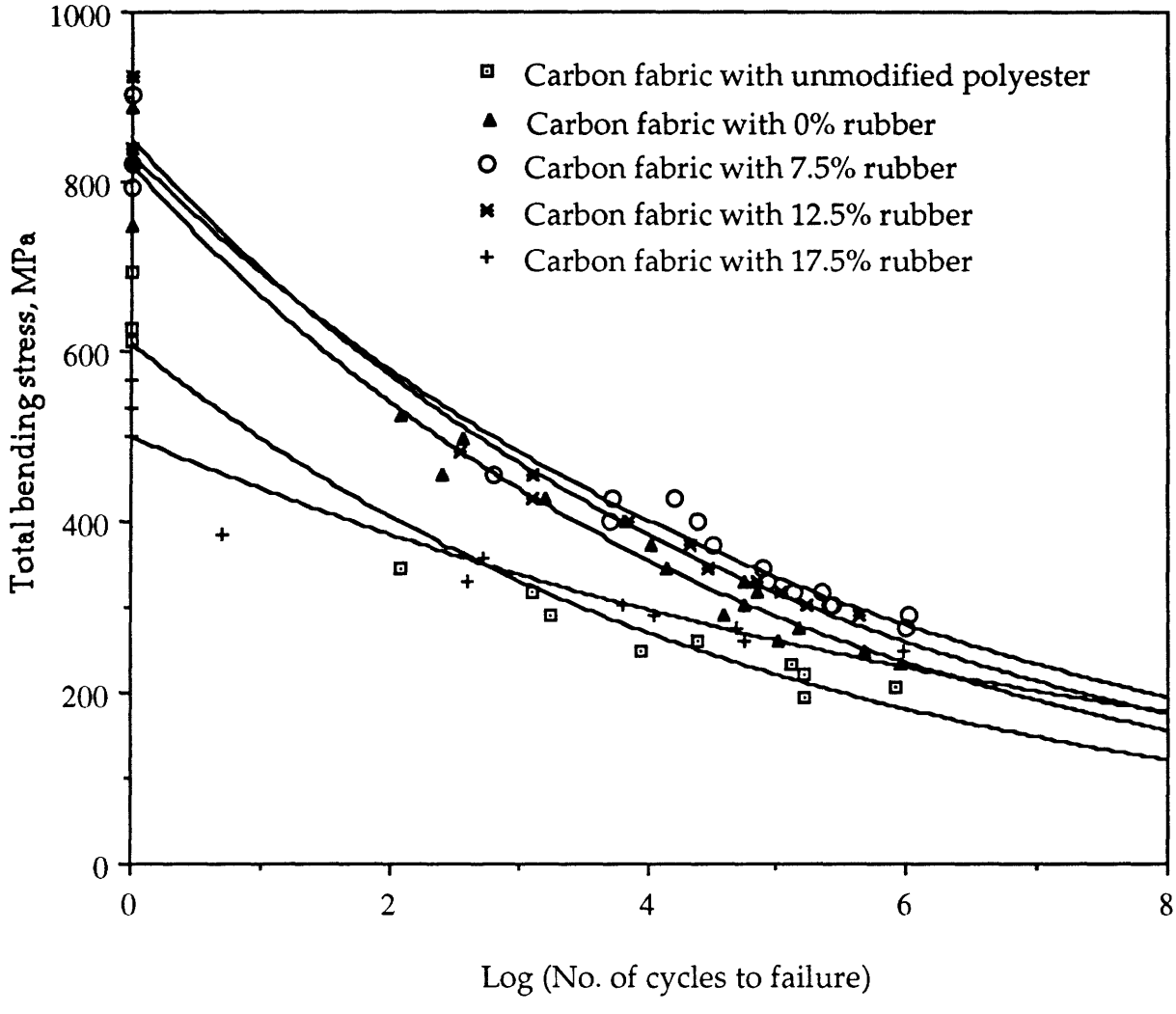

Fig : 53 : Comparison of total stress S-N curves for carbon fabric with unmodified polyester, MNS with 0%, 7.5%, 12.5% and 17.5% rubber, R=-1

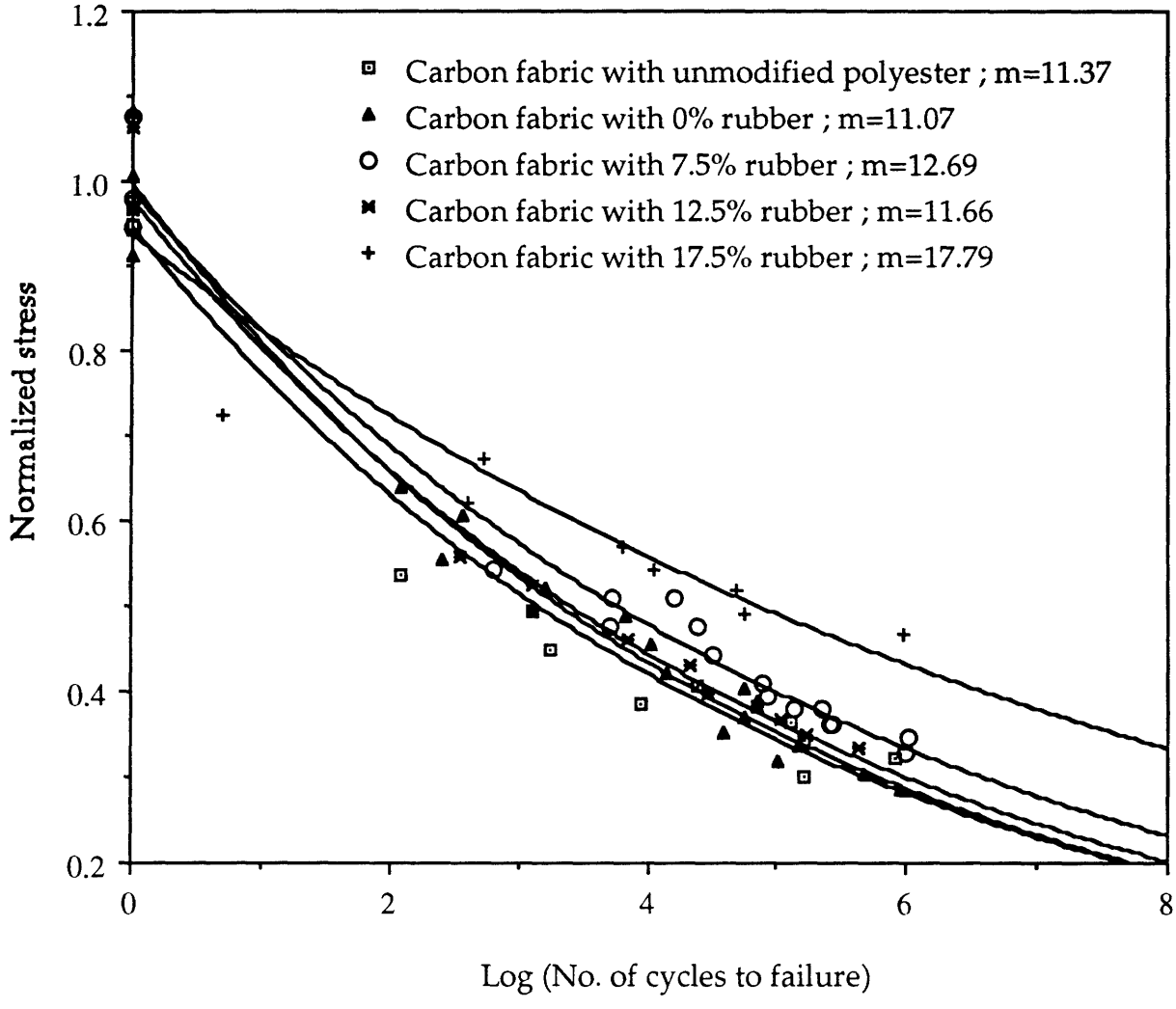

Fig : 54 : Comparison of normalized stress S-N curves for carbon fabric with unmodified polyester, MNS with 0%, 7.5%, 12.5% and 17.5% rubber, R=-1

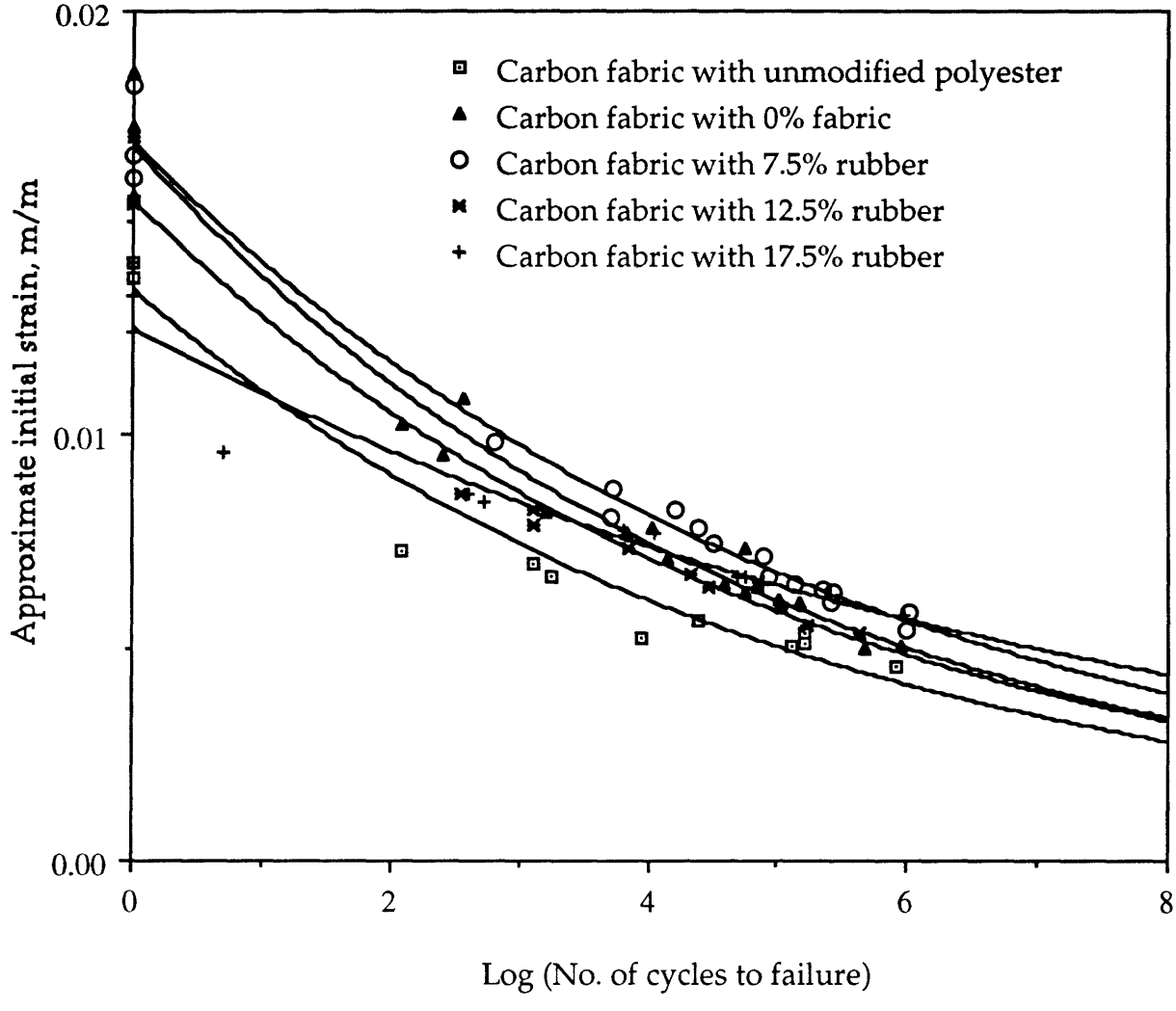

Fig : 55 : Comparison of initial strain-N curves for carbon fabric with unmodified polyester, MNS with 0%, 7.5%, 12.5% and 17.5% rubber, R=-1

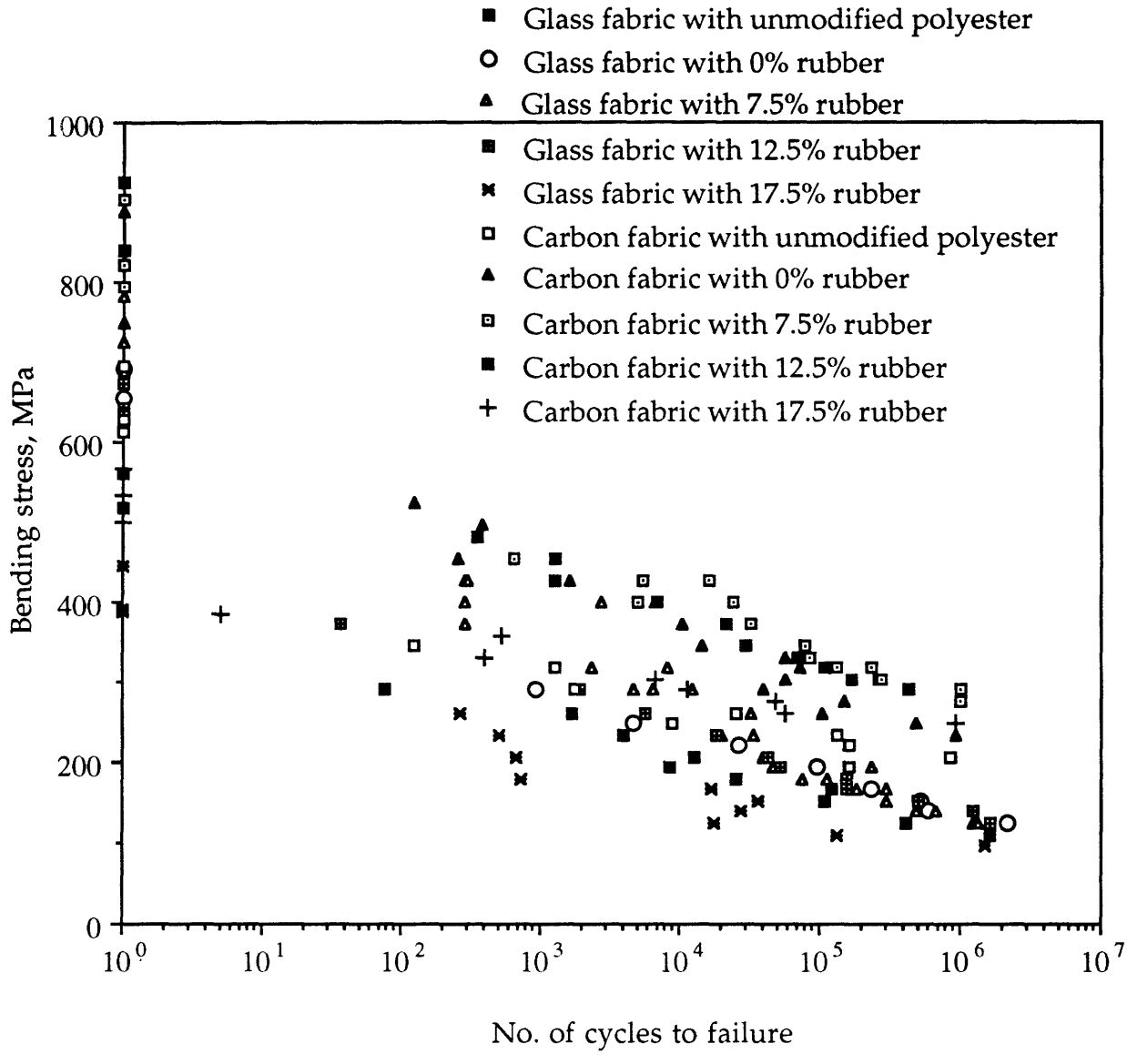

Fig : 56 : Comparison of total stress S-N curves for all Glass fabric and Carbon fabric composites.

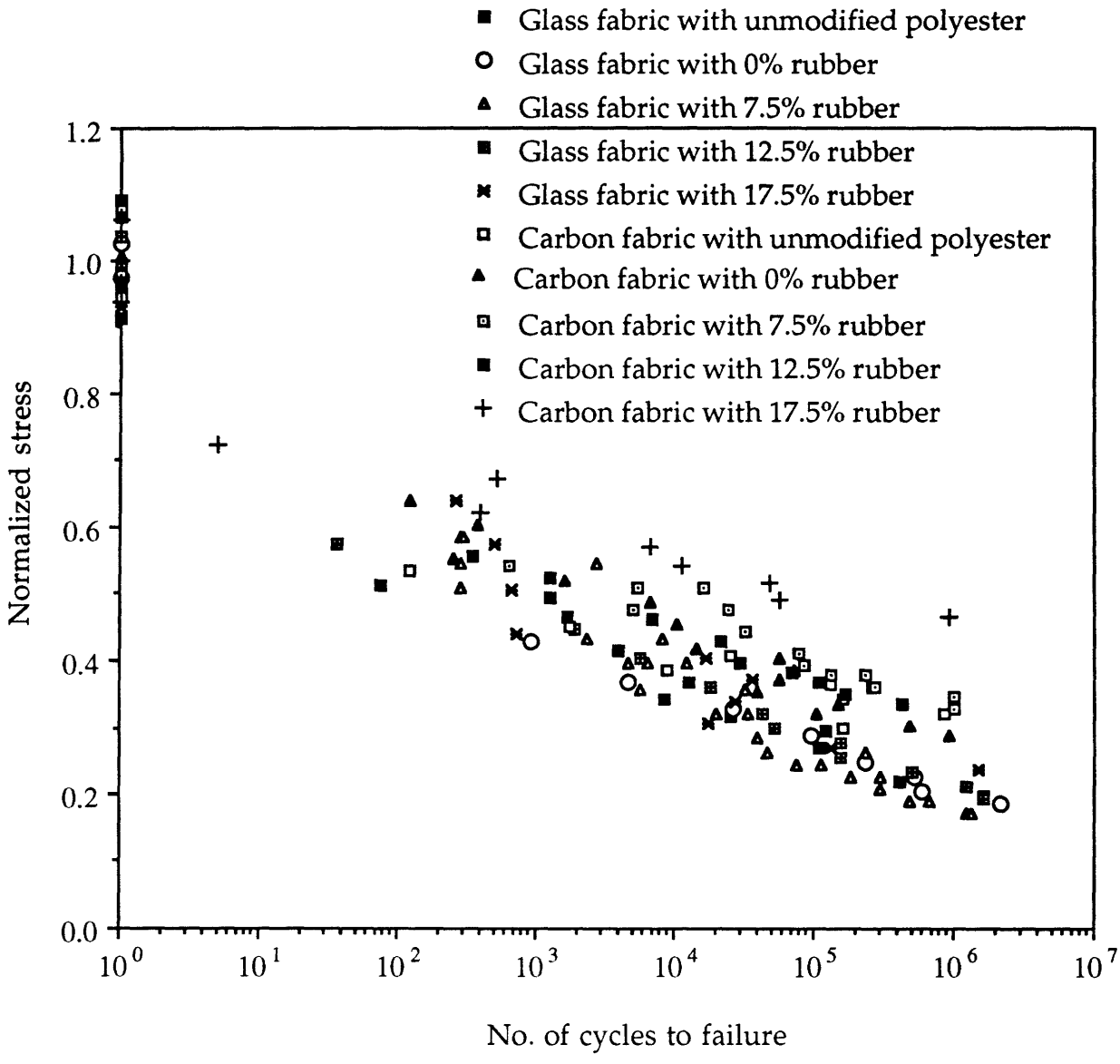

Fig : 57 : Comparison of normalized stress S-N curves for all glass fabric and Carbon fabric composites

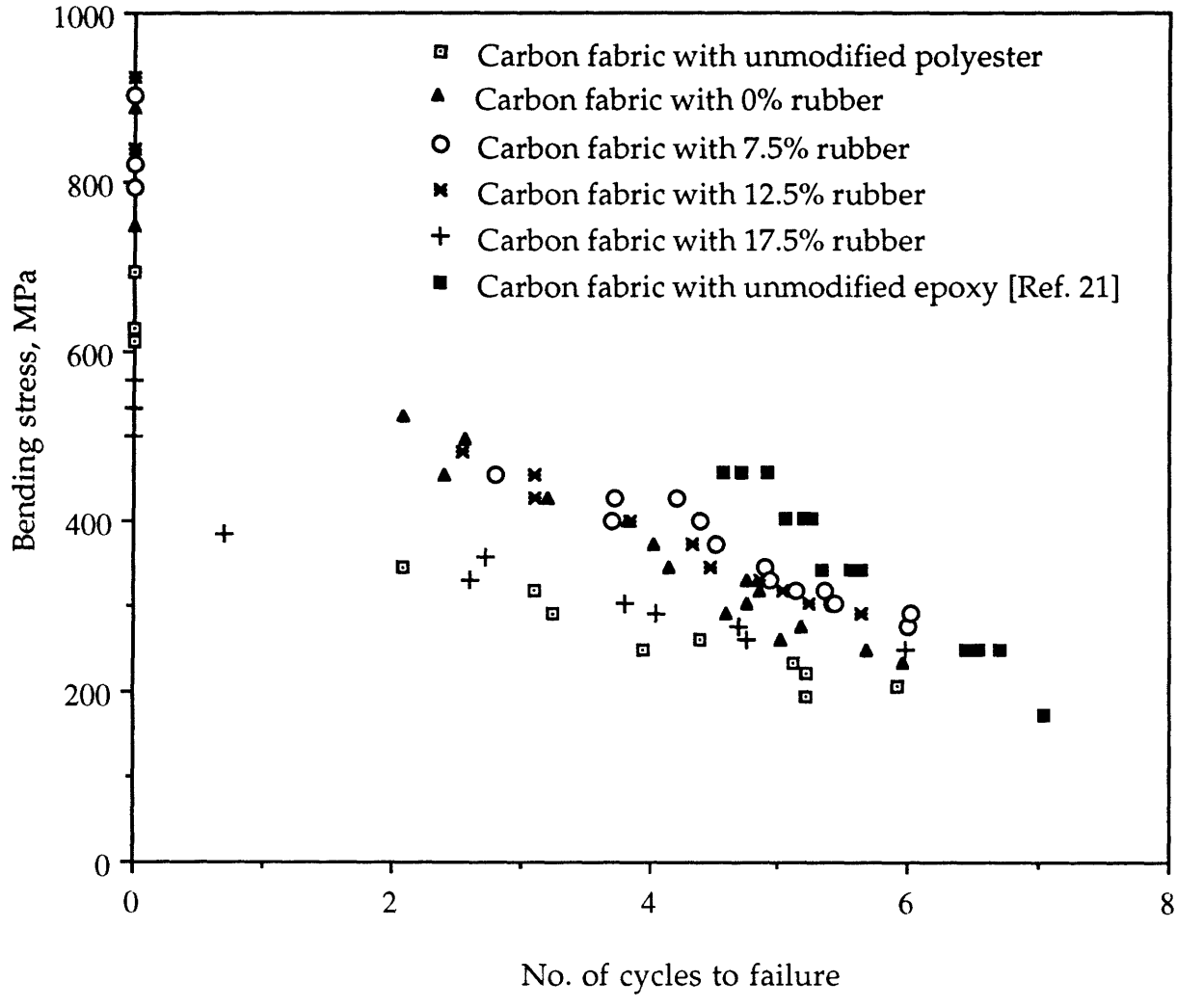

Fig : 58 : Comparison of total stress S-N curve for plain weave carbon fabric with unmodified epoxy [Ref. 21] to the S-N curves for carbon fabric with unmodified polyester, MNS with 0%, 7.5%, 12.5% and 17.5% rubber, R=-1.

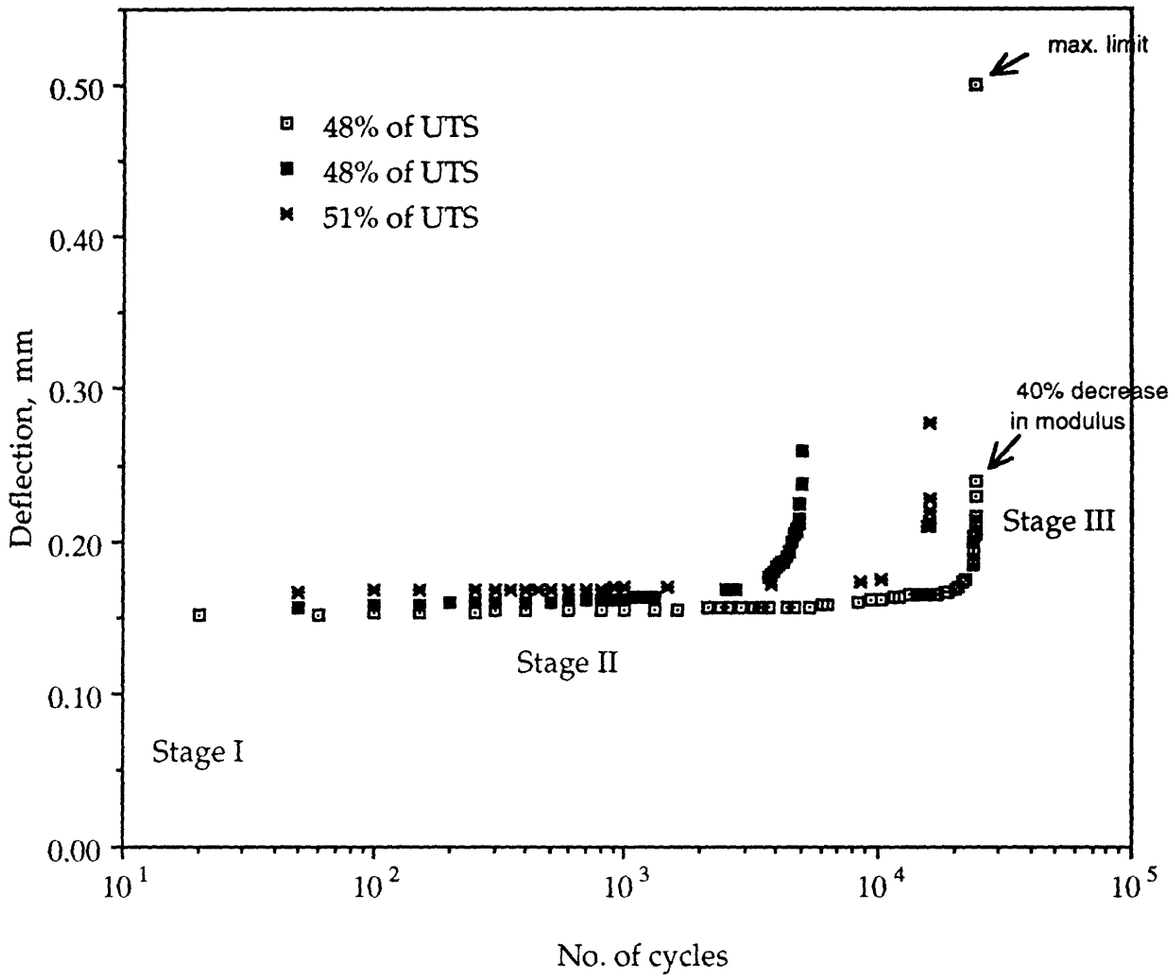

Fig : 59 : Deflection Vs. No. of cycles for carbon fabric/MNS with 7.5% rubber laminate

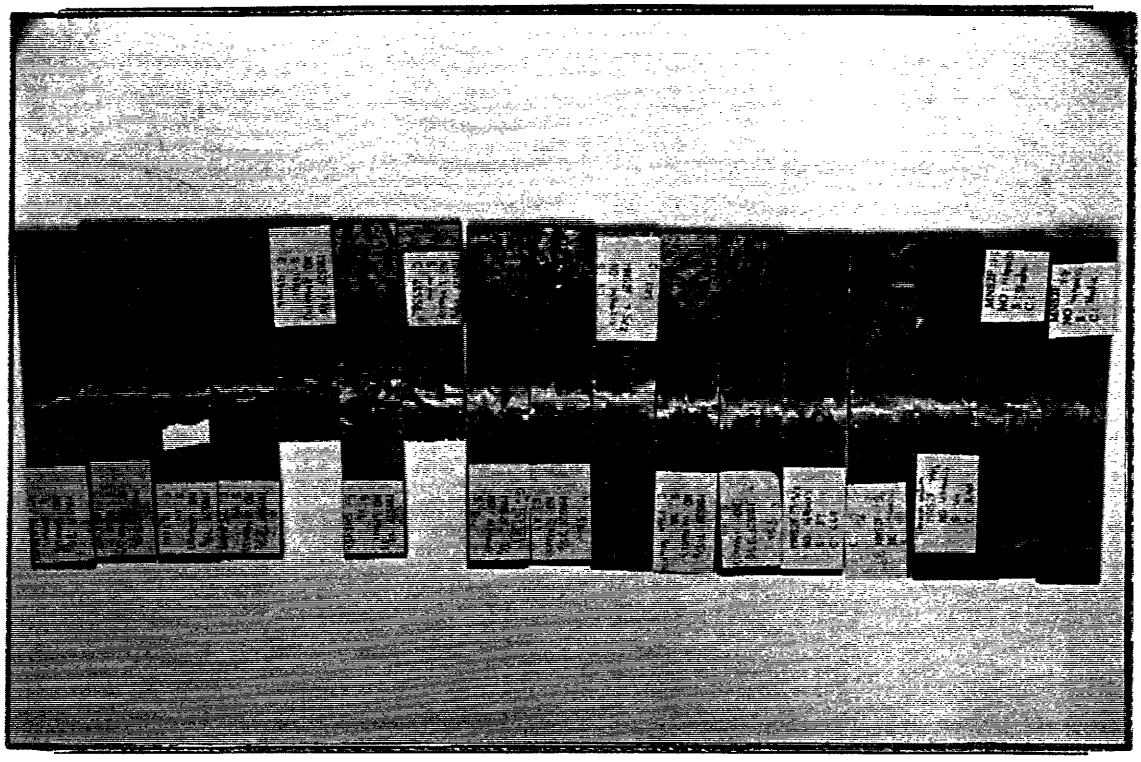

Fig. 60 : Photograph of the damage zone in fatigue tests performed on chopped strand mat/MNS with 7.5% rubber.

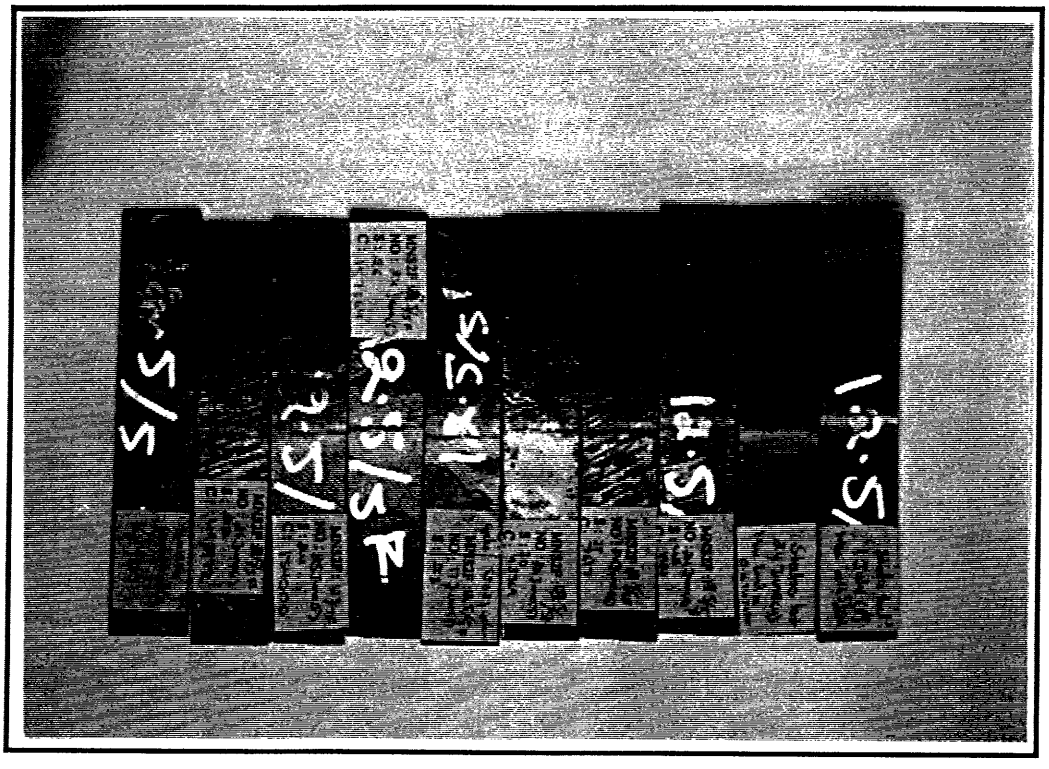

Fig. 61 : Photograph of the damage zone in fatigue tests performed on chopped strand mat/MNS with 12.5% rubber.

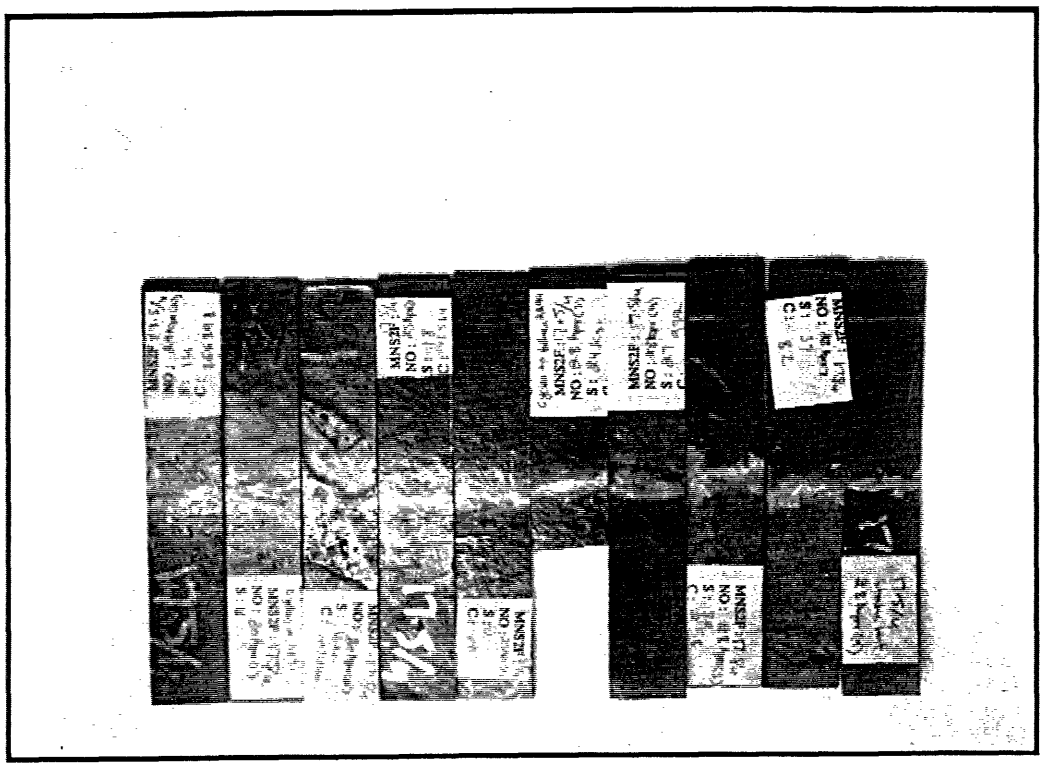

Fig. 62 : Photograph of the damage zone in fatigue tests performed on chopped strand mat/MNS with 17.5% rubber.

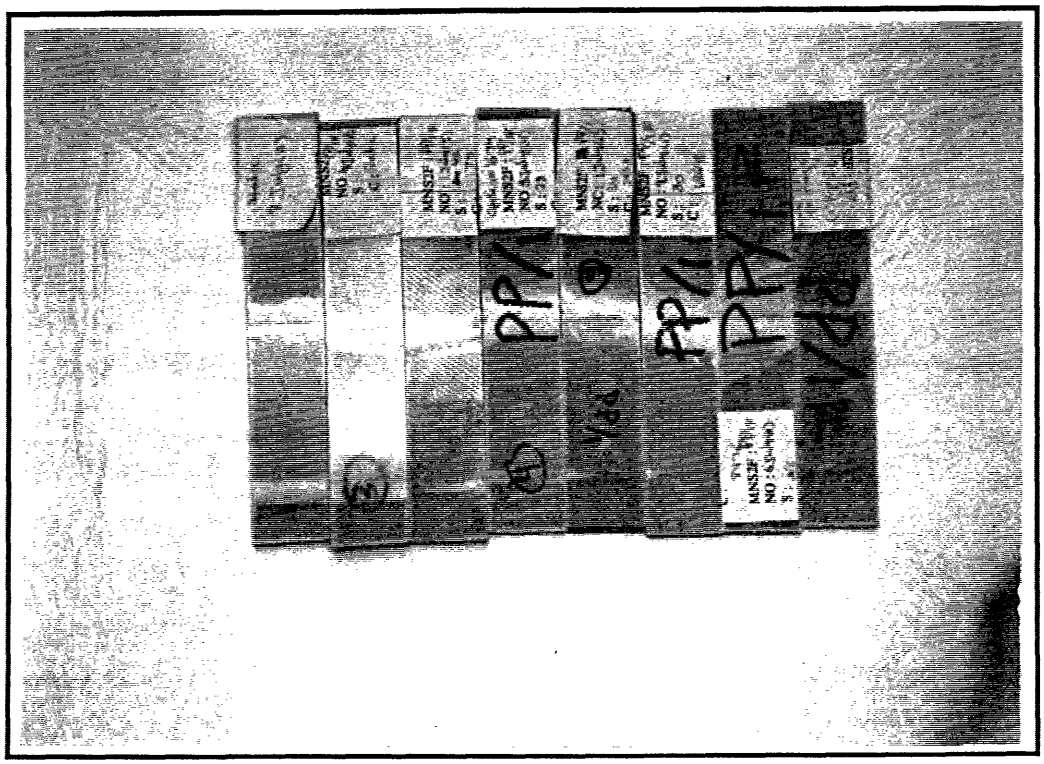

Fig. 63 : Photograph of the damage zone in fatigue tests performed on glass fabric/unmodified polyester.

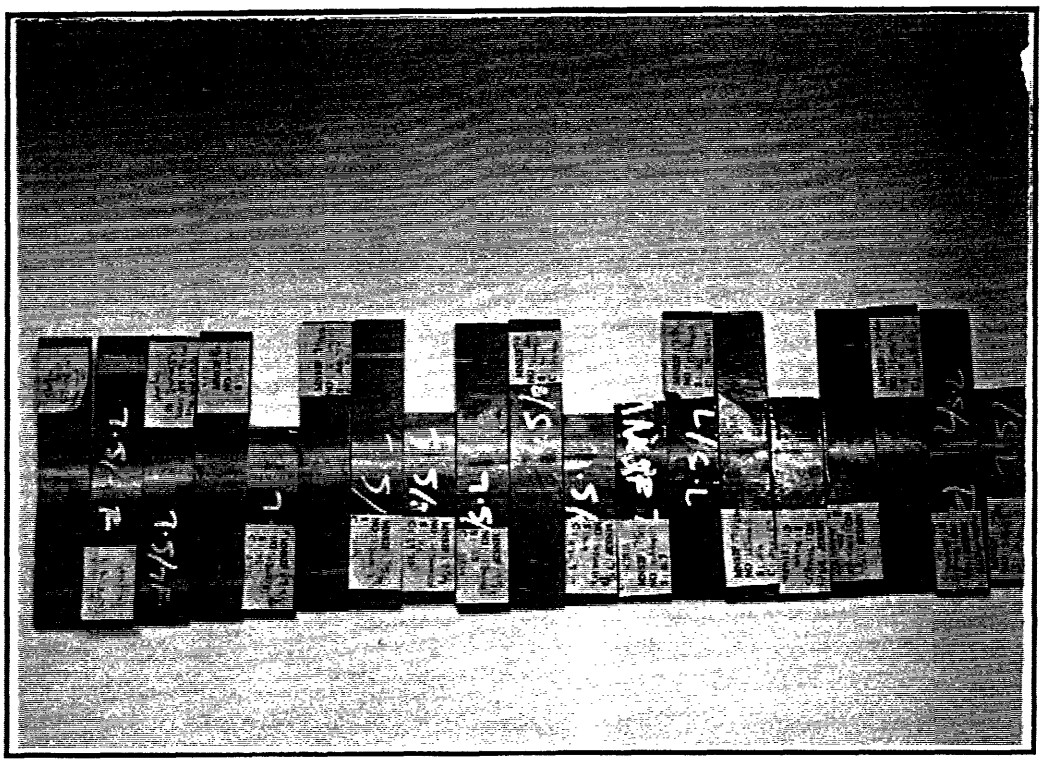

Fig. 64 : Photograph of the damage zone in fatigue tests performed on glass fabric/MNS with 7.5% rubber.

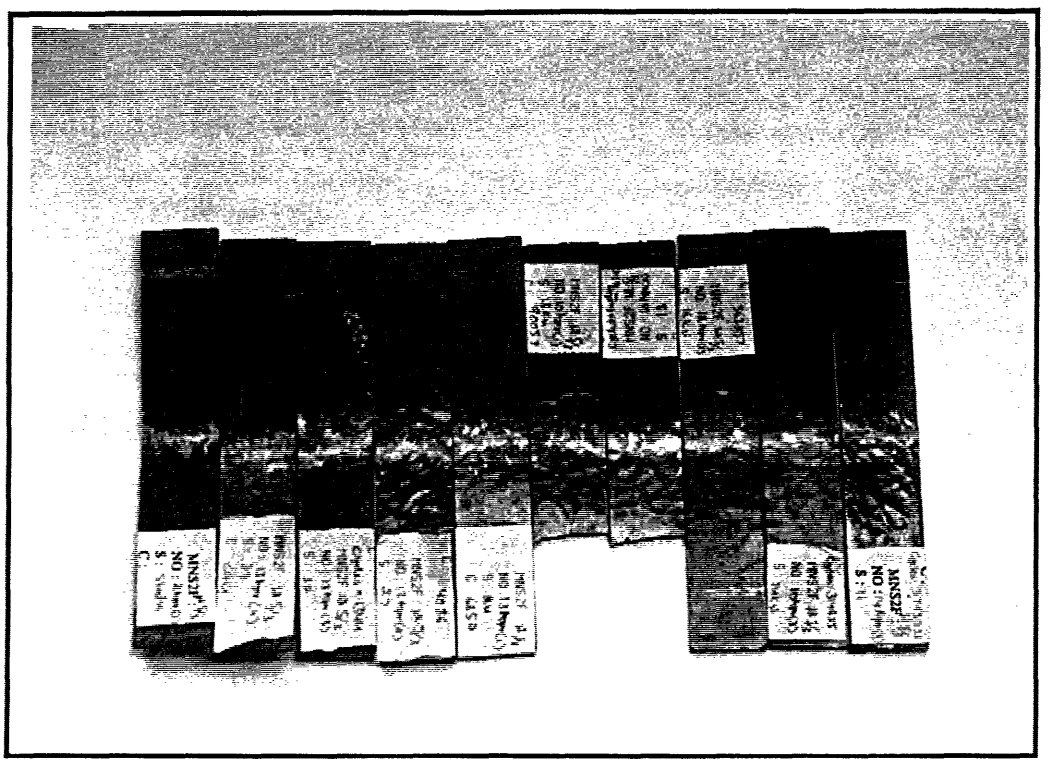

Fig. 65 : Photograph of the damage zone in fatigue tests performed on glass fabric/MNS with 12.5% rubber.

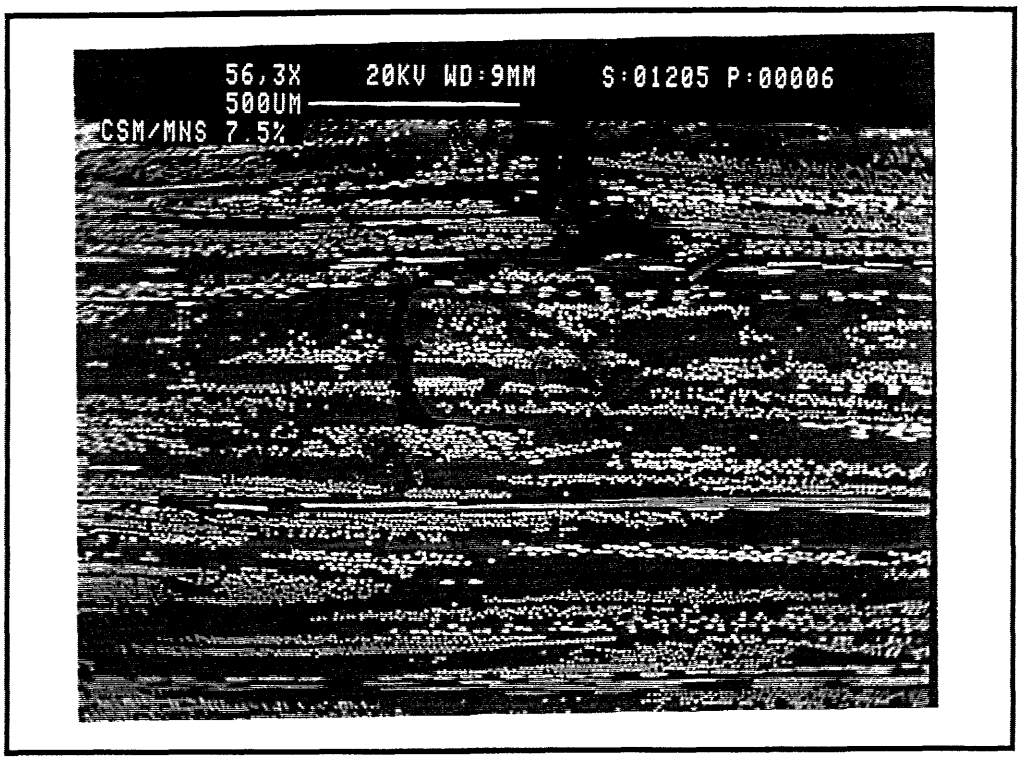

(a)

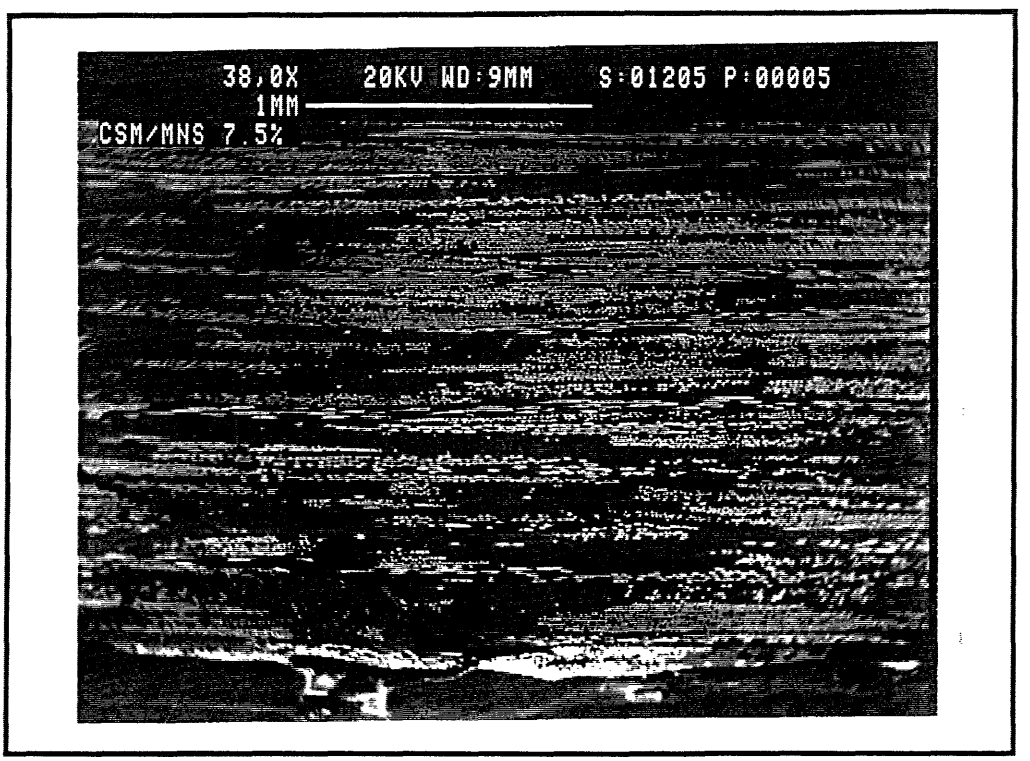

(b)

Fig. 66 : SEM micrographs of the fracture surface (longitudinal view) of chopped strand mat with 7.5% rubber (a) Top surface (b) Bottom surface.

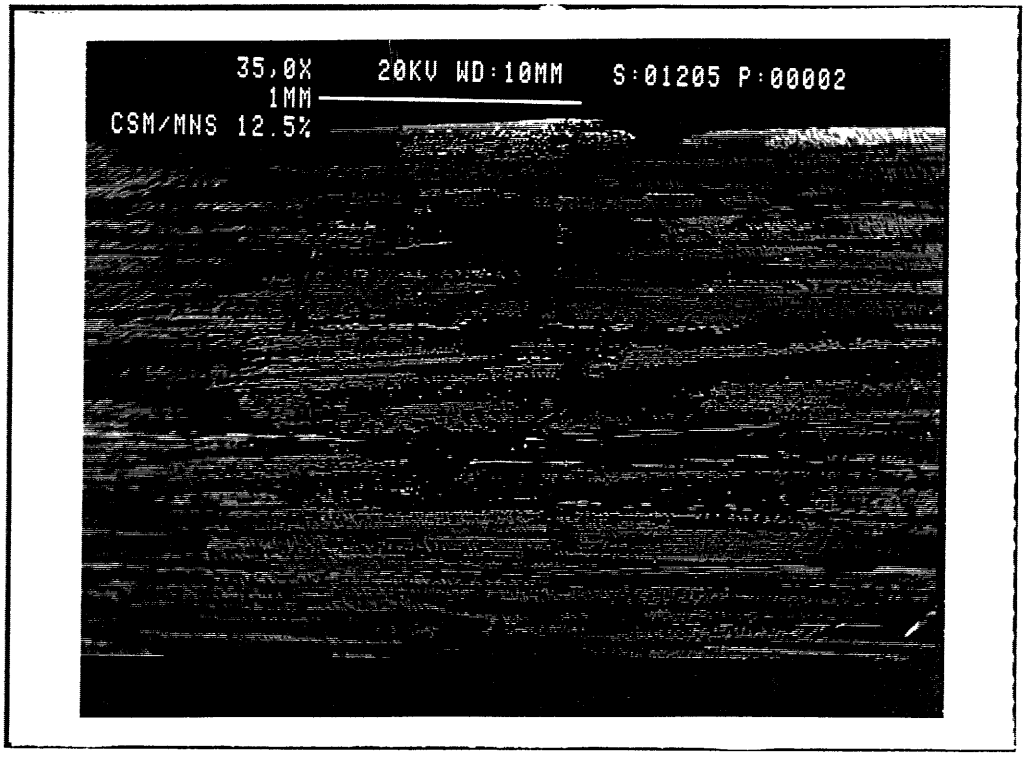

(a)

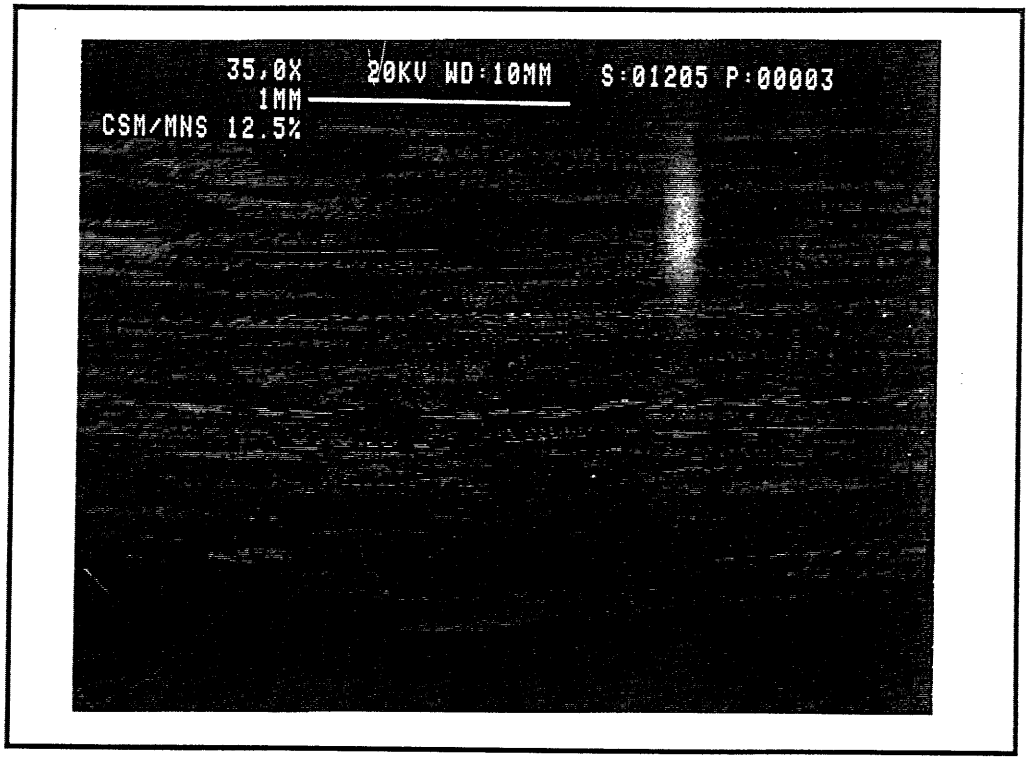

(b)

Fig. 67 : SEM micrographs of the fracture surface (longitudinal view) of chopped strand mat with 12.5% rubber (a) Top surface (b) Bottom surface.

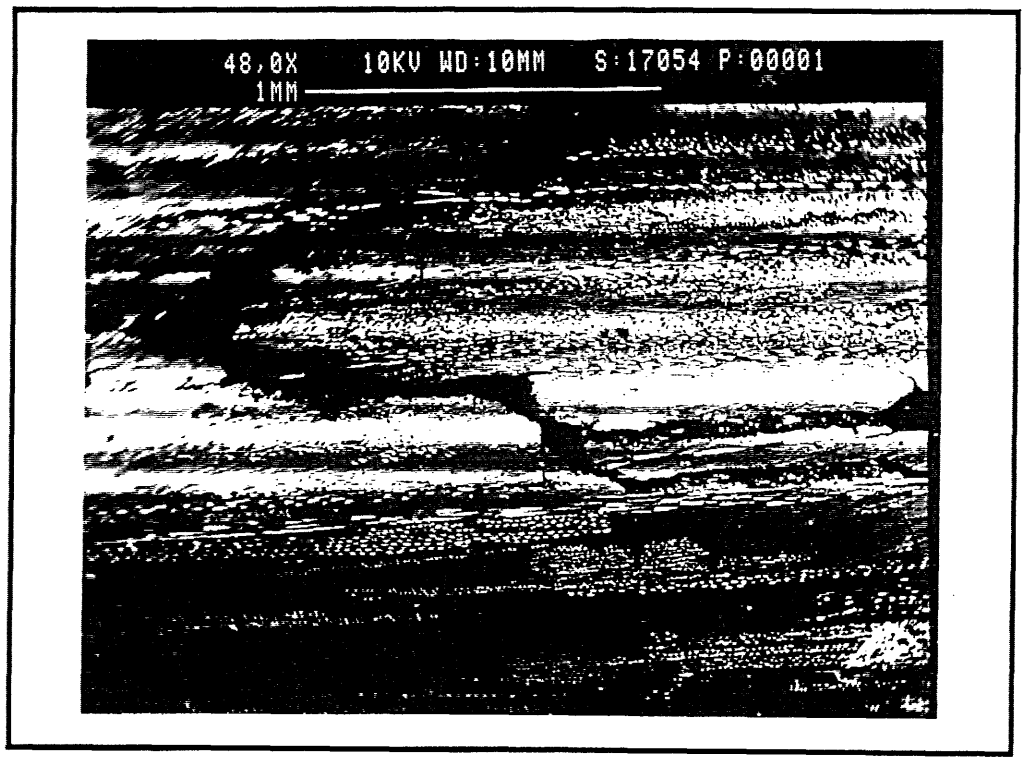

(a)

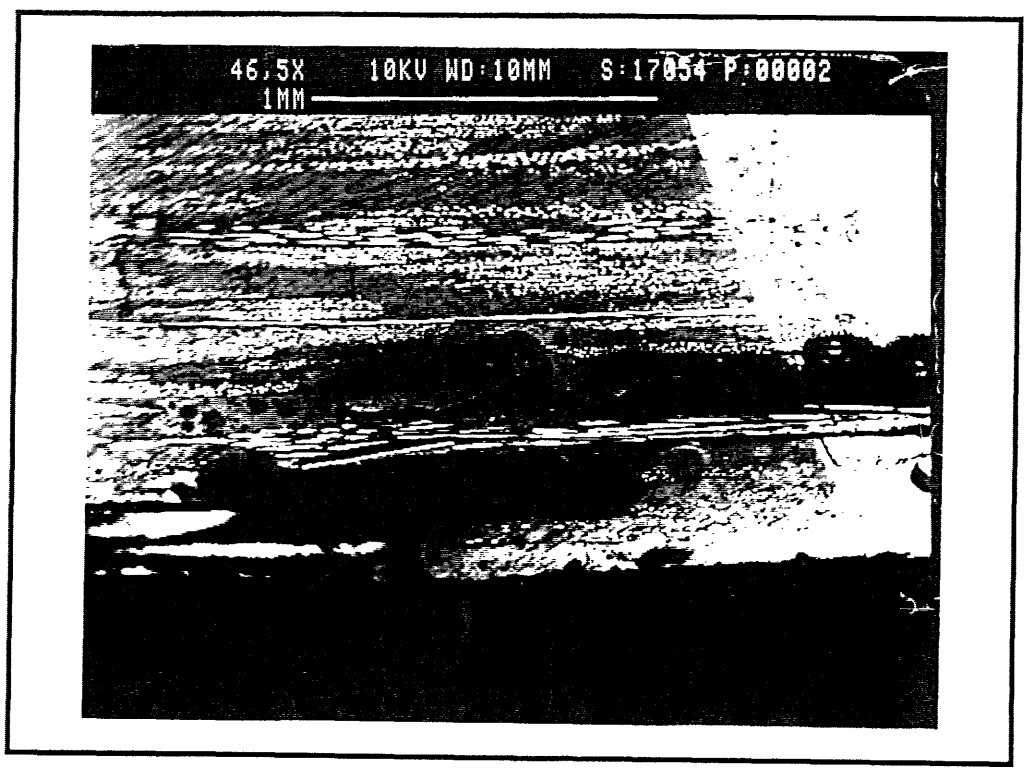

(b)

Fig. 68 : SEM micrographs of the fracture surface (longitudinal view)of chopped strand mat with 17.5% rubber (a) Top surface (b) Bottom surface.

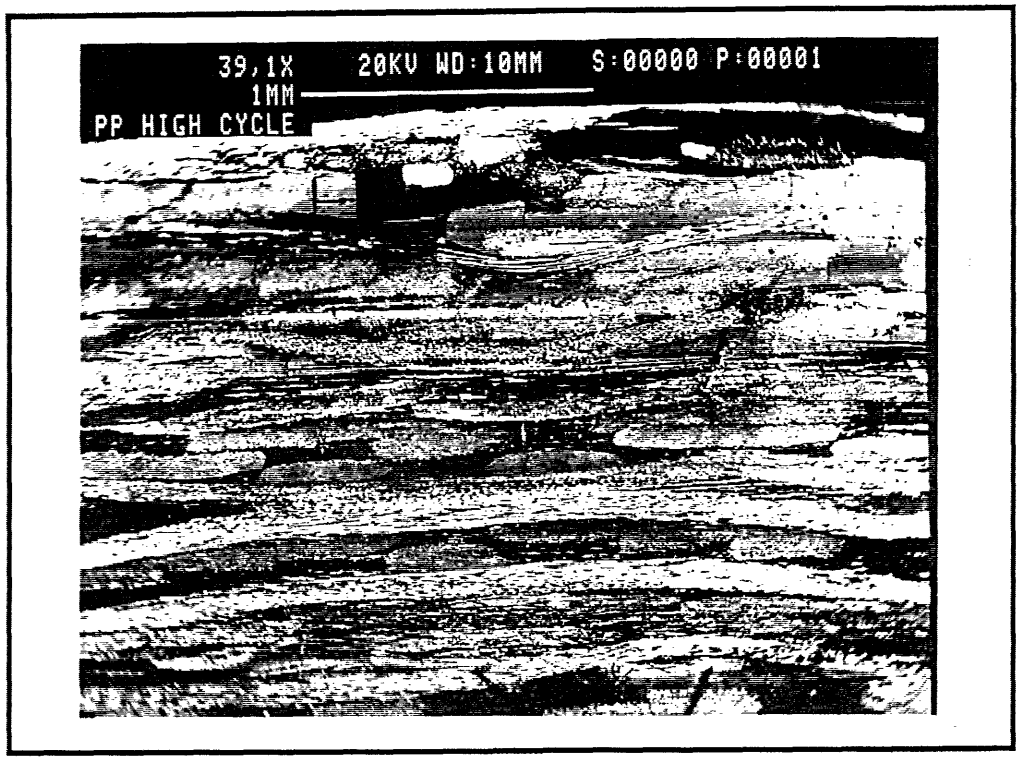

(a)

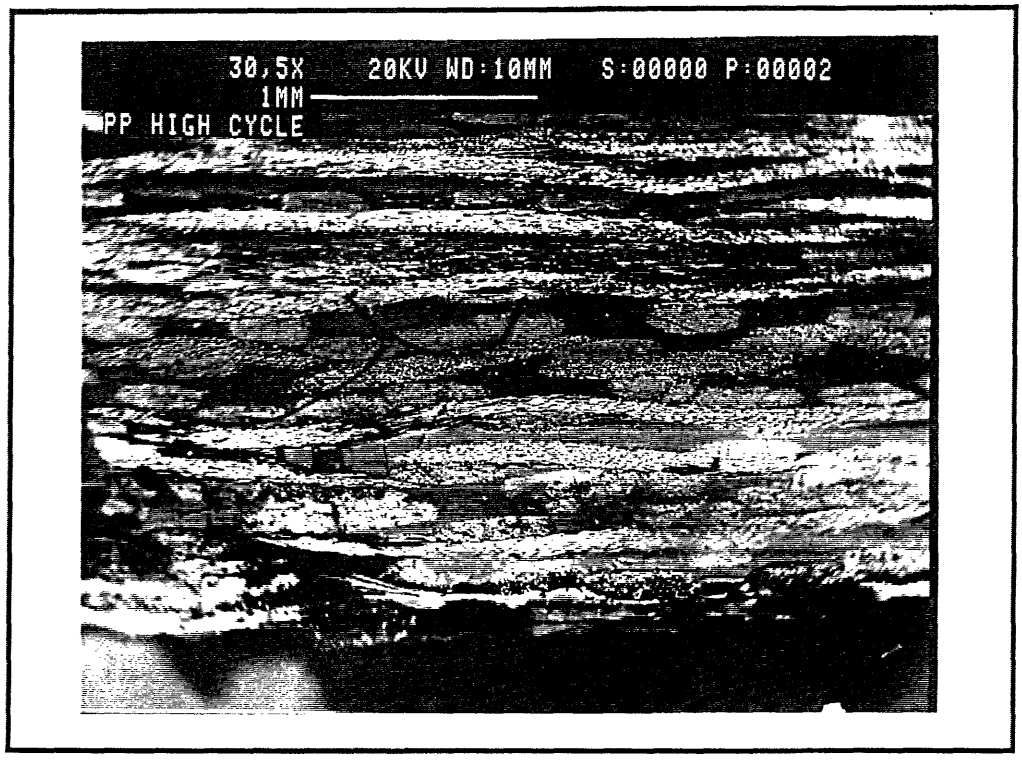

(b)

Fig. 69: SEM micrographs of the fracture surface (longitudinal view) of glass fabric with unmodified polyester (a) Top surface (b) Bottom surface.

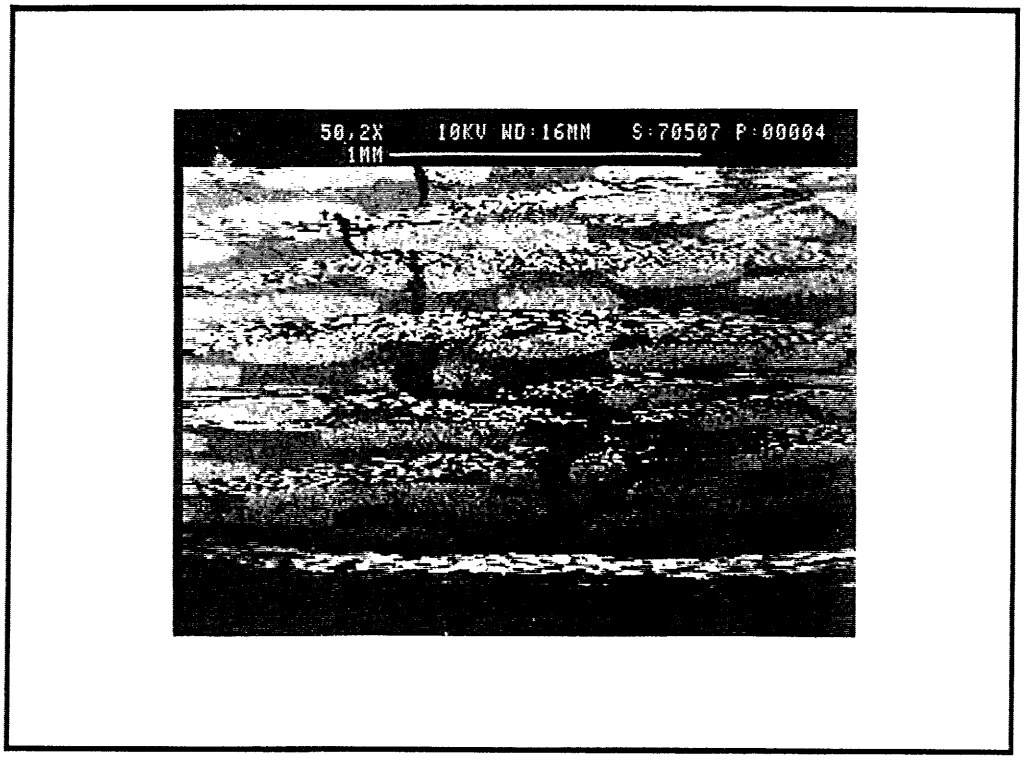

(a)

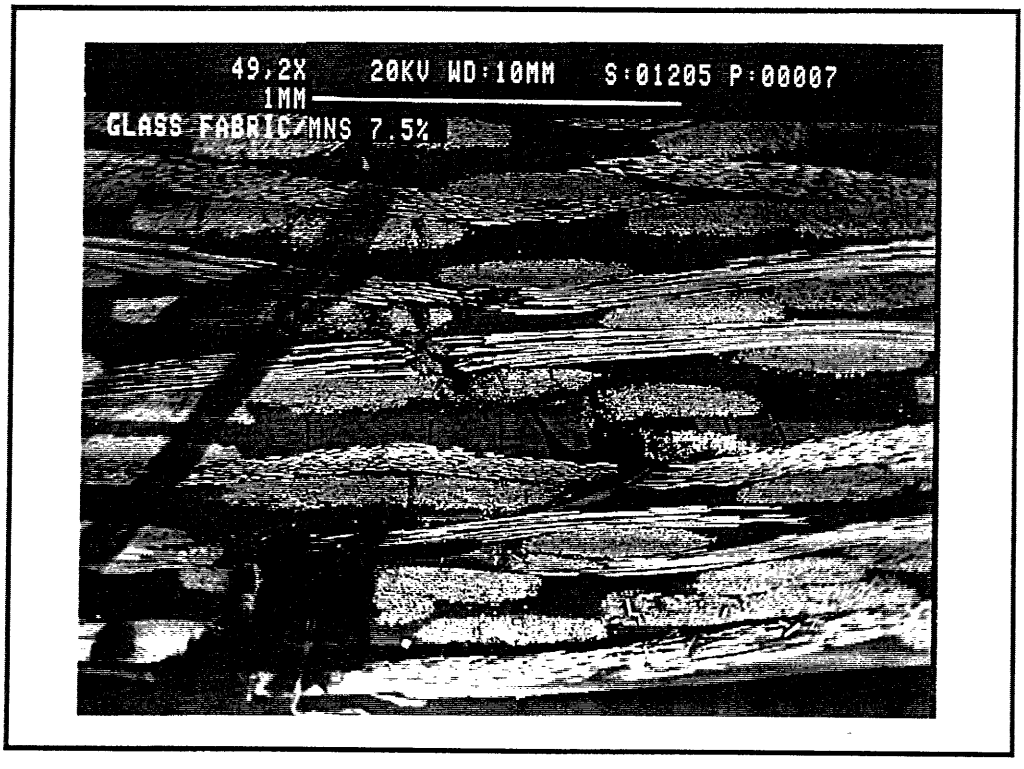

(b)

Fig. 70 : SEM micrographs of the fracture surface (longitudinal view) of glass fabric with 7.5% rubber (Two different specimens are shown).

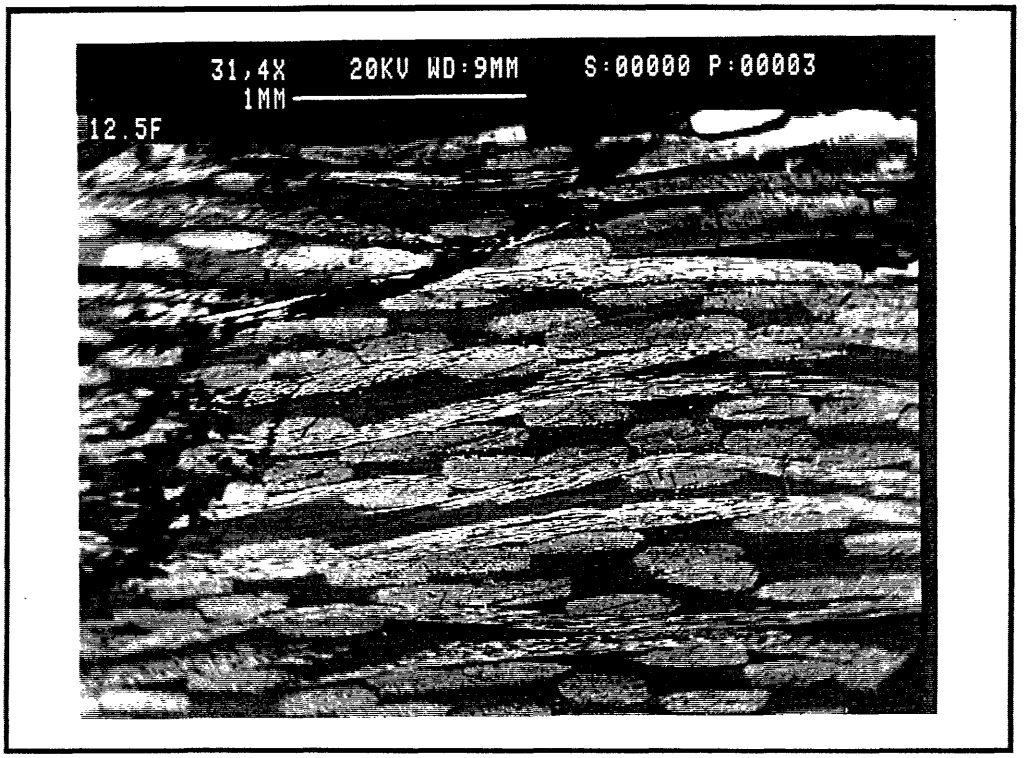

Fig. 71 : SEM micrograph of the fracture surface (longitudinal view) of glass fabric with 12.5% rubber composite (Top surface).

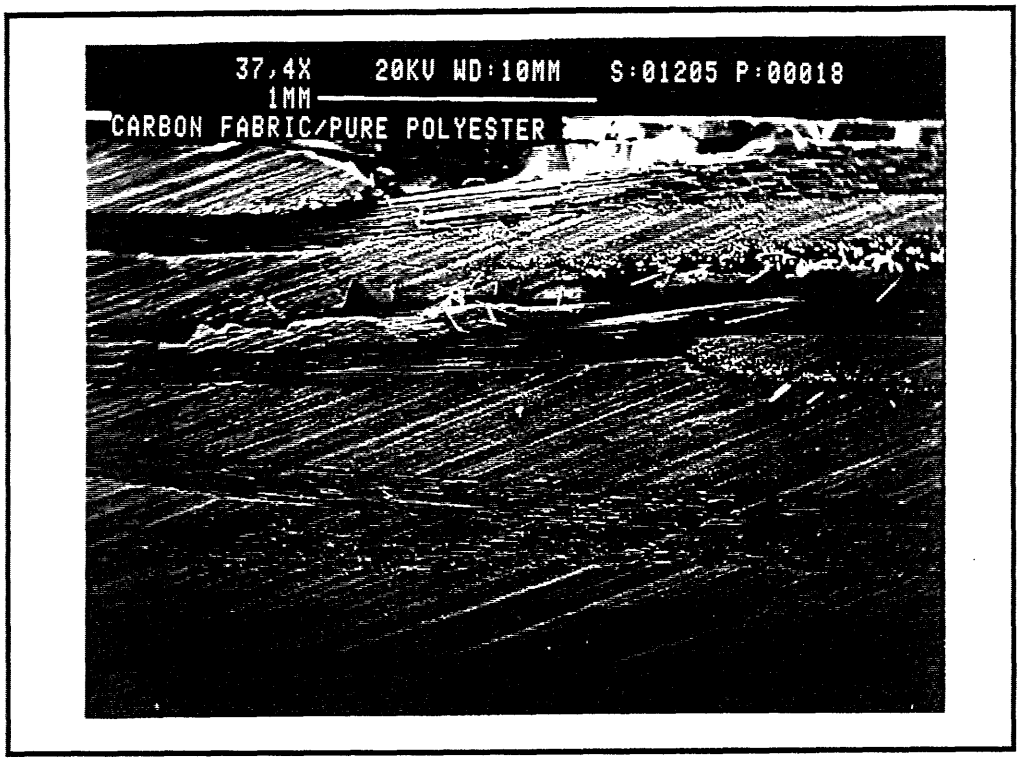

(a)

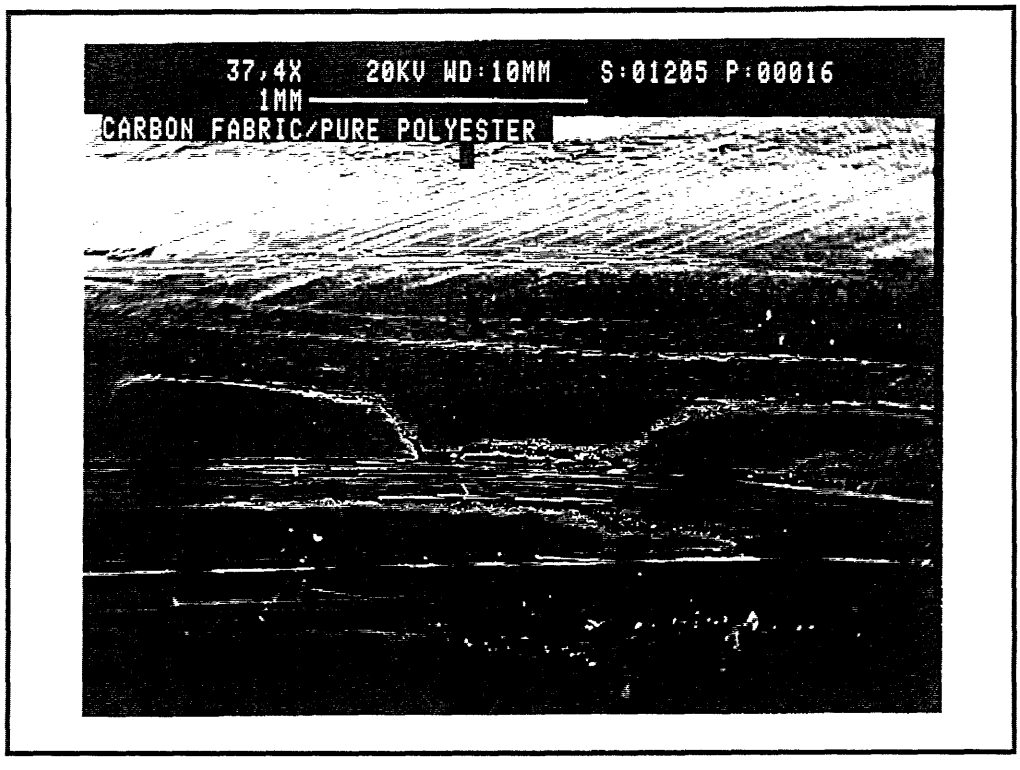

(b)

Fig. 72 : SEM micrographs of the fracture surface (longitudinal view) of carbon fabric with unmodified polyester (a) Top surface (b) Bottom surface.

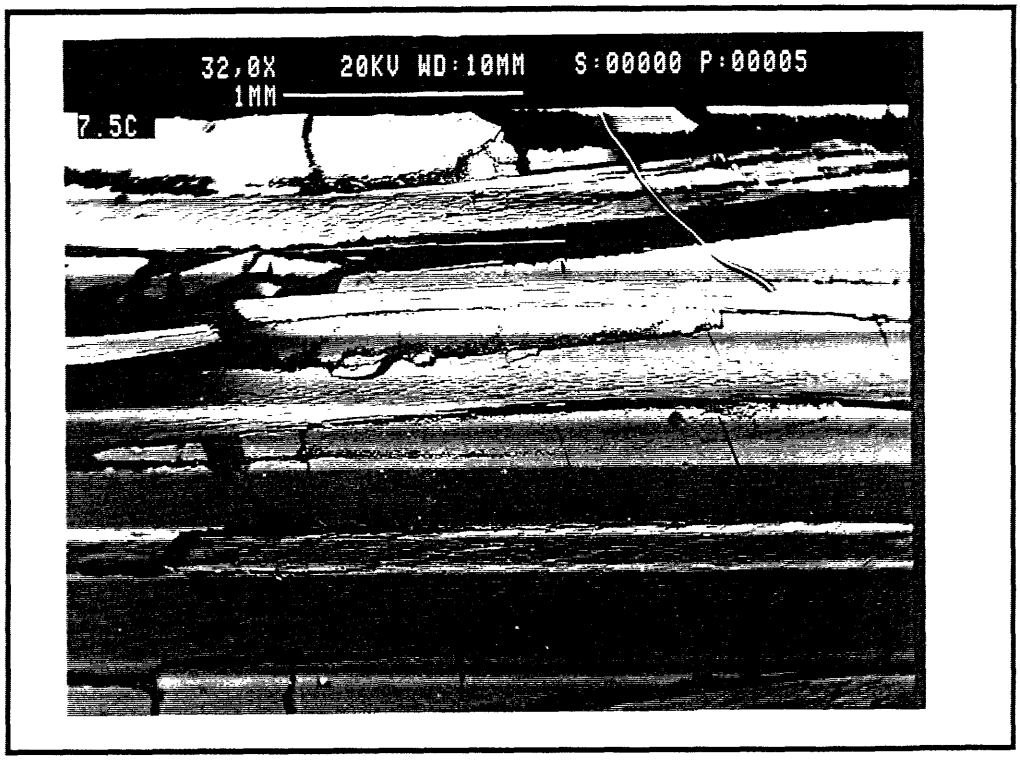

(a)

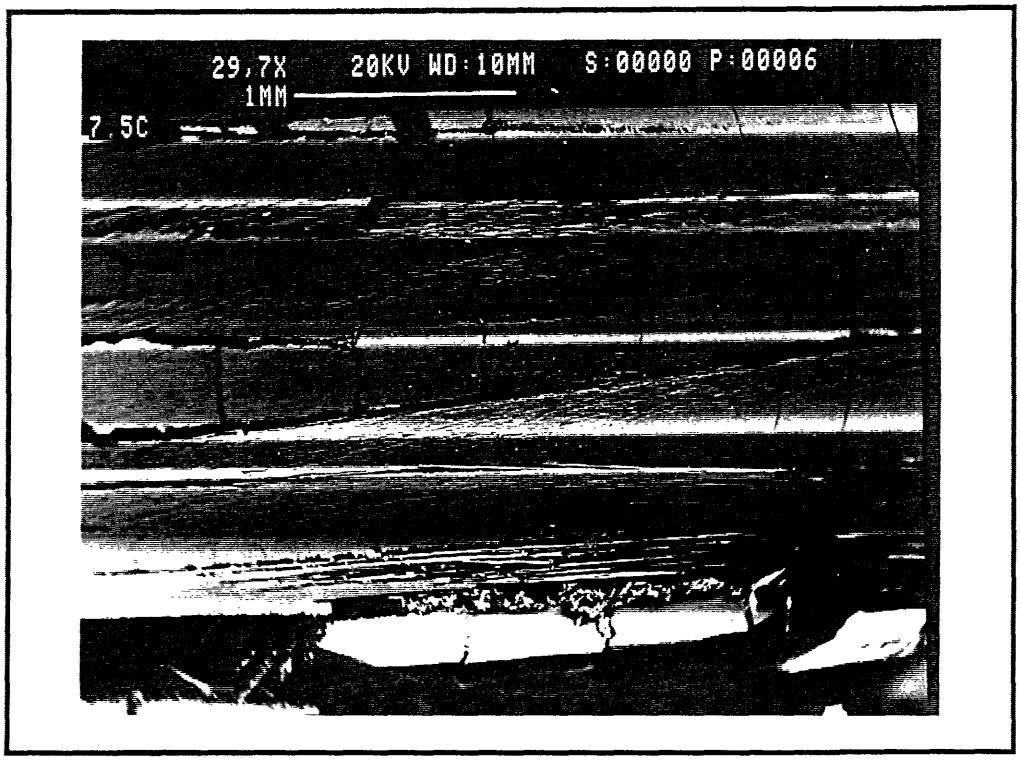

(b)

Fig. 73 : SEM micrographs of the fracture surface (longitudinal view) of carbon fabric with 7.5% rubber (a) Top surface (b) Bottom surface.

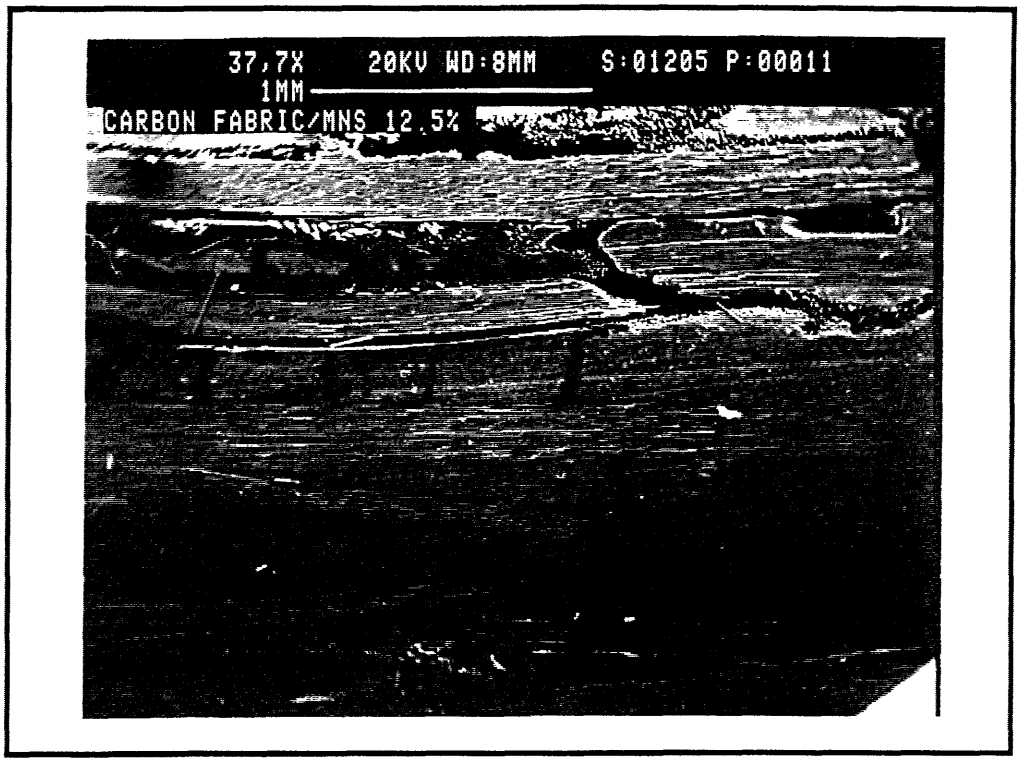

(a)

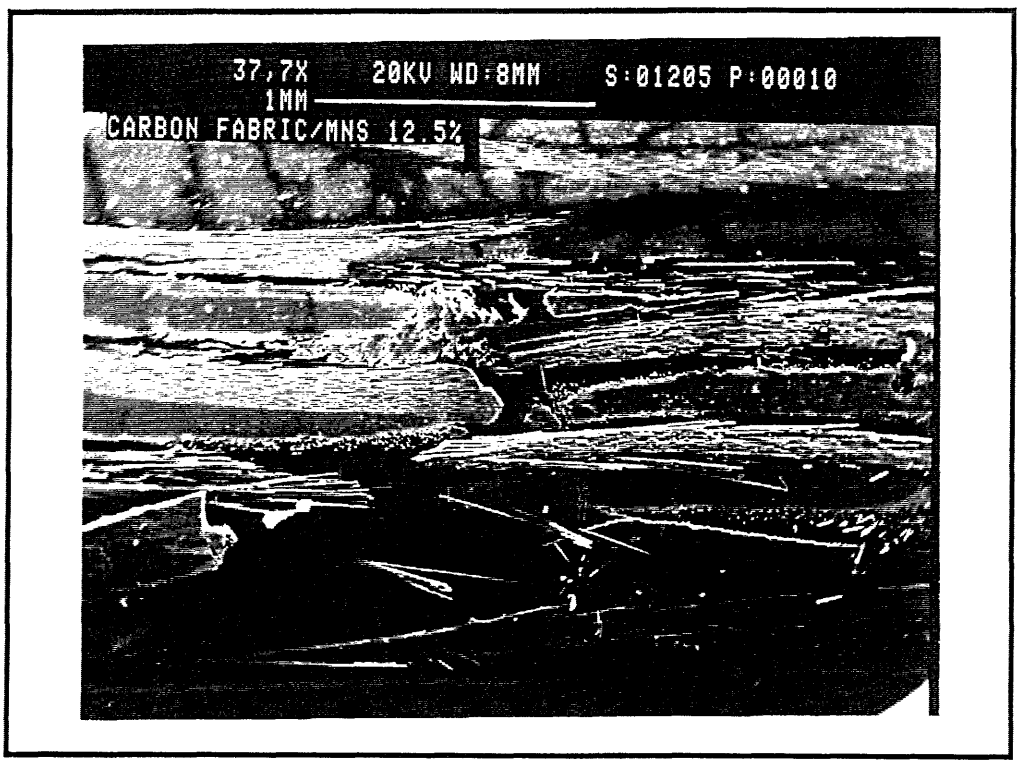

(b)

Fig. 74 : SEM micrographs of the fracture surface (longitudinal view) of carbon fabric with 12.5% rubber (a) Top surface (b) Bottom surface.

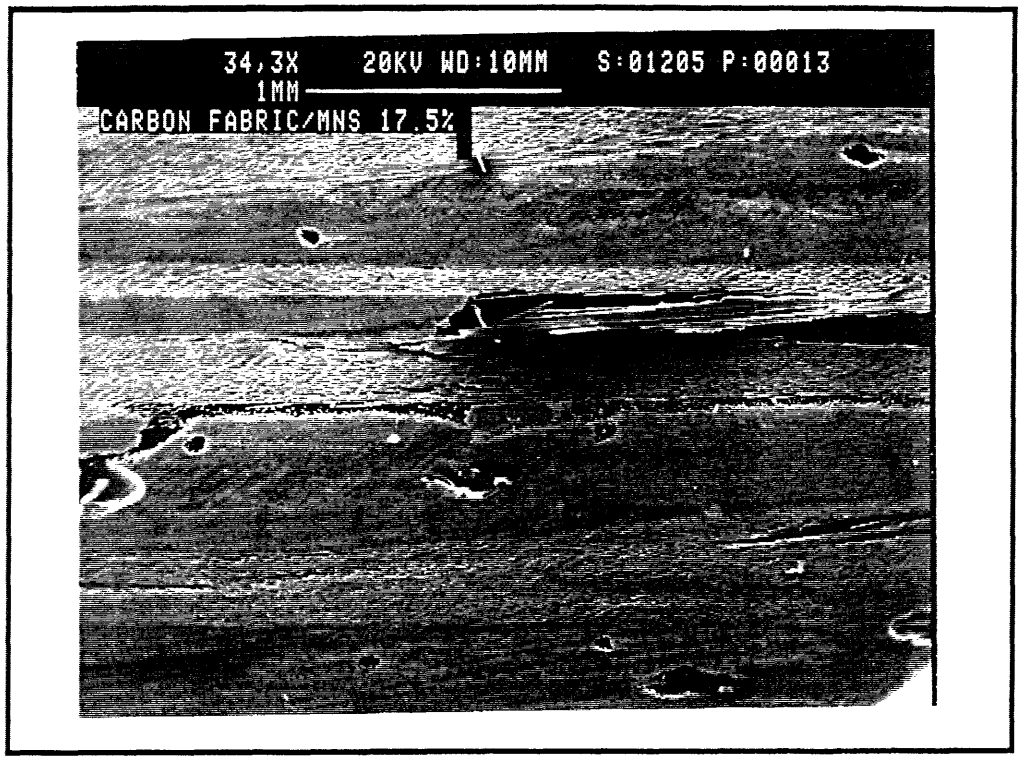

(a)

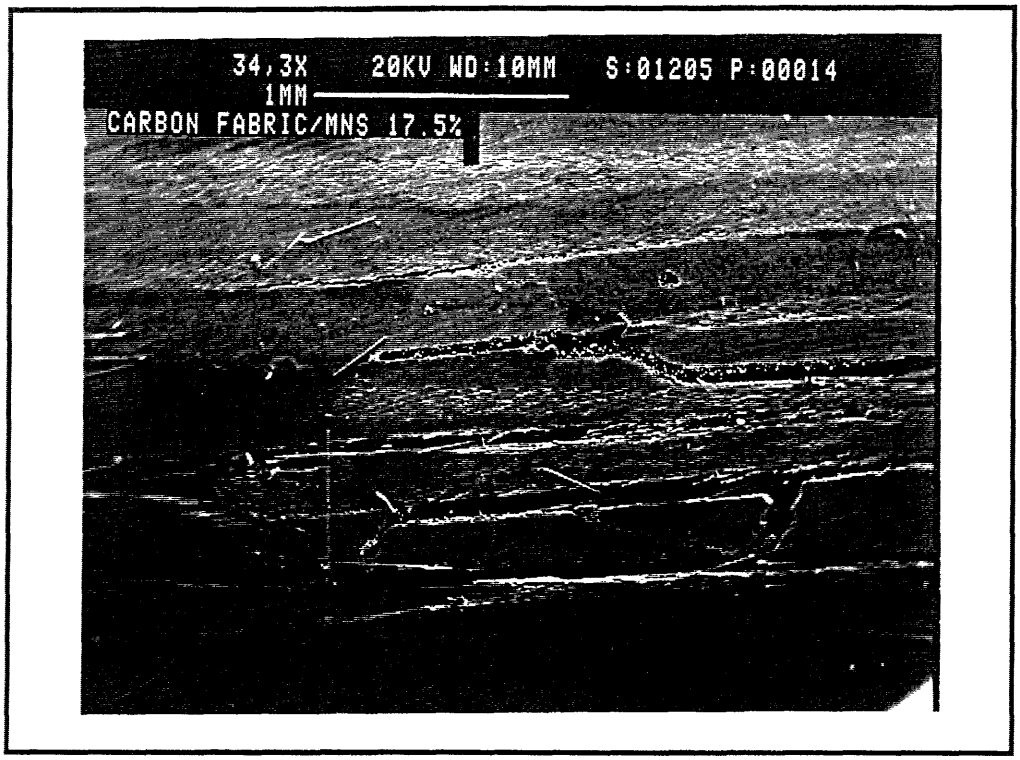

(b)

Fig. 75 : SEM micrographs of the fracture surface (longitudinal view) of carbon fabric with 17.5% rubber (a) Top surface (b) Bottom surface.

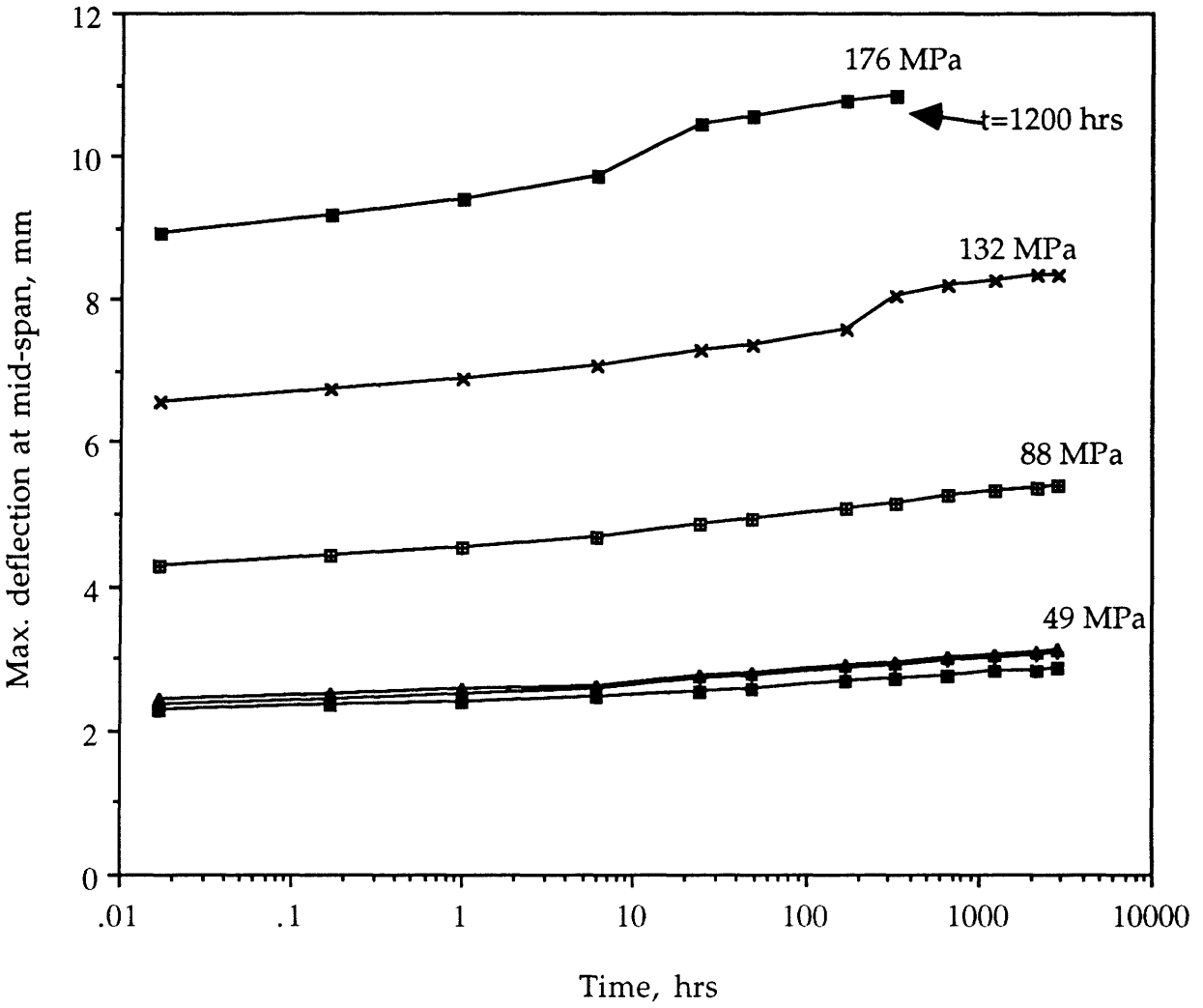

Fig : 76 : The deflection Vs. time curve in a creep test on chopped strand mat with 7.5% rubber.

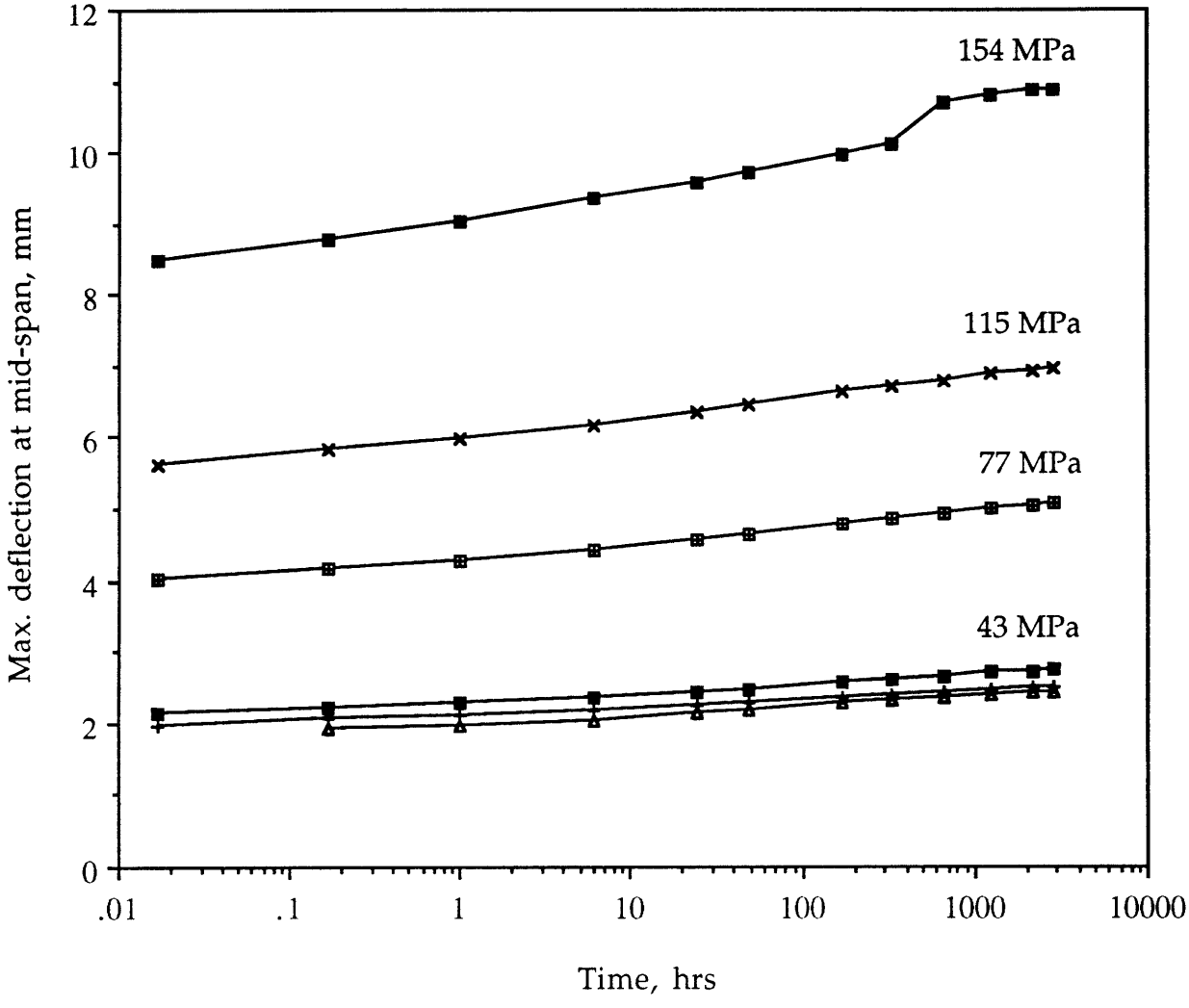

Fig : 77 : The deflection Vs. time curve in a creep test on chopped strand mat with 12.5% rubber.

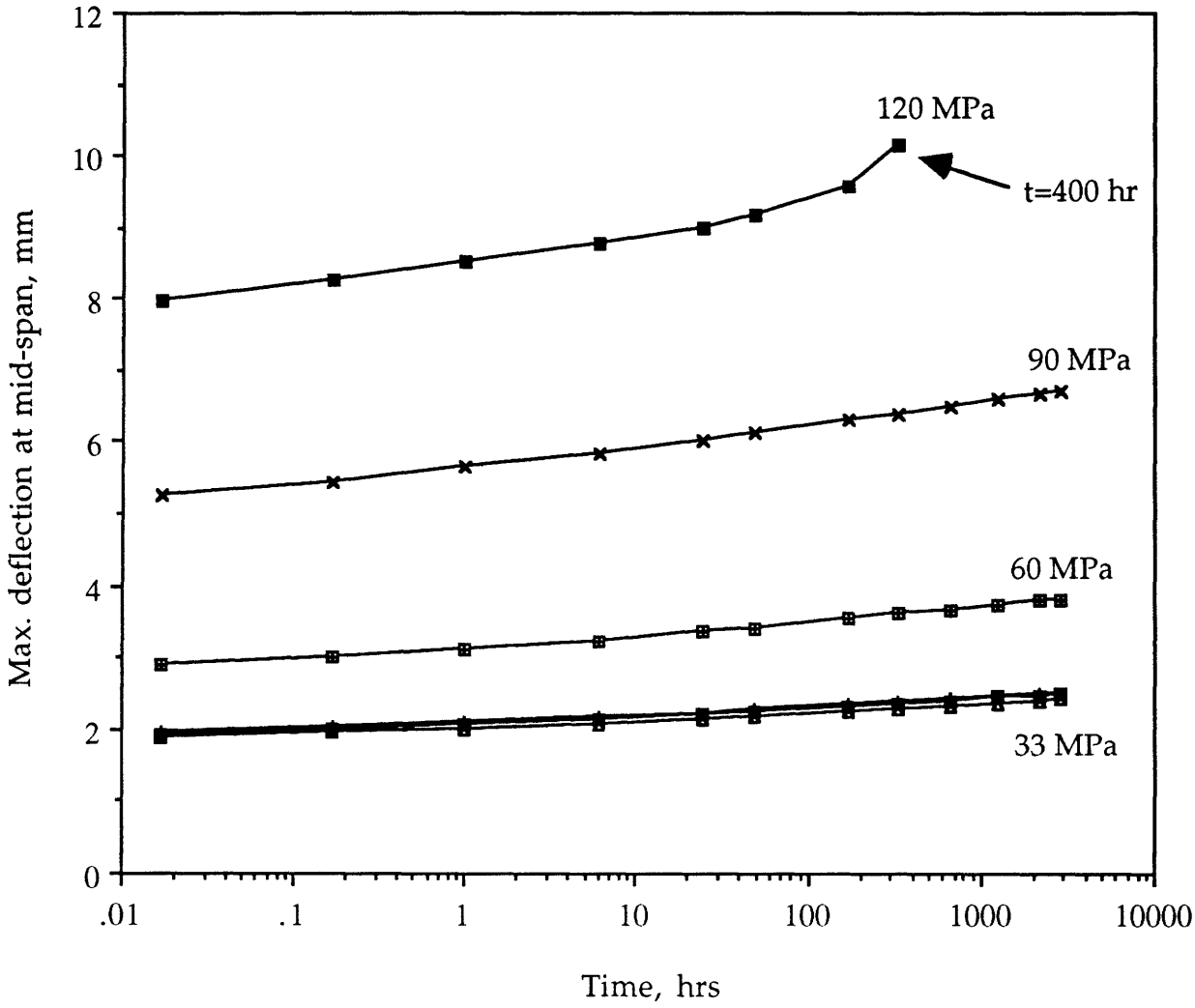

Fig : 78 : The deflection Vs. time curve in a creep test on chopped strand mat with 17.5% rubber.

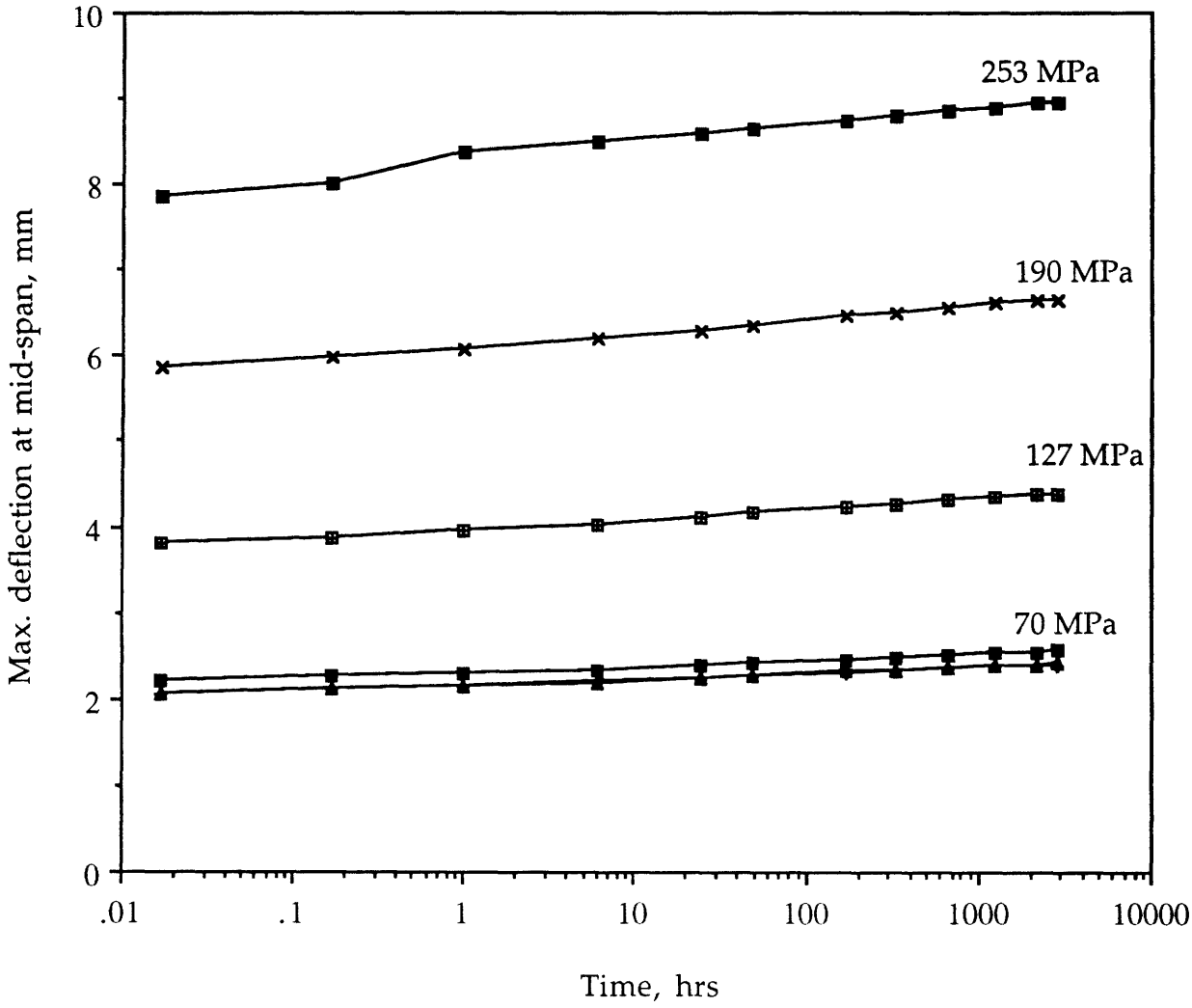

Fig : 79 : The deflection Vs. time curve in a creep test on glass fabric with 7.5% rubber.

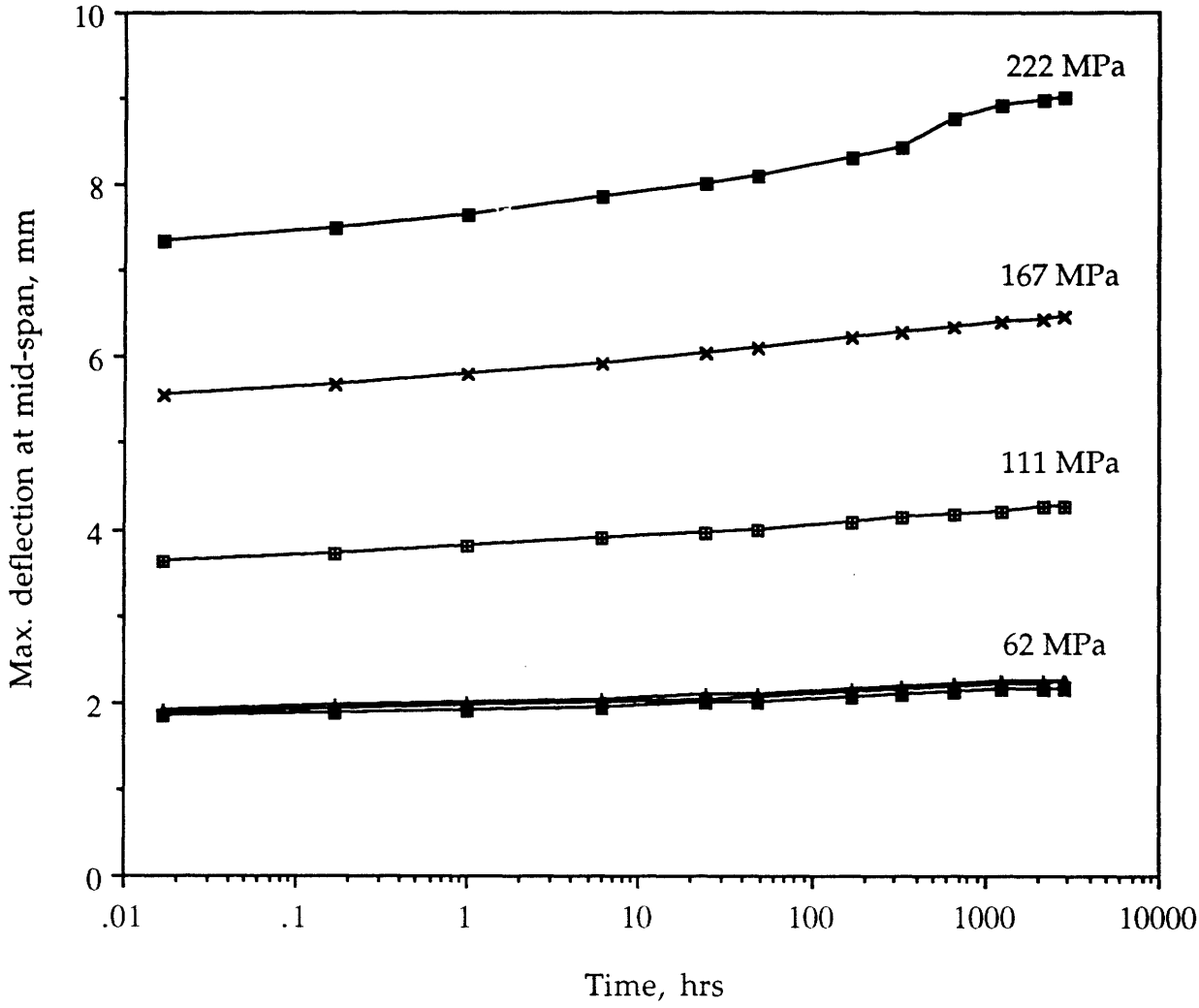

Fig : 80 : The deflection Vs. time curve in a creep test on glass fabric with 12.5% rubber.

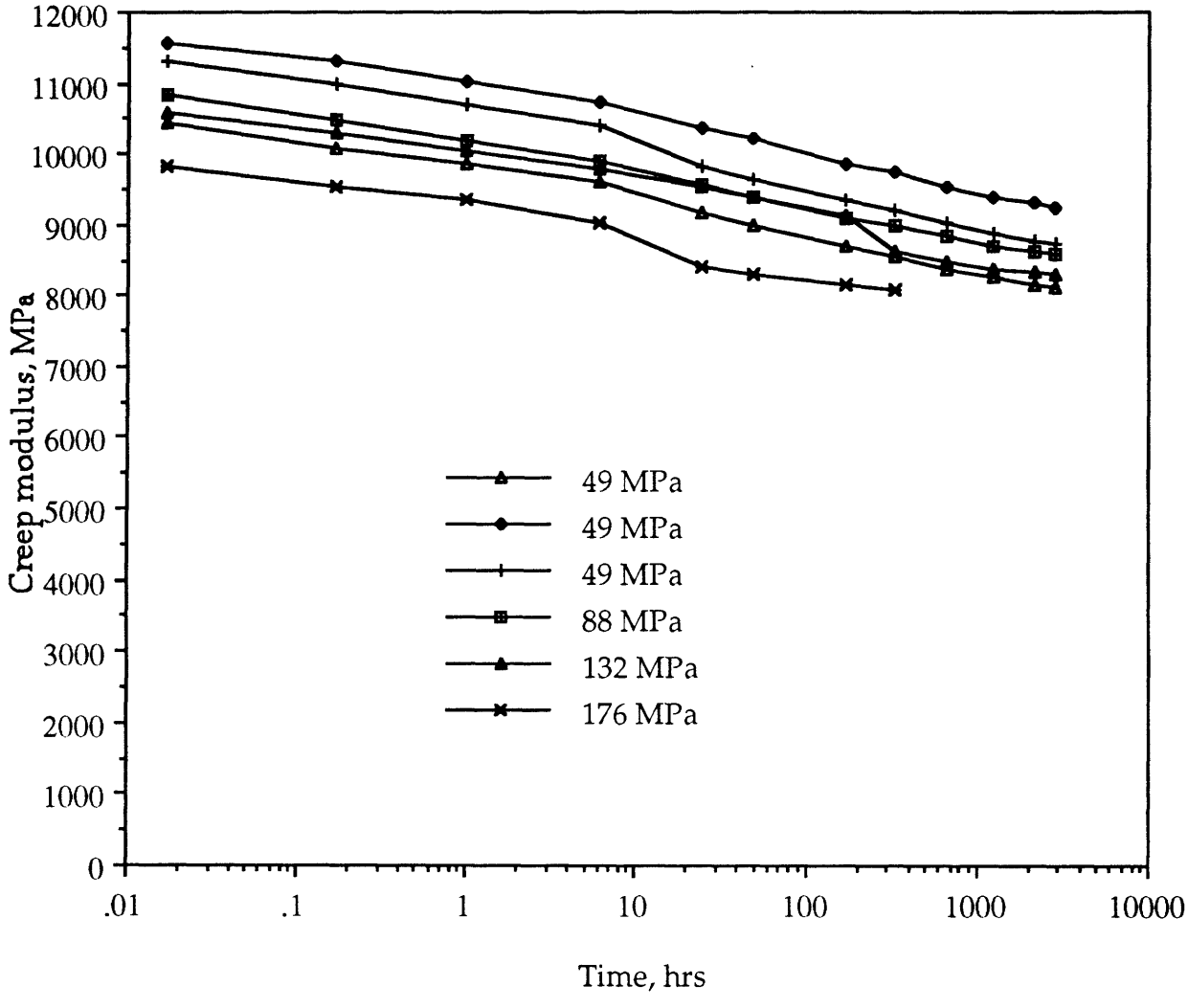

Fig : 81 : The creep modulus Vs. time curve for chopped strand mat with 7.5% rubber.

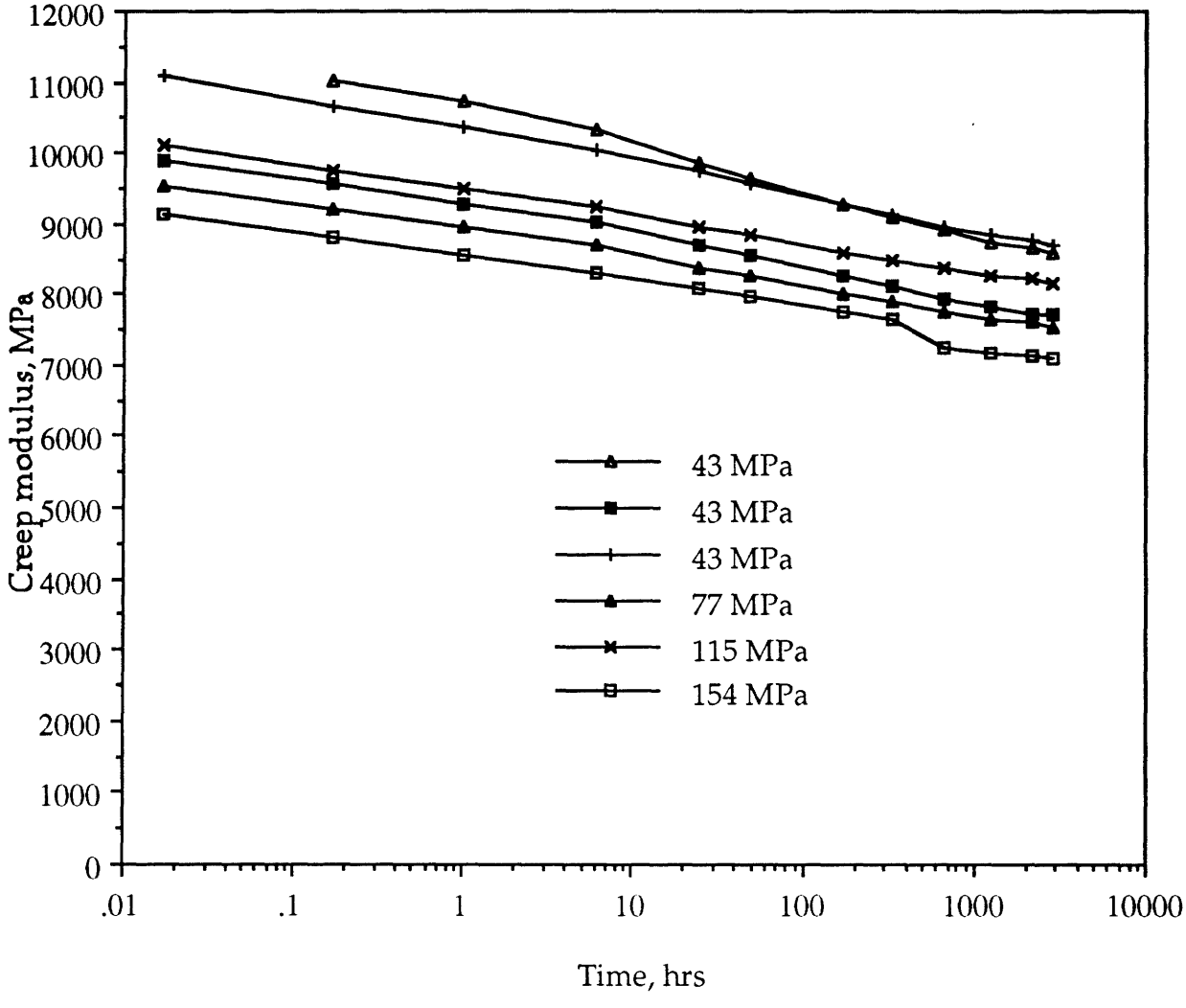

Fig : 82 : The creep modulus Vs. time curve for chopped strand mat with 12.5% rubber.

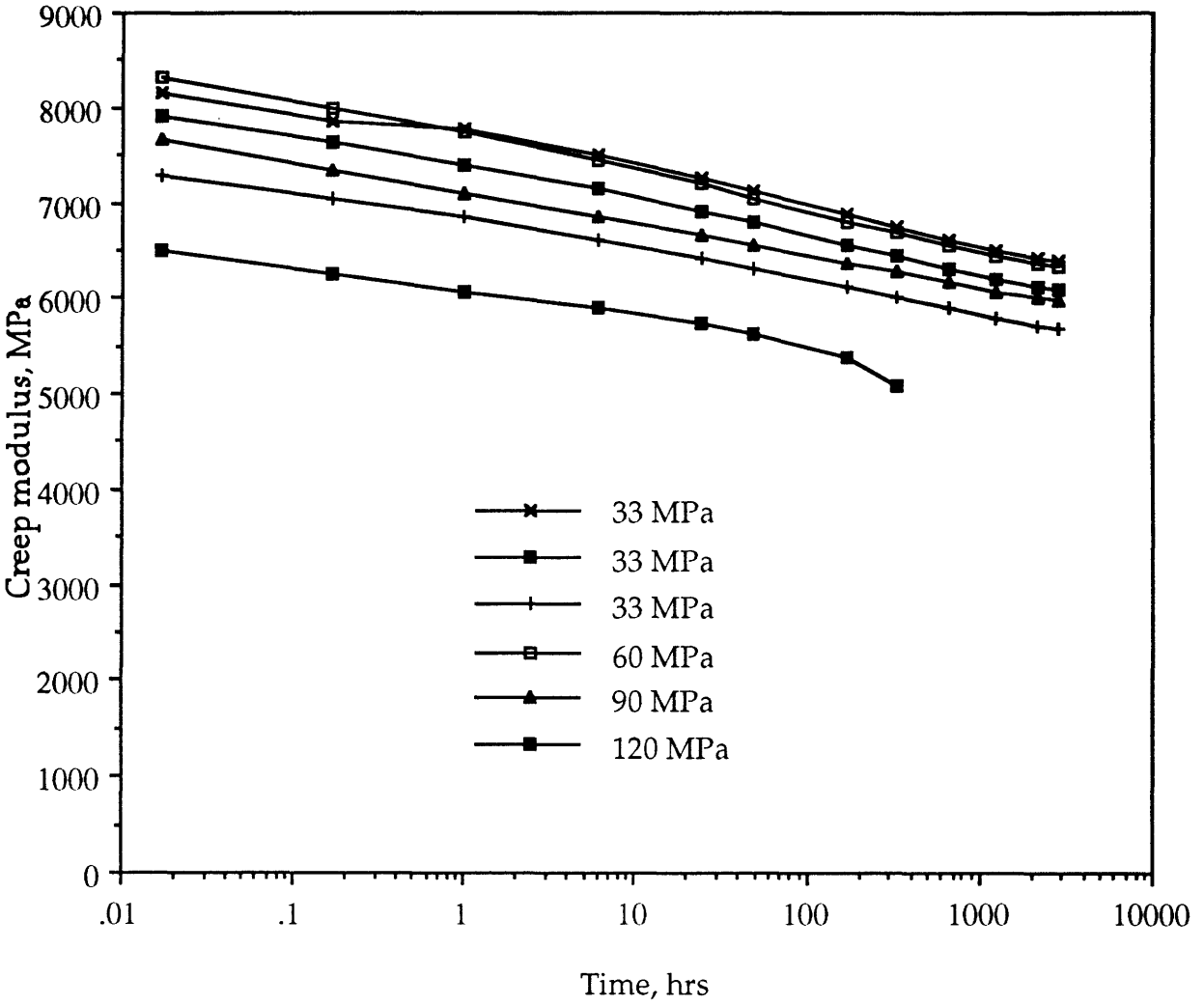

Fig : 83 : The creep modulus Vs. time curve for chopped strand mat with 17.5% rubber.

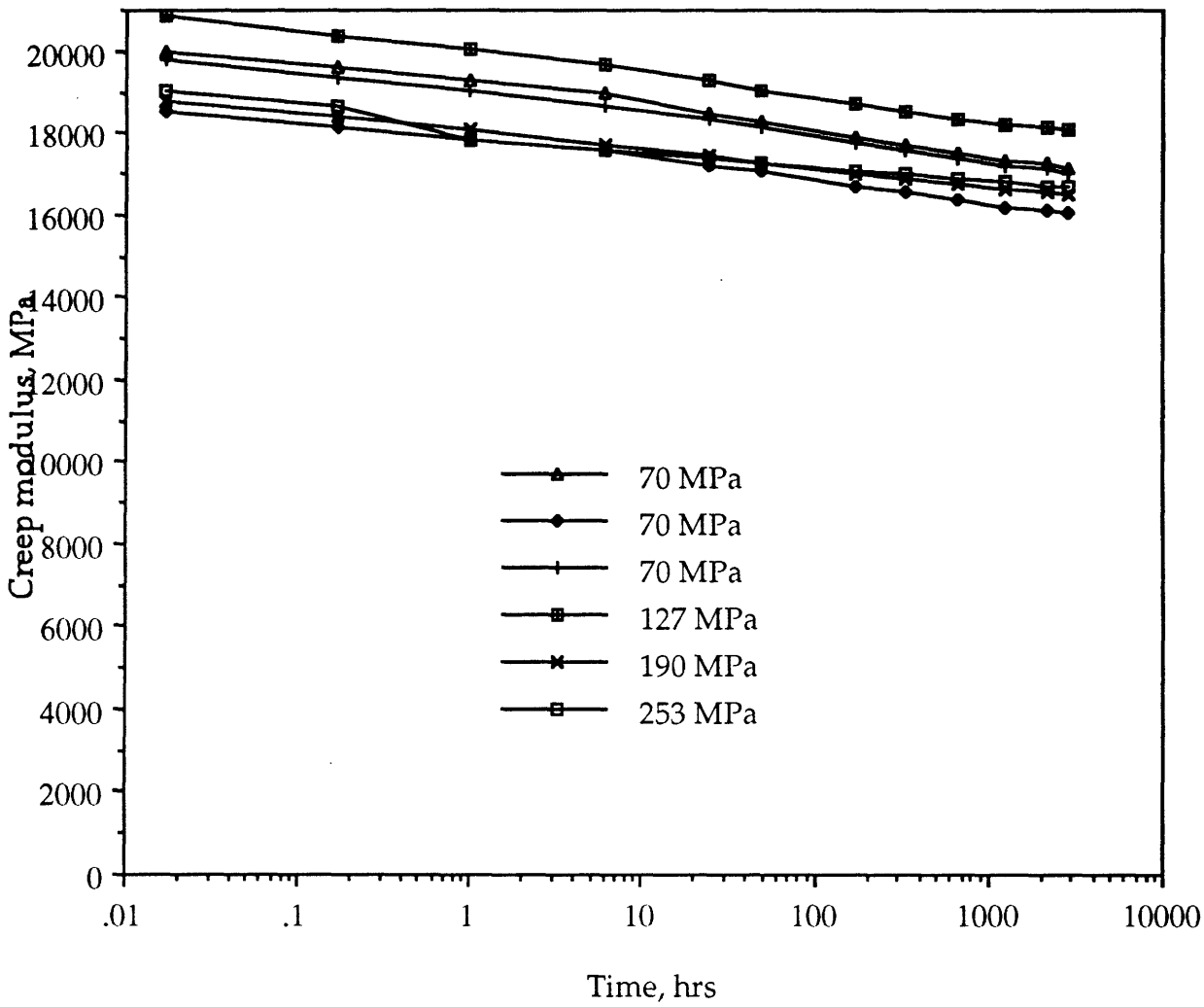

Fig : 84 : The creep modulus Vs. time curve for glass fabric with 7.5% rubber.

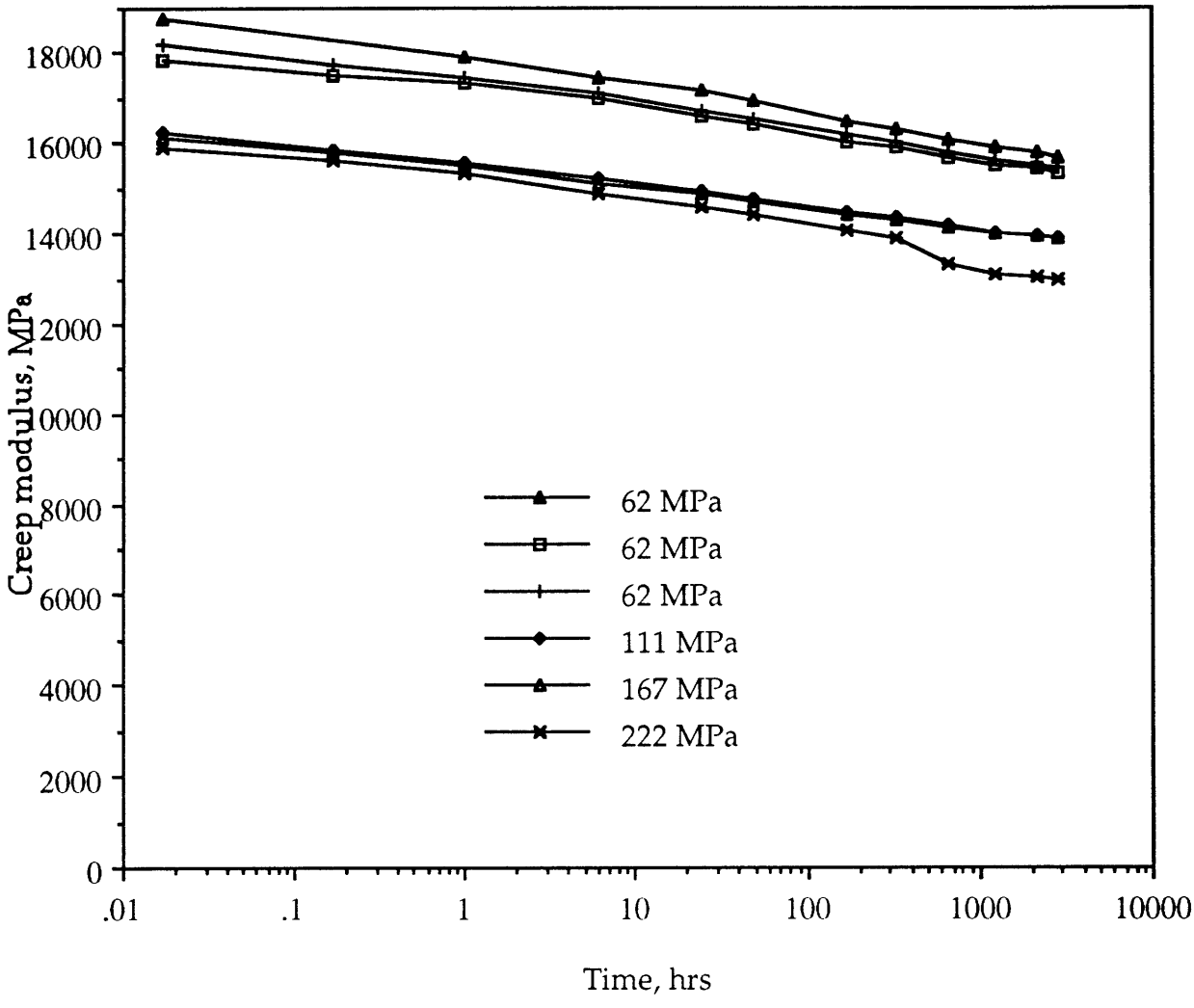

Fig : 85 : The creep modulus Vs. time curve for glass fabric with 12.5% rubber.

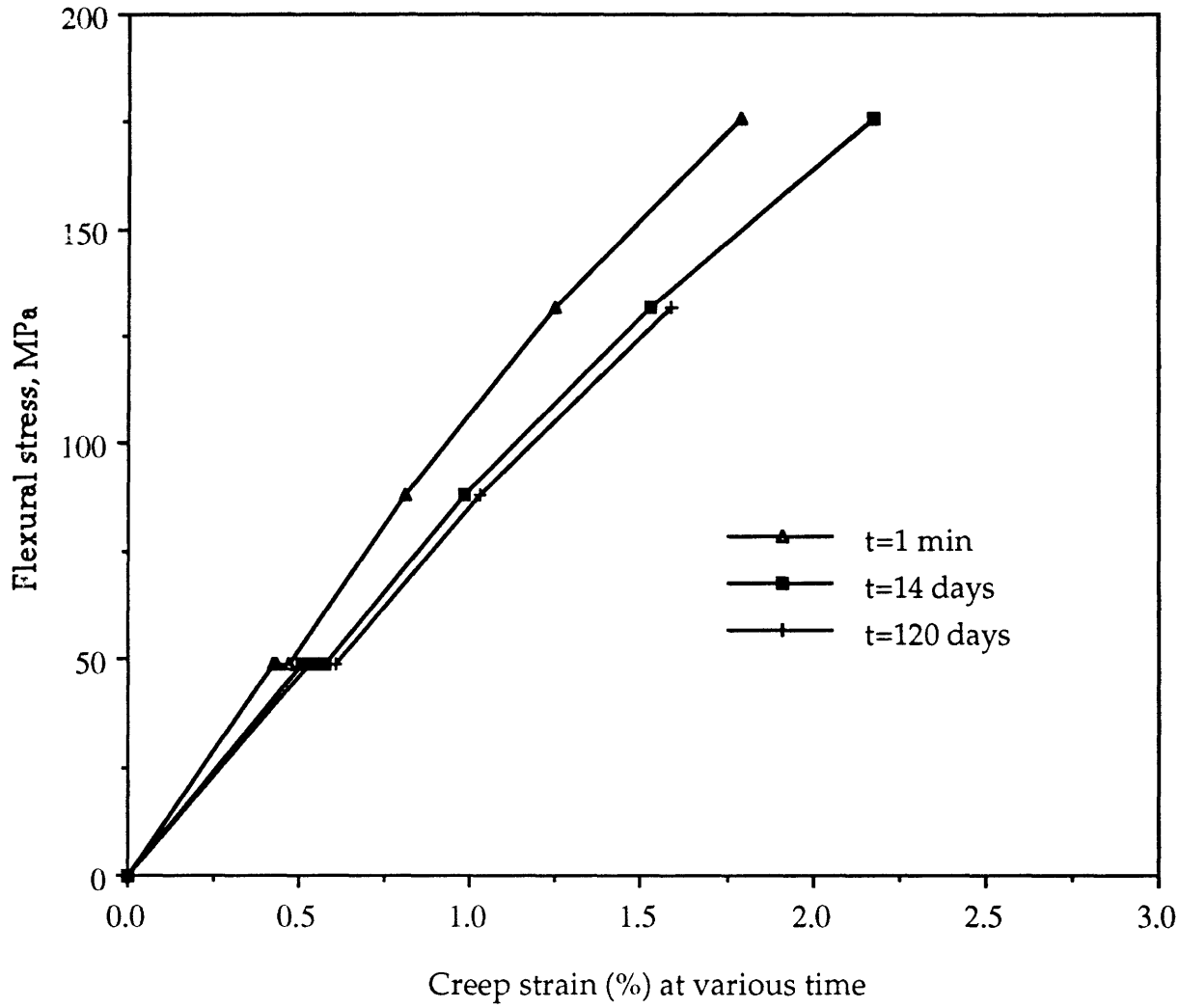

Fig : 86 : Isochronous stress-strain curve for chopped strand mat with 7.5% rubber at various times.

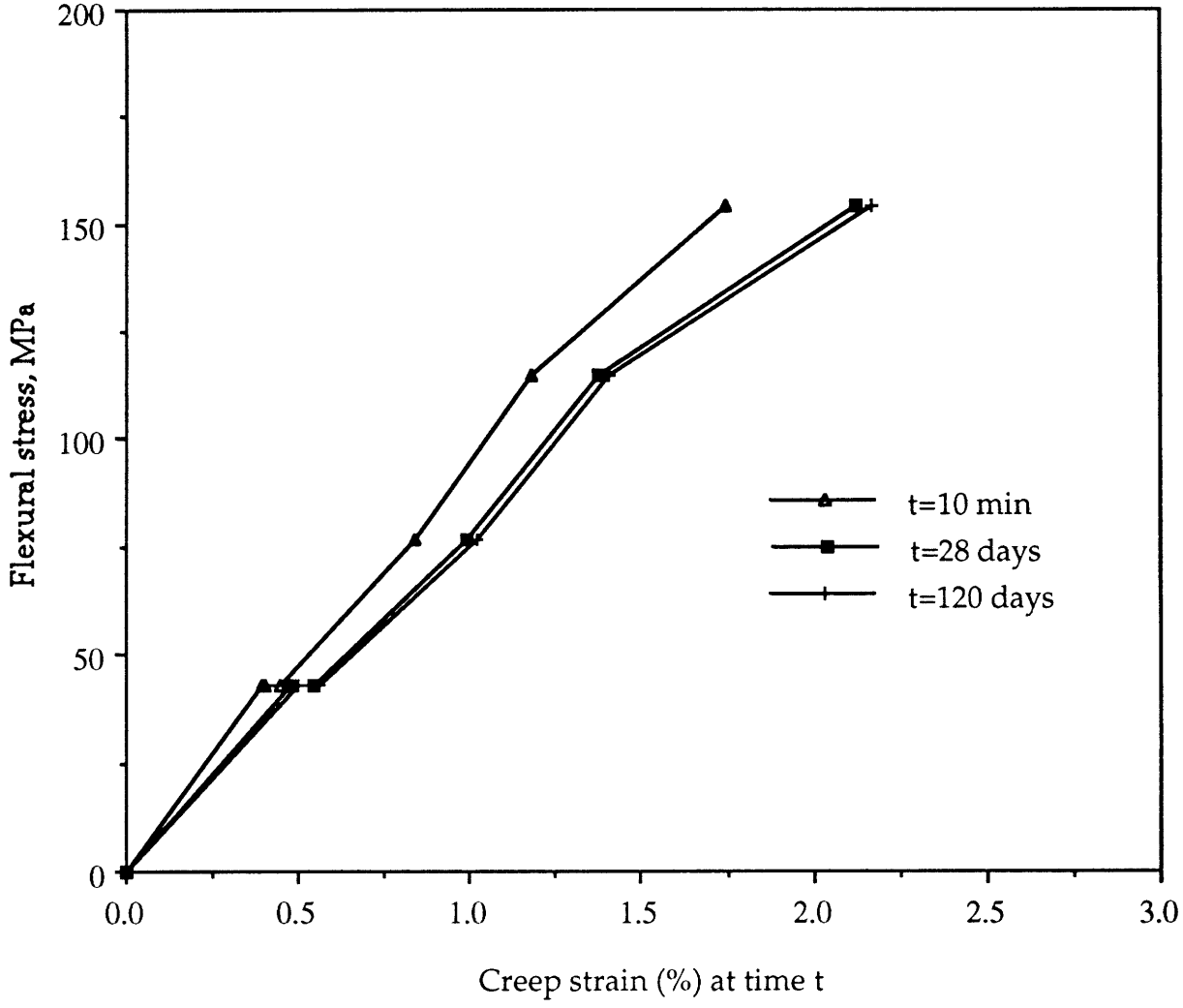

Fig : 87 : Isochronous stress-strain curve for chopped strand mat with 12.5% rubber at various times.

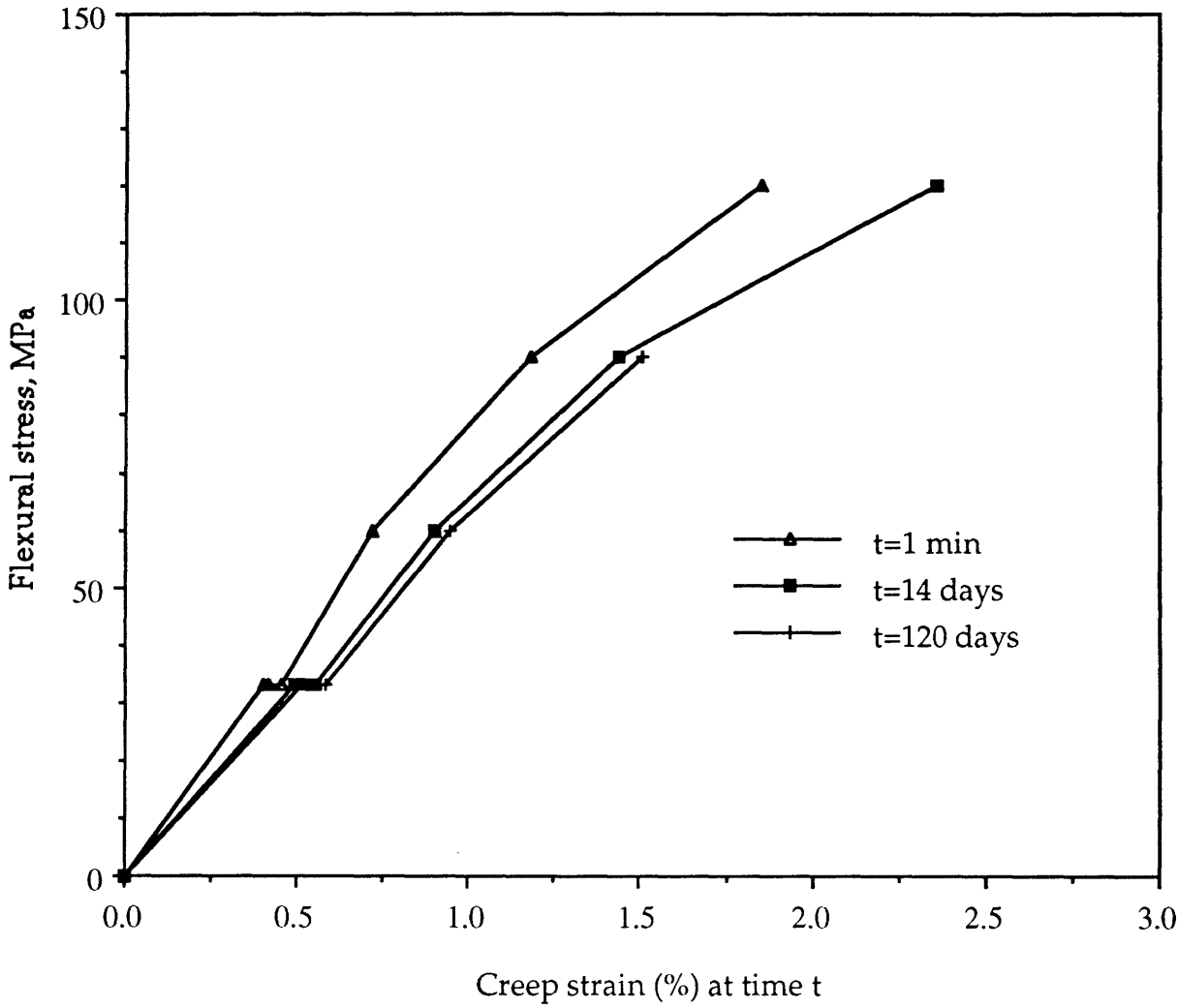

Fig : 88 : Isochronous stress-strain curve for chopped strand mat with 17.5% rubber at various times.

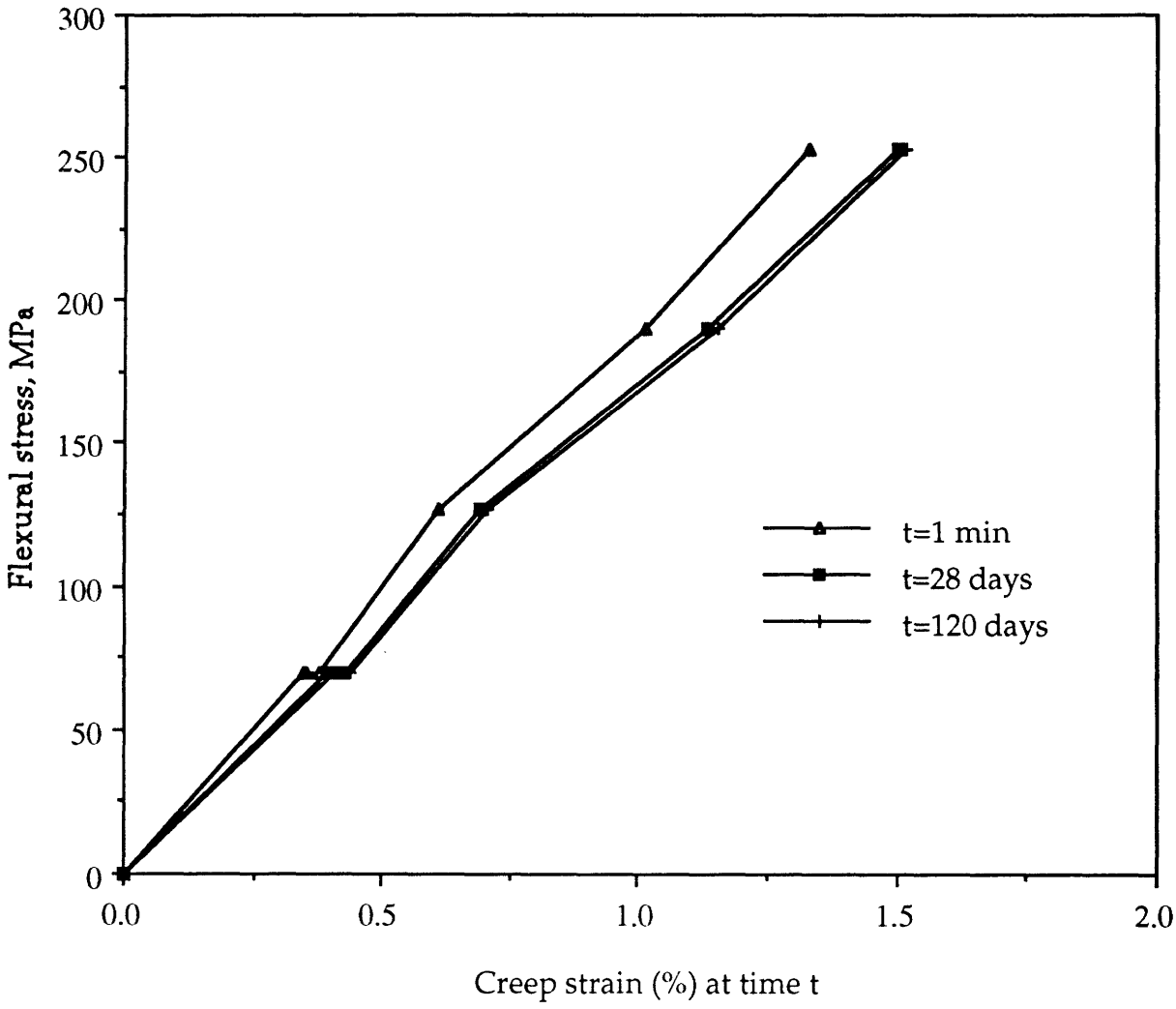

Fig : 89 : Isochronous stress-strain curve for glass fabric with 7.5% rubber at various times.

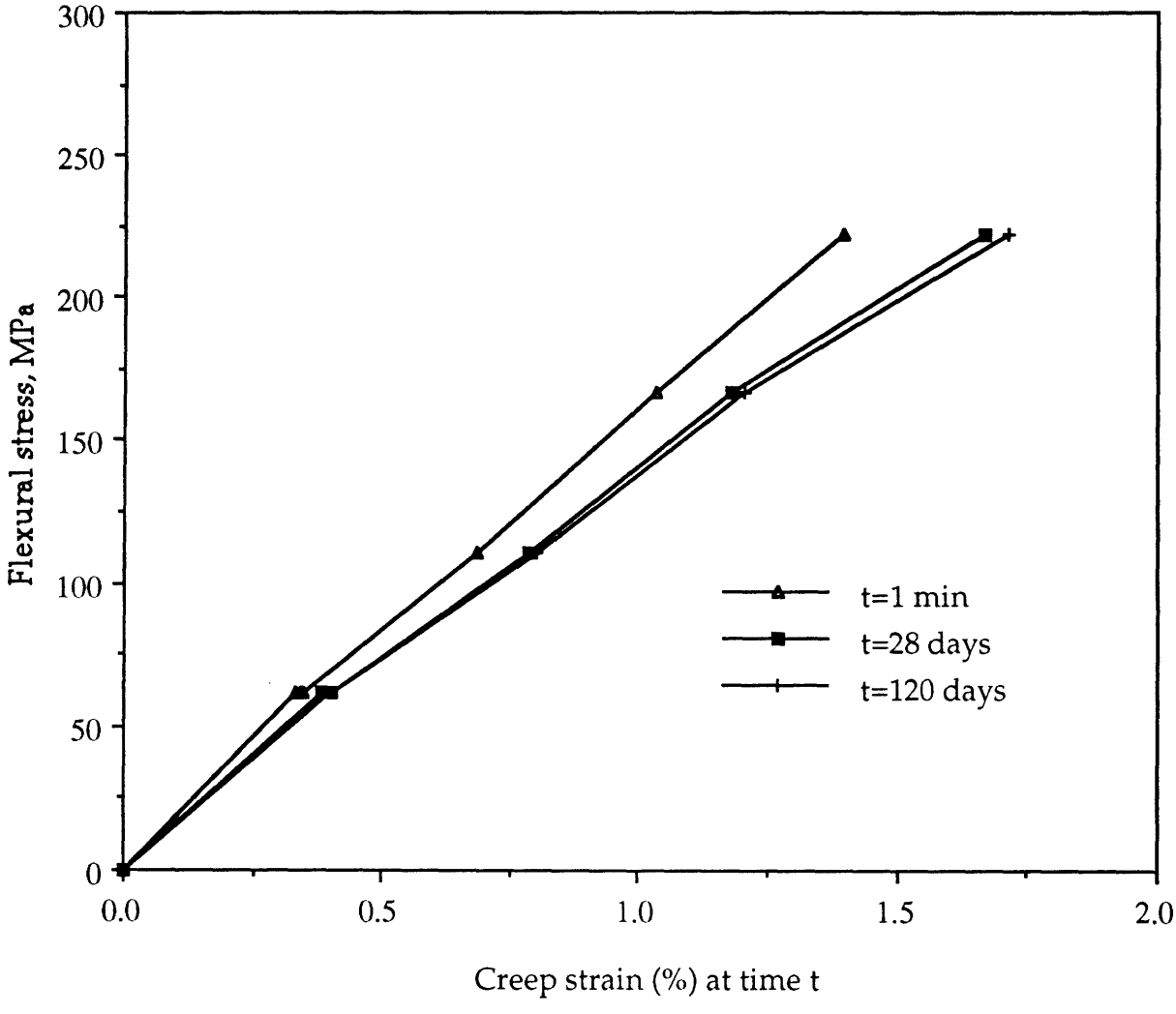

Fig : 90 : Isochronous stress-strain curve for glass fabric with 12.5% rubber at various times.

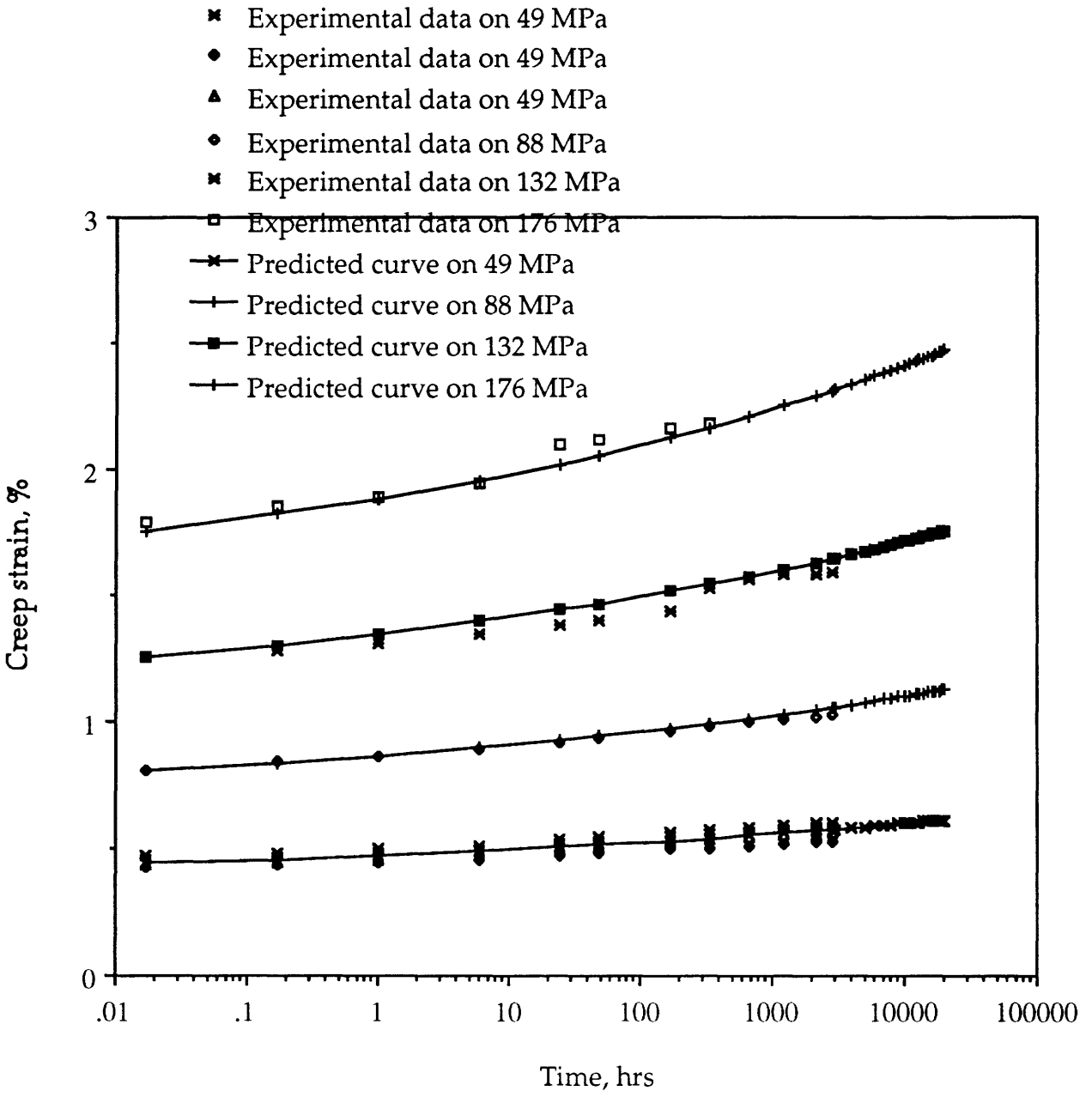

Fig : 91 : Predicted and experimental creep strain Vs. time curve for chopped strand mat with 7.5% rubber .

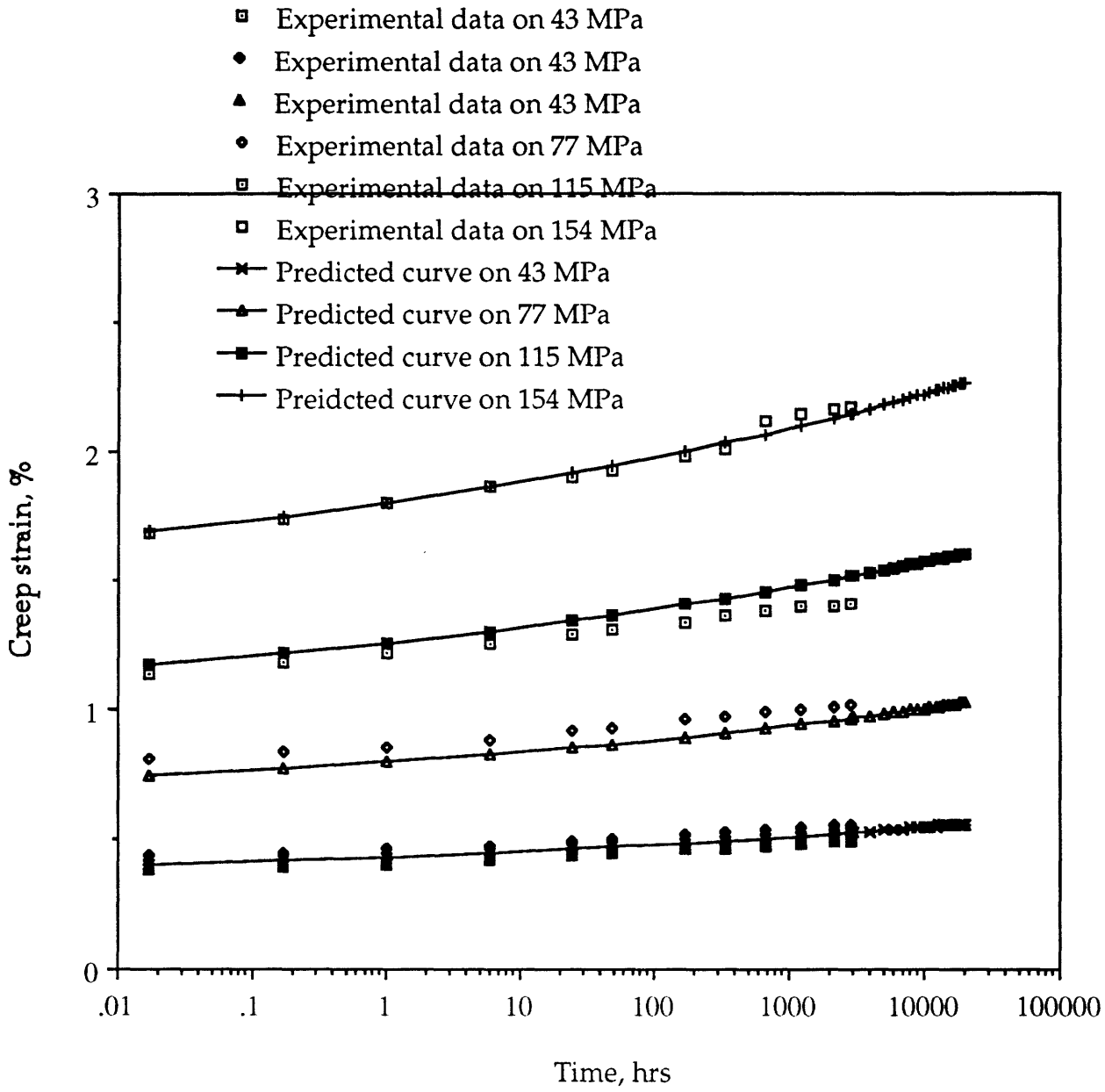

Fig : 92 : Predicted and experimental creep strain Vs. time curve for chopped strand mat with 12.5% rubber.

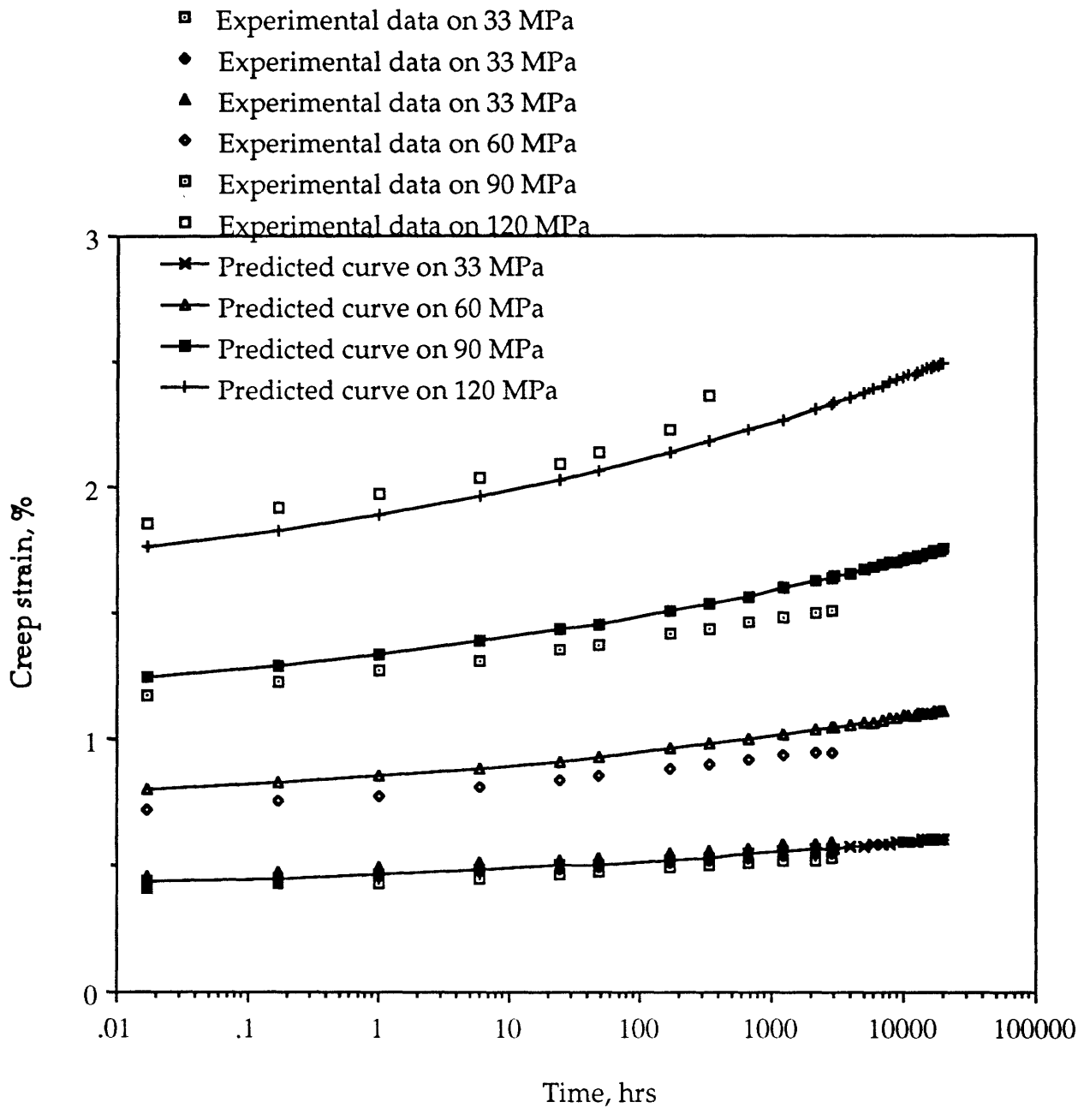

Fig : 93 : Predicted and experimental creep strain Vs. time curve for chopped strand mat with 17.5% rubber.

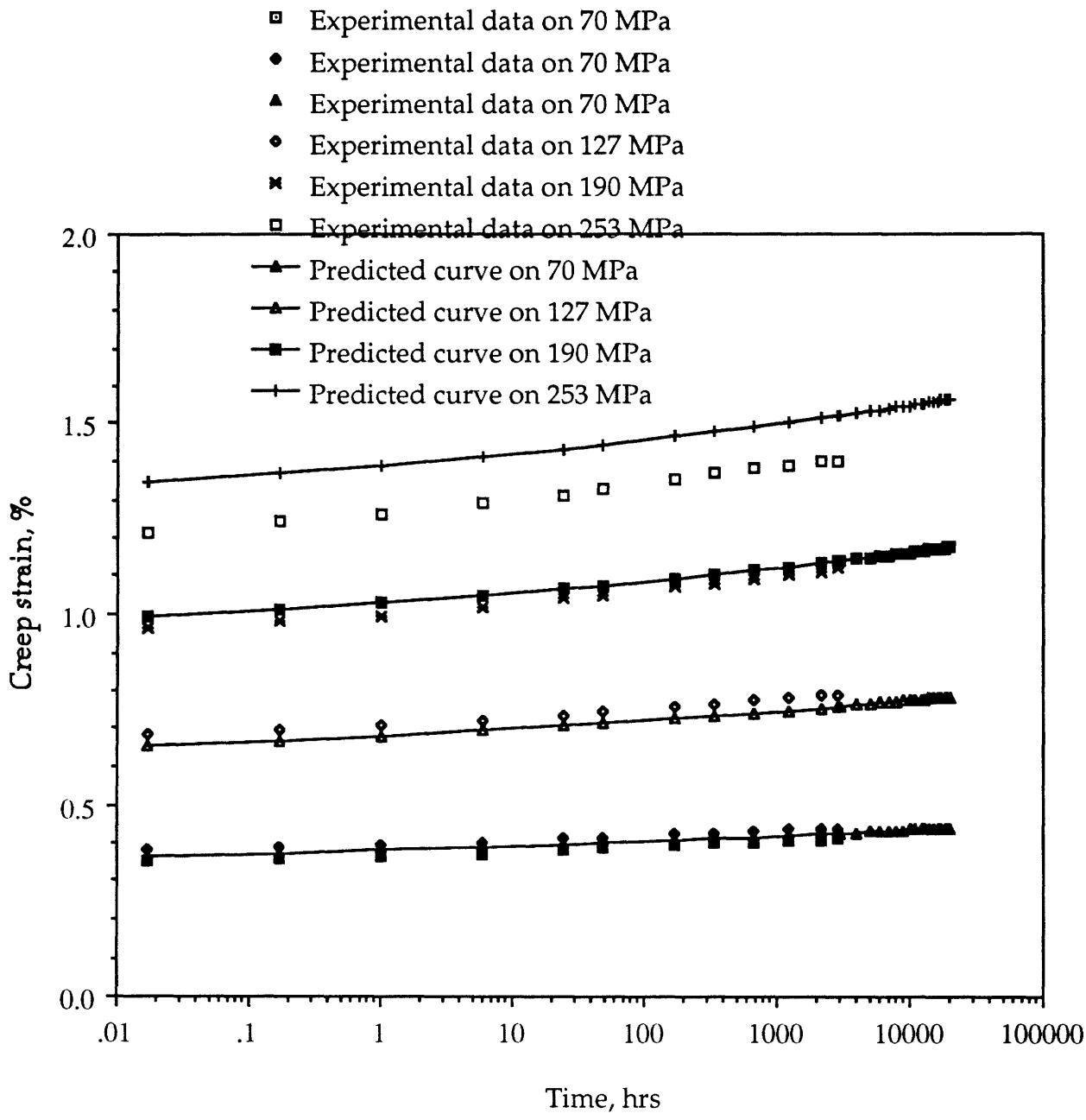

Fig : 94 : Predicted and experimental creep strain Vs. time curve for glass fabric with 7.5% rubber.

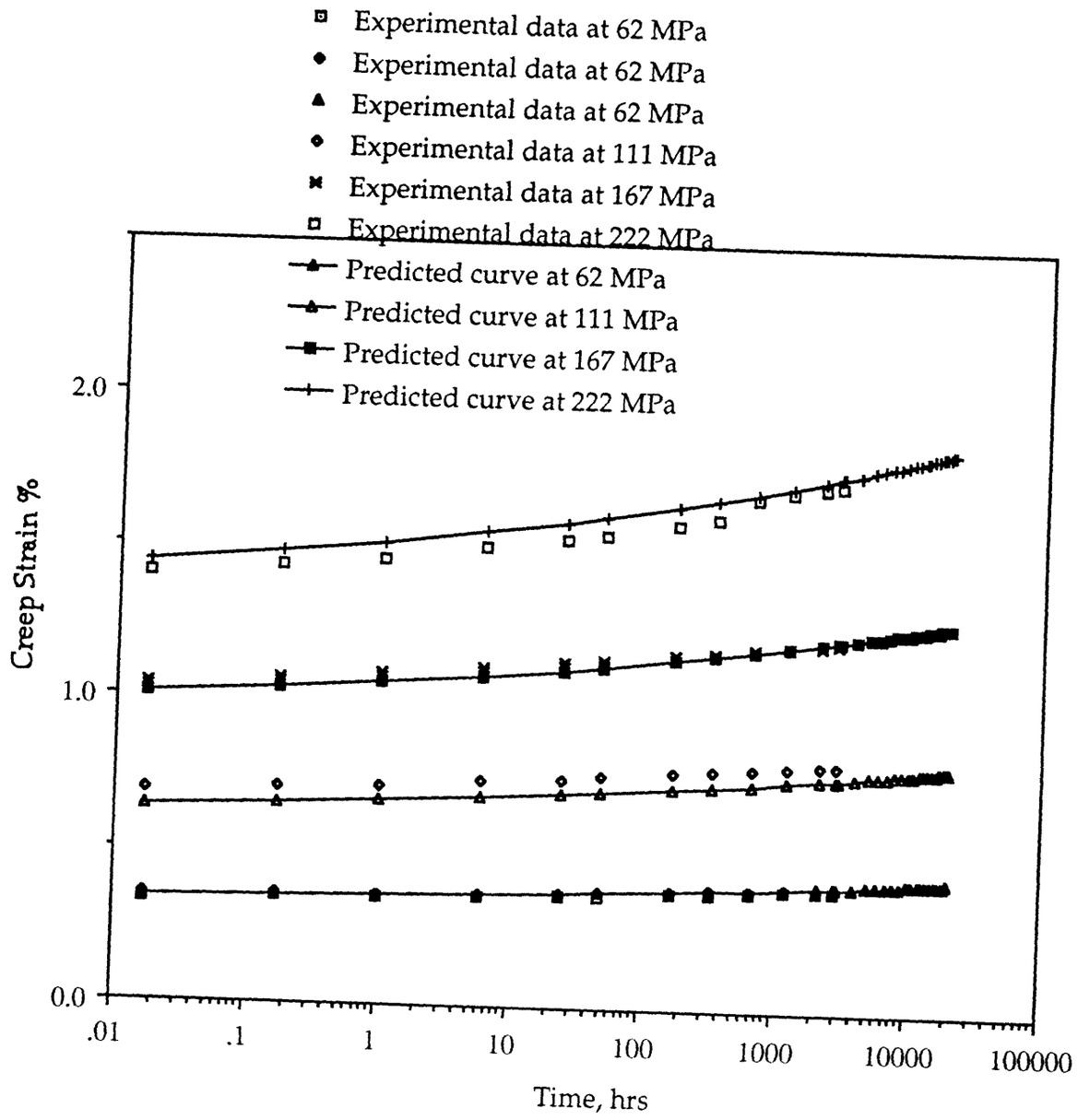

Fig : 95 : Predicted and experimental creep strain Vs. time curve for glass fabric with 12.5% rubber.

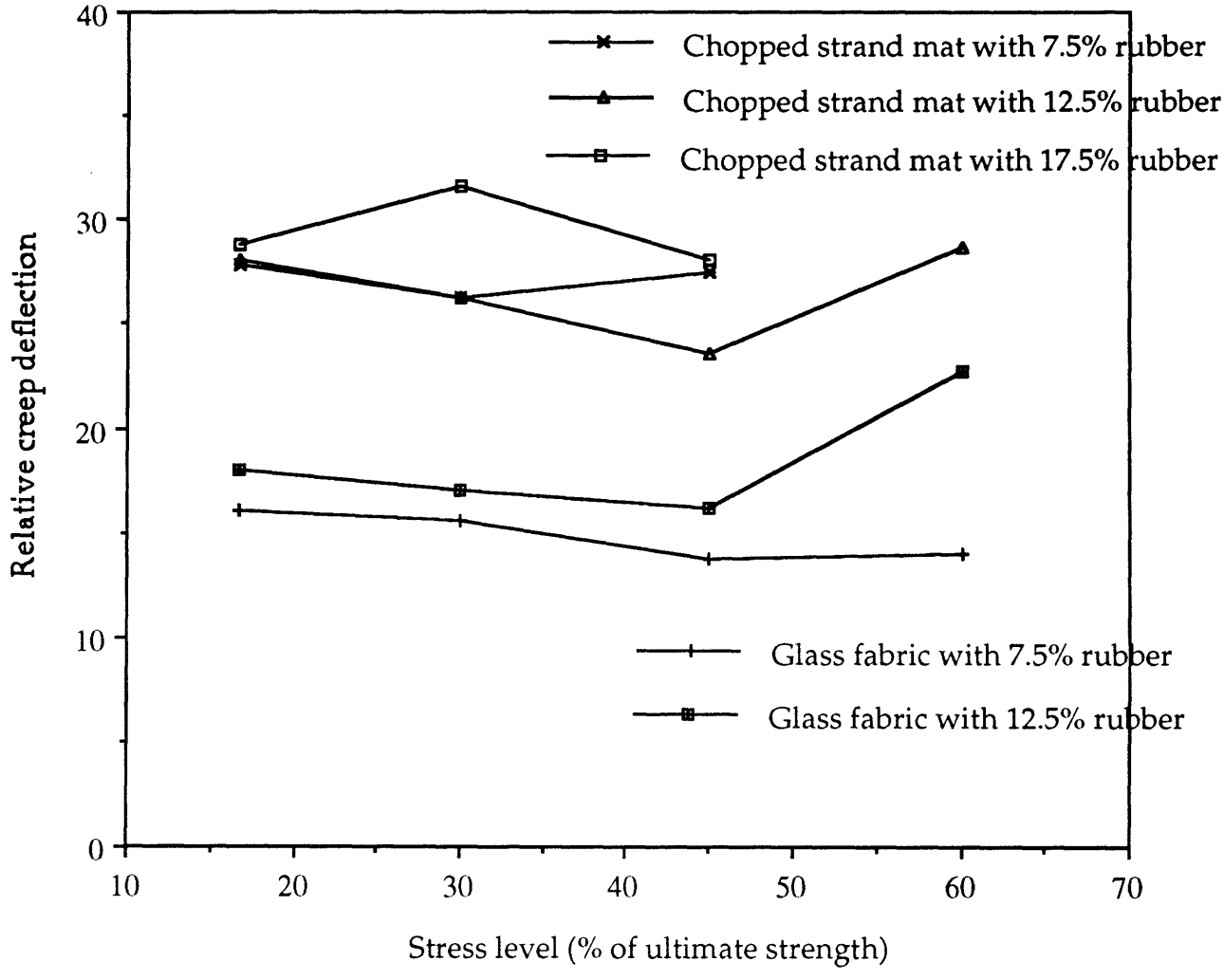

Fig : 96 : Relative creep deflection Vs. stress level (on which the creep test is performed) for different composites

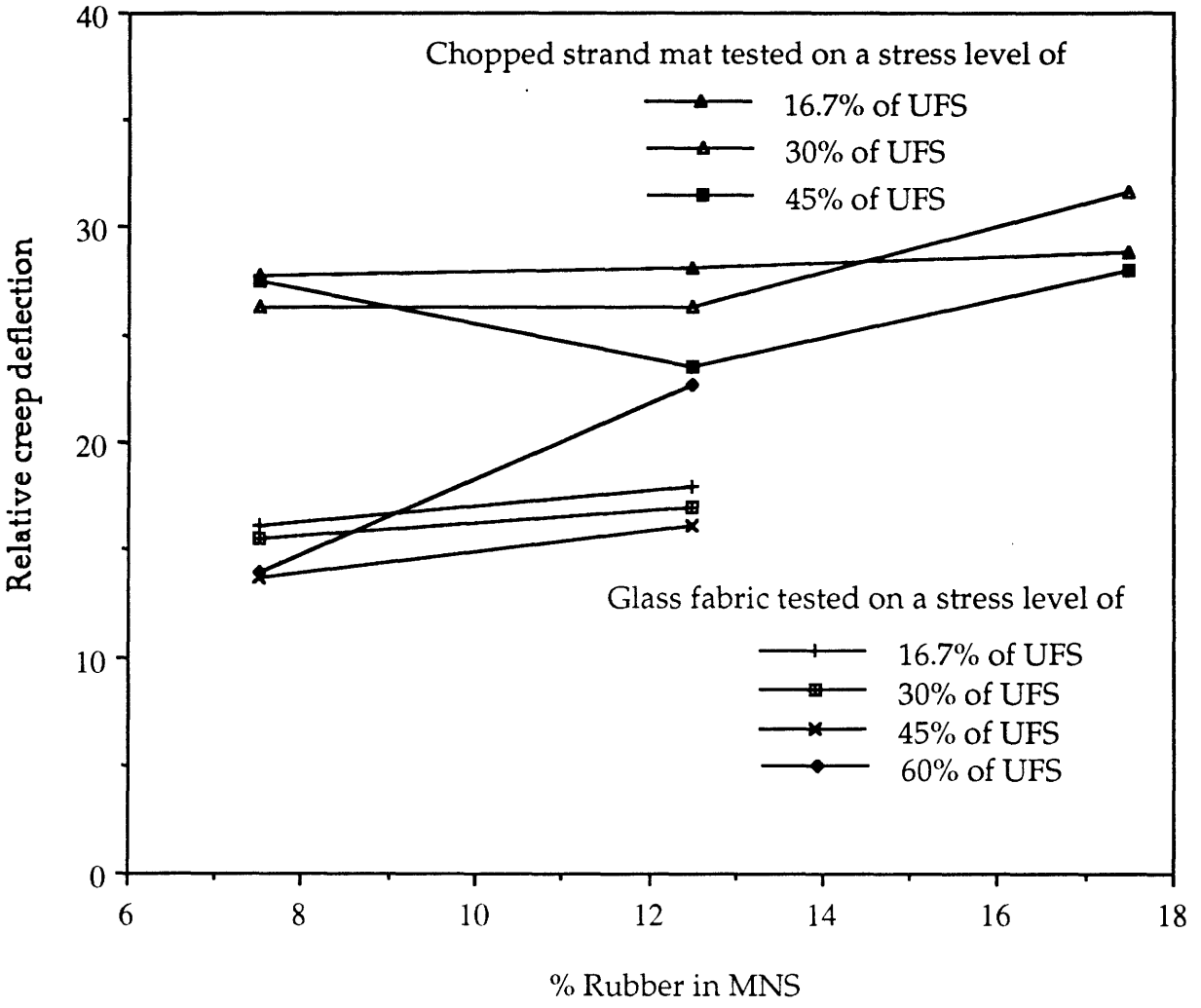

Fig : 97 : Relative creep deflection Vs. rubber content in MNS at different stress level.

References

1. Subramaniam, R. , Flüeler, Peter H. , McGarry, F. J. , "Composite based on Molecular Network system".
2. McGarry, F. J. , Subramaniam, R. , "Molecular Network System : A Toughened Crosslinked Polyester System".
3. Osborn, Jason W. , "The effect of full flexural fatigue on the flexural strength composites", Master of Science Thesis, MIT (1991).
4. Kim, Ran Y. , "Fatigue Behavior", Composite Design 4th Ed. (Stephen W. Tsai, ed.), p 19-1, Think Composites (1988).
5. Talreja, Ramesh, "Fatigue of Composite Materials", Technomic Publishing Company (1987).
6. Oldyrev, P. P. , "Construction of Fatigue curves in hard high-cycle loading of reinforced plastics", Mechanics of Composite Materials, v. 23, n. 3, Nov 1987, p 319-325.
7. Murkani, R. , Noriaki, S. , Kusumato, N. and Yoshiaki, M. , "Tensile Fatigue Characteristic of Polymer Blends" Kobunshi Robunshu, Eng. Ed. , Vol. 5, n 3 (1976).
8. Hertzberg, Richard W. , Manson, John A. , "Fatigue of Engineering Plastics", Academic Press Inc (1980).
9. Joneja, Surendra K. , "Matrix Contribution to Fatigue Behavior of Glass Reinforced Polyester Composites", Journal of Reinforced Plastics and Composites, Vol. 6, n. 4 (1987).
10. Curtis, P. T. , "The Fatigue Behavior of Fibrous Composite Materials", Journal of Strain Analysis, Vol. 24, No. 4 (1989).
11. Konur, O. , Matthews, F. L. , "Effect of the properties of the constituents on the fatigue performance of composites : a review", Composites, Vol. 20, No. 4 (1989).
12. Mandell, J. F. , Huang, D. D. , McGarry, F. J. , "Tensile Fatigue Performance of Glass Fiber Dominated Composites", Research Report R80-4, MIT (1980).
13. Jones, C. J. , Dickson, R. F. , Adam, T. , Reiter, H. and Harris, B. , "The environmental fatigue behavior of reinforced plastics", Proc. Royal Soc. London, A 396, p. 315-338 (1984).
14. Mandell, J. F. , "Fatigue behavior of short fiber composite materials" Fatigue of Composite Materials Vol. 4 (Ken L. Reifsnider, ed.), p. 231-337, Elsevier Science Publishers (1991).

15. Rotem, A. , "The Fatigue Behavior of Composite Laminates under Various Mean Stresses", Composites Structures, Vol. 17, p 113-126 (1991).
16. Nguyen, D. H. and Ogale, A. A. , "Compressive and Flexural Creep Behavior of Carbon Fiber/PEEK composites", Journal of Thermoplastic Composite Materials, p. 83-99, Vol. 4 (1991).
17. Zhang, S. Y. , Xiang, X. , Y. , "Creep Characterization of a Fiber Reinforced Plastic Material", Journal of Reinforced Plastics and Composites, p. 1187-1194, Vol. 11 (1992).
18. Ward, I. M. , "Mechanical Properties of Solid Polymers", Second Edition, John Wiley & Sons (1983).
19. ASTM D 790-90 Flexural Properties of Unreinforced and Reinforced Plastics and Electrical Insulating Materials, Annual Book of ASTM Standards (1990).
20. ASTM D 671 Flexural Fatigue of Plastics by Constant-Amplitude-of-Force, Annual Book of ASTM Standards (1990).
21. Chou, Shen , Chen, Hong-Chu and Lai, Che-Chun, "The fatigue properties of weft-knit fabric reinforced epoxy resin composites", Composites Science and Technology 45, p. 283-291 (1992).
22. Hayashi, I. , Asanuma, K. , Niwa, K. , Fukano, M. and Maruyama, N. , "Mechanism of Damage Propagation in CFRP/AFRP Hybrid Laminates under Fatigue Flexural Loading", JSME International Journal, Series I, Vol. 34, No. 2 (1991).
23. Newaz, Golam M. , "Influence of Matrix Material on Flexural Fatigue Performance of Unidirectional Composites", Composites of Science and Technology 24, p. 199-214 (1985).
24. Shih, G. C. , Ebert, L. J. , "The Effect of the Fiber/Matrix Interface on the Flexural Fatigue Performance of Unidirectional Fiberglass Composites", Composites Science and Technology 28, p. 137-161 (1987).
25. ASTM D 2990-90 Standard Test Methods for Tensile, Compressive, and Flexural Creep and Creep-Rupture of Plastics, Annual Book of ASTM Standards (1990).
26. Flueler, P. , Motavalli, M. , "Creep Behavior of MNS-Composites Reinforced with Chopped Glass Mats and Woven Glass fabrics", EMPA Nr. 148465, September 1993.

27. Tuttle, M. E. , Brinson, H. F. , "Prediction of the Long-Term Creep Compliance of General Composite Laminates", Experimental Mechanics, 36(1), p. 89-102 (1986).
28. Dillard, D. A. , "Viscoelastic behavior of laminated composite materials", Fatigue of Composite Materials Vol. 4 (Ken L. Reifsnider, ed.), p. 339-384, Elsevier Science Publishers (1991).
29. Schapery, R. A. , "On the Characterization of Nonlinear Viscoelastic Materials", Polymer Engineering and Science, Vol. 9, No. 4, p. 295-310 (1969).